


Spring 5-2-2017

AN EXACT ANALYSIS FOR FOUR-ORDER ACOUSTO-OPTIC BRAGG DIFFRACTION WHICH INCORPORATES BOTH INCIDENT LIGHT ANGLE AND SOUND FREQUENCY DEPENDENCIES

Adeyinka Sunday Ademola
University of Texas at Tyler

Follow this and additional works at: https://scholarworks.uttyler.edu/ee_grad

 Part of the [Aerospace Engineering Commons](#), [Biomedical Commons](#), [Computational Engineering Commons](#), [Controls and Control Theory Commons](#), [Electrical and Electronics Commons](#), [Electronic Devices and Semiconductor Manufacturing Commons](#), [Nuclear Engineering Commons](#), [Operational Research Commons](#), [Other Electrical and Computer Engineering Commons](#), [Other Operations Research](#), [Systems Engineering and Industrial Engineering Commons](#), [Signal Processing Commons](#), [Systems and Communications Commons](#), [Systems Engineering Commons](#), and the [VLSI and Circuits, Embedded and Hardware Systems Commons](#)

Recommended Citation

Ademola, Adeyinka Sunday, "AN EXACT ANALYSIS FOR FOUR-ORDER ACOUSTO-OPTIC BRAGG DIFFRACTION WHICH INCORPORATES BOTH INCIDENT LIGHT ANGLE AND SOUND FREQUENCY DEPENDENCIES" (2017). *Electrical Engineering Theses*. Paper 31.
<http://hdl.handle.net/10950/565>

This Thesis is brought to you for free and open access by the Electrical Engineering at Scholar Works at UT Tyler. It has been accepted for inclusion in Electrical Engineering Theses by an authorized administrator of Scholar Works at UT Tyler. For more information, please contact tbianchi@uttyler.edu.

AN EXACT ANALYSIS FOR FOUR-ORDER ACOUSTO-OPTIC BRAGG
DIFFRACTION WHICH INCORPORATES BOTH INCIDENT LIGHT ANGLE
AND SOUND FREQUENCY DEPENDENCIES

by

ADEMOLA ADEYINKA SUNDAY

A thesis submitted in partial fulfillment
of the requirements for the degree of
Master of Science in Electrical Engineering
Department of Electrical Engineering

R. Pieper, Ph.D., Committee Chair

College of Engineering

The University of Texas at Tyler
May 2017

The University of Texas at Tyler
Tyler, Texas

This is to certify that the Master's Thesis of

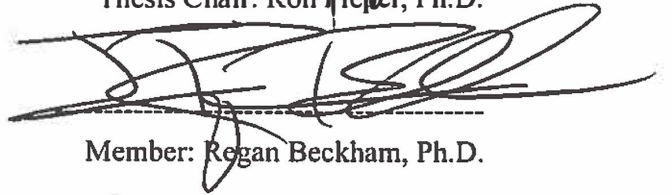
ADEMOLA ADEYINKA SUNDAY

has been approved for the thesis requirement on
March 31, 2017
for the Master of Science in Electrical Engineering

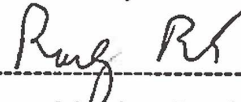
Approvals:



Thesis Chair: Ron Pieper, Ph.D.



Member: Regan Beckham, Ph.D.



Member: Randy Back, Ph.D.



Member: Premantanda Indic, Ph.D.



Chair: Hassan El-Kishky, Ph.D.



Michael McGinnis, Ph.D., P. E.
Interim Dean, College of Engineering.

Dedication

I dedicate this research to God Almighty, and to my Late father, Mr. David Ajibade Ademola, of blessed memory.

Acknowledgement

I would like to appreciate my thesis supervisor, Dr. R. J. Pieper, for his immense contribution toward the success of this research work. Similarly, the incessant supports of my parents, Mr. and Mrs. Isaac Olakojo is highly appreciated. My inestimable gratitude to my mum, Mrs. Ademola Abiodun, and all my siblings- Adedapo, Olusola, Adedamola, Aderonke and Adesoji. Thanks to my niece, Oluwadarasimi, and nephew, Adebayo, and at large, my extended family members. My heartfelt also goes to my bosom friend who is also my brother in-law, Mr. Adekunle Emmanuel Bankole, and his sweetheart, Miss Iyiola Odunayomi. Also, the prayers rendered by Dr. and Mrs. Adewuyi, Dr. and Mrs. Olawepo, Pst. and Mrs. Babalola, Pst. and Mrs. Adekugbe, Engr. and Mrs. Abidoeye, and the church of God at large is well recognized. I would not fail to recognize the love and care shown to me by the entire family of Mrs. Donna McDonald, Jasmine, Michaela, Sky, Storm and Shiloh. Similarly, I would say thank you to Dr. and Dr. (Mrs.) Onime for their kindness at all times. Also, Miss Nora Isioma Anazia is appreciated in everything. Above all, the unflinching support coupled with the mutual understanding of both my priceless wife, Janet Adewunmi, and that of my lovely and adorable daughter, Adesewa Gloria, is well valued. And to everyone too numerous to mention I would like to say thanks a million. God bless you all.

Table of Contents

List of Tables.....	v
List of Figures	vi
Abstract	viii
Chapter One	1
Introduction	1
1.1 Review of Prior Work	2
1.2 Objectives and Framework.....	4
1.3 Organization of the Research	5
Chapter Two.....	6
Background	6
2.1 Basic Principles of Acousto-Optics.....	6
2.2 AO Analysis based on Korpel Plane Wave Formalism.....	9
2.3 An Exact Four-Order Analysis with Restriction	11
2.4 Solutions for the Four-Order Problem.....	12
2.5 Ferrari Approach in Determining the Quartic Roots (2.35)	19
2.6 Overview of Chapter Two	21
Chapter Three.....	22
A Comprehensive Four-Order Exact Solution Analysis of Acousto-Optic	22
3.1 Translating the Physical Four-Order AO Problem to Mathematical System of First Order Linear Homogenous Coupled Differential Equations in Field Terms $\{\psi_1, \psi_0, \psi_{-1}, \psi_{-2}\}$	22

3.2 Steps taken to remove Coupling and generate the 4 th Order Homogenous Linear Differential Equation for $\psi_{-2}(\xi)$	25
3.3 Generating the Characteristic Equation (Quartic) for the Fourth Order Differential Equation of $\psi_{-2}(\xi)$	26
3.4 Predicting the Four Roots for the Quartic Characteristic Equation.....	26
3.5 A General Form of Solution for $\{\psi_1(\xi), \psi_0(\xi), \psi_{-1}(\xi), \psi_{-2}(\xi)\}$ in Terms of Four Undetermined Coefficients $\{A, B, C, D\}$	28
3.6 The Development of a Transition Matrix Solution	32
3.7 The General Solution and Selected Sample Cases	35
3.8 Overview of Chapter Three	36
Chapter Four.....	37
Matlab Simulations and Discussion of Results	37
4.1 Numerical and Analytical Simulation via Matlab yielding Confirmation of Four-Order AO Analytic Model	37
4.2 Flowchart Description for Implementation of Numerical and Analytical Methods	37
4.2.1 Numerical and Analytical Analysis of Space (ξ) Variation.....	37
4.2.2 Numerical and Analytical Analysis of Frequency ($\bar{\Omega}$) Variation.....	39
4.2.3 Numerical and Analytical Analysis of Angle ($\bar{\phi}_0$) Variation	42
4.3 Test Cases Demonstrating Variation in Normalized Space, Normalized Frequency, and Normalized Angle.....	44
4.3.1 Test case(s) for normalized space variation	44
4.3.2 Test case(s) for normalized frequency variation.....	48
4.3.3 Test cases for normalized angle variation.....	53

4.4 Concluding Remarks for Chapter Four	57
Chapter Five	58
Additional Topics.....	58
5.1 Divine Proportion Analysis	58
5.2 Energy Conservation for Unitary Transition Matrices.....	60
5.3 Numerical Demonstration that Roots are Real.....	61
5.4 Analysis and Demonstration for Consistency of Roots satisfying Vieta's Formulas [38].....	63
5.5 Demonstration that Transition Matrix " $\Gamma(\xi)$ " is Unitary.....	64
5.6 Concluding Remarks for Chapter Five.....	69
Chapter Six.....	70
Conclusion and Future Work	70
References	72
Appendix A: Obtaining the Fourth-Order Differential Equation [20]	76
Appendix B: Derivation of Fourth-Order Differential Equation	77
Appendix C: Obtaining the Quartic Roots using the Ferrari Approach.....	80
Appendix D: Test of Roots as Related to Coefficients (Vieta's Theorem)	86
Appendix E: Derivation of Homogeneous Solution of All Order.....	90

List of Tables

Table 1. Fundamental Parameters (After Pieper et al. [14, 21])	6
Table 2. Normalized Parameters ^a (Pieper et al. [20]).....	11

List of Figures

Figure 1. A typical Acousto-Optic device.....	2
Figure 2. Conservation of momentum triangle.....	8
Figure 3. Sound angular spectrum profile.....	8
Figure 4. General AO interaction diagram showing (dashed) Bragg lines (after Pieper et al. [14,21]).....	10
Figure 5. Comparison for four-order numerical and analytical solutions; all power is initially in the 0-order [20]	16
Figure 6. Comparison for four-order numerical and analytical solutions; all power is initially in the -1-order [20]	17
Figure 7. Comparison for four-order numerical and analytical solutions; all power is initially in the +1-order [20]	18
Figure 8. Comparison for four-order numerical and analytical solutions; all power is initially in the -2-order [20]	18
Figure 9. Flowchart of space variation numerical analysis.....	38
Figure 10. Flowchart of space variation analytical analysis	39
Figure 11. Flowchart of frequency variation numerical model.....	40
Figure 12. Flowchart of frequency variation analytical model	41
Figure 13. Flowchart of angle variation numerical model.....	43
Figure 14. Flowchart of angle variation analytical model	44
Figure 15. Comparison for four-order numerical and analytical solutions; all power is initially in the 0-order	45
Figure 16. Comparison for four-order numerical and analytical solutions; all power is initially in the -1-order.....	45
Figure 17. Comparison for four-order numerical and analytical solutions; all power is initially in the +1-order.....	46
Figure 18. Comparison for four-order numerical and analytical solutions; all power is initially in the -2-order.....	46
Figure 19. Comparison for four-order numerical and analytical solutions; power is initially 50% in both the 0th order and -1 order	47
Figure 20. Comparison for four-order numerical and analytical solutions in terms of acoustic frequency, all power is initially in the 0-order	48
Figure 21. A two-order numerical solutions and a four-order analytical solution in terms of acoustic frequency, with all power is initially in the 0-order	49
Figure 22. Comparison for four-order numerical and analytical solutions in terms of acoustic frequency, all power is initially in the -1-order	50
Figure 23. Comparison for four-order numerical and analytical solutions in terms of acoustic frequency, all power is initially in the +1-order	50
Figure 24. Comparison for four-order numerical and analytical solutions in terms of acoustic frequency, with all power is initially in the -1-order.....	51
Figure 25. Comparison for four-order numerical and analytical solutions for normalized frequency variation; power is initially 50% in both the 0-order and -1-order	52

Figure 26. Comparison for four-order numerical and analytical solutions for normalized frequency variation; power is initially 50% in both the +1-order and -2-order	52
Figure 27. Comparison for four-order numerical and analytical solutions in terms of optical angle with all power is initially in the 0-order.....	53
Figure 28. Comparison for four-order numerical and analytical solutions in terms of optical angle with all power is initially in the -1-order	54
Figure 29. Comparison for four-order numerical and analytical solutions in terms of optical angle with all power is initially in the +1-order	55
Figure 30. Comparison for four-order numerical and analytical solutions in terms of optical angle with all power is initially in the -1-order	55
Figure 31. Comparison for four-order numerical and analytical solutions for normalized angle variation; power is initially 50% in both the 0-order and -1-order.....	56
Figure 32. Comparison for four-order numerical and analytical solutions for normalized angle variation; power is initially 50% in both the +1-order and -2-order	56
Figure 33. Test of roots with normalized angle variation	61
Figure 34. Test of roots with normalized frequency variation.....	62
Figure 35. Test of roots with sound factor variation.....	62
Figure 36. Test of roots with quality factor (Q_c) variation.....	63
Figure 37. Demonstration of matrix unitary condition with normalized angle variation	67
Figure 38. Demonstration of matrix unitary condition with normalized frequency variation	67
Figure 39. Demonstration of matrix unitary condition with sound factor variation	68
Figure 40. Demonstration of matrix unitary condition with quality factor variation...	68

Abstract

AN EXACT ANALYSIS FOR FOUR-ORDER ACOUSTO-OPTIC BRAGG DIFFRACTION WHICH INCORPORATES BOTH INCIDENT LIGHT ANGLE AND SOUND FREQUENCY DEPENDENCIES

Ademola Adeyinka Sunday

Thesis Chair: Ron Pieper, Ph.D.

The University of Texas at Tyler
March 2017

This thesis extends the prior work which produced an exact solution to the four-order acousto-optic (AO) Bragg cell with assumed fixed center frequency and with exact Bragg angle incident light. The extension predicts the model that incorporates the dependencies of both the input angle of light and the sound frequency. Specifically, a generalized 4th order linear differential equation (DE), is developed from a simultaneous analysis of four coupled AO system of DEs. Through standard methods, the characteristic roots, which requires solving a quartic equation, is produced. Subsequently, a derived system of homogeneous solutions, which absorbs the roots obtained using Ferrari's approach, is formalized into a transition matrix operator which predicts the diffracted light orders at the exit of the AO cell in terms of the same diffracted light orders at the entrance. Numerical tests are used to test the hypothesis that the state of transition matrix is unitary. It is shown that this unitary matrix condition is sufficient to guarantee energy conservation. Three different types of tests: normalized space variation, normalized angle variation, and normalized frequency variation, have been used to demonstrate the agreement between analytical solutions and numerical predictions, which validate the formalism. Lastly, all four generated eigenvalues from the four-order acousto-optic differential matrix operator can be expressed simply in terms of Euclid's Divine Proportion.

Chapter One

Introduction

In what is now referred to as the topic of surface acoustic waves, Lord Raleigh, in 1885, attempted to analyze the effect of an earthquake by setting in motion the field of acoustics. About thirty seven years later, one facet of Raleigh's earlier concept was transformed into what is now termed Acousto-Optics [1]. Acousto-Optics (AO), first predicted by Léon Brillouin in 1922, is a branch of physics that deals with the interaction (either weak or strong) between sound and light [2, 3]. Similarly, by assuming both light and sound particles are well-defined in terms of energy ($\hbar\omega$ and $\hbar\vec{k}$) and momenta ($\hbar\Omega$ and $\hbar\vec{K}$) respectively, and in the absence of heat lost, AO will be explained in quantum mechanics as the elastic collision between the photons and phonons [4]. This interaction can result in light beam deflection, amplitude modulation, phase modulation, and frequency shifting [5].

Originally, AO was proposed to determine if the spectrum of thermal sound fluctuations in matter (solid, liquid or gas) could be measured by analyzing the amount of light they scattered [2, 6]. To achieve this, a Bragg cell (sound cell) has been introduced. It works simply by applying an electric field to a piezoelectric transducer such that a periodic sound wave is generated in the medium (such as glass) [7] as shown in Fig. 1. Consequently, this has the effect of deforming the material, causing an internal strain which results in a change in the refractive index. Thereafter, the strain is transmitted to the acousto-optic medium which is mechanically coupled to the transducer. An incident light on the acousto-optic medium will scatter off (diffract) the variation of the refractive index - compression and rarefaction [8]. Meanwhile, the analysis given by Brillouin to explain the heuristic theory was closely related to X-ray diffraction in crystals [9]. There have been two independent experimental verifications carried out by both the American and French scientists - Debye and Sears, and R. Lucas and P. Biquard in 1932 [10,11], Brillouin's predictions earlier analyzed using retarded potential Green's function method in the first Born approximation [12] were separately verified. Their analysis predicted that

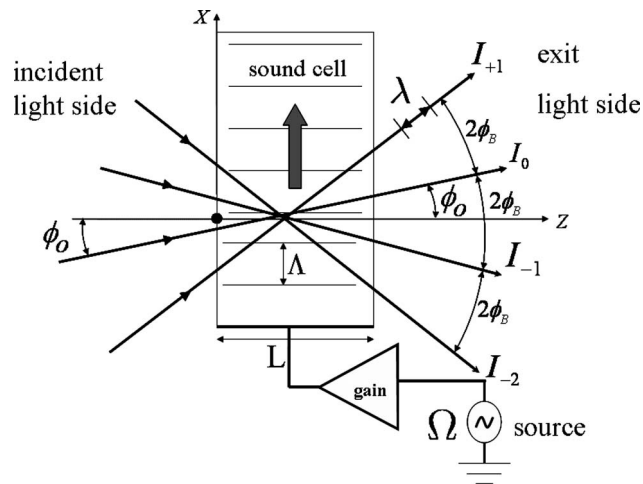


Figure 1. A typical Acousto-Optic device

the sound atomic planes cause multiple reflections (also called diffraction or scattering) of an incident electromagnetic plane wave. These reflections interfere constructively for certain critical angles of incidence, to cause enhanced overall reflection [13]. Shapewise, atomic planes are sharply defined in location and regular in structure, whereas, sound waves on the other hand are essentially sinusoidal and, when limited in the transverse direction, spread as they propagate. This results in very complex density distributions and wavefronts [9]. Besides, the movement of sound wavefronts makes the diffracted light either Doppler downshifted or upshifted (i.e., negative frequency shift or positive frequency shift) [5]. Doppler shifts in the sound has been predicted by Brillouin. To a first approximation the analogy is very useful [9]. However, in acoustic diffraction, the counterpart of the atomic planes in X-ray diffraction are planes of compression and rarefaction, induced by ultrasonic waves with frequency between 1 MHz and 2 GHz. Therefore, AO diffraction effects are similar to X-ray diffraction effects which occur as in crystals [9].

1.1 Review of Prior Work

Because it has been observed that light can be scattered into several orders when interacting with sound [11], there has been a keen interest in developing an efficient means for determining the conditions in which only one order of light is significantly diffracted. Although the application of numerical methods is essential to generating physical solutions for mathematically intractable problems for a wide range of AO designs [14, 15], an analytic solution, if possible, is usually preferred. Advantages of practical interest typically include computation speed required to

generate a solution, which is usually higher for analytic solutions. Also, analytic solutions provide more physical insight into the parameter functional dependencies. Lastly, direct methods for sensitivity analysis are well established for analytic solutions.

Based on the Feynman diagram techniques [16], Poon and Korpel in the 1980s, worked out an approximate analytic solution involving four diffracted orders. Their solution took the form of an infinite series in powers of $1/Q$, where Q is the Klein-Cook parameter and that the practical computation requires that the series has being truncated. Afterwards, an exact solution involving four diffracted orders was worked out by Poon, which assumes 100% of the energy is present in the 0th order and incident at the exact Bragg angle [17]. With boundary conditions specified relative to both initial 0 and -1-order field values, as well as their corresponding space derivatives, a four-order solution was derived from simultaneous analysis of two 2nd-order differential equations. The validity of the solution was checked by confirming that it met the energy conservation rule.

In the mid-80's, Blomme and Leroy [18] worked out an exact four-order solution that was applicable to arbitrary angles of incidence, but again was derived only with boundary conditions in which 100% of the optical power was initialized in the 0-order. The development of a four-order solution for arbitrary boundary conditions would be necessary to establish the equivalent of a four-order matrix formalism comparable to the two-order matrix formalism [19].

Subsequently, Pieper, Koslover and Poon, in 2008, developed an exact solution to the four-order AO Bragg diffraction problem with arbitrary initial optical power distribution but restrictive conditions such as exact Bragg angle incident light for 0-order and working at the AO cell center frequency [20]. The solution was formalized into a transition matrix operator predicting diffracted light orders at the exit of AO cell for arbitrary selection of the distribution of optical power for four orders incident on the AO cell. It was proven that the transition matrix is unitary which was sufficient to guarantee energy conservation. Moreover, the approach taken to find the four-order solution has led to the unveiling of the Golden Ratio, also known as the Divine Proportion [20].

In 2009, Ndwata and Pieper, introduced a design technique to increase the acousto-optic diffraction bandwidth for diffraction from 0-order into the first order.

For a high percentage of AO applications a broader bandwidth for first order diffraction improves the performance [21]. They combined both phased array and Hamming sound field apodization methods. Following this experiment, comparison of the combination of Hamming sound apodization and a three-cell phased array relative to either Hamming sound field apodization or a phased array shows that there was about 15% improvement over the phased array method alone [15] and 37% improvement over Hamming sound field apodization alone[14].

The range of AO effect applications is extensive. In one of the first system applications, as described by Korpel et al, AO deflector was the horizontal deflection in a laser TV display. While water was used as the interaction medium, a 3-dB resolution of about 200 resolvable TV elements were achieved using beam steering [22]. Subsequently, improvement in the resolution was attainable via cascade of two deflectors [23]. AO modulators, however, has gained ground over the years due to its numerous advantages, such as a low drive power, high extinction ratio, insensitivity to temperature changes, and simplicity in design and construction. AO effect has made versatile contributions in signal processing. This includes pulse compression [24, 25], optical correlation [26] and spectrum analysis of RF signals [26]. A thorough review of acousto-optical signal processors was given by Damon *et al.* [27]. In addition, the Acousto-optic effect has found numerous applications in practical devices such as optical modulators [28], deflectors [29], spectrometer [30], switches [21], filters, isolators, frequency shifters, and spectrum analyzers [7]. Similarly, encryption and decryption of signal processing has been conceived in AO, such that a message signal is added to a dc value, which is centered on the pass band and fed as an input bias of a Bragg cell. The heterodyne receiver is then designed for the decryption of the modulated message signal, which could be matched to transmitter key, thus generating an unmodulated chaos [31, 32].

1.2 Objectives and Framework

While the prior work was limited to space variations with the transducer's operation at center frequency and exact Bragg angle simultaneously [20], this research has been extended to incorporate input angle of light and acoustic frequency variation. With the derivation of a more generalized 4th -order DE, prior conditions were imposed as a check on the previous work (space variation). Thereafter, the boundary

conditions were relaxed by varying from unity, either normalized incident angle of optical, or normalized acoustic frequency.

The physical, practical and mathematical model employed in this research was closely related to that of Pieper's, Koslover's and Poon's work, [8], that is based on Korpel's 1979 paper [14] on two dimensional strong solutions, which can be conveniently programmed for a variety of boundary conditions, and it compares favorably with a normalized numerical analysis solution using Euler's method. To validate the formalism, a comparison between the analytical solutions and numerical predictions for the normalized space, angle and frequency will be presented. Although not directly tied into the mathematics of the approach taken to find the more generalized four-order solution, this result also reaffirmed the Golden Ratio, also known as the Divine Proportion [34], found in specimens and examples from arts, biology, architecture, and mathematics, which appears in the mathematics of four-order considered here. To avoid ambiguous notation, the convention follows that vectors are typeset in boldface; scalars and matrices are both in lightface but can be readily distinguished by context.

1.3 Organization of the Research

This thesis is divided into six chapters. Following the introduction in Chapter One, Chapter Two provides, among other things, a physical background and analysis of prior work. Chapter Three presents the comprehensive development of the 4th order generalized exact model, and its solution. The solution formalism into transition matrix is also presented. Chapter Four discusses the results using numerous test cases. Chapter Five presents additional topics such as the divine proportion and energy conservation analysis. Chapter Six contains conclusion and future work.

Chapter Two

Background

2.1 Basic Principles of Acousto-Optics

By generally predicting AO as a light-sound interaction, a Bragg cell (sound cell) is designed simply by applying an electric field to a piezo-electric transducer such that a periodic sound wave is generated in the medium (such as glass) [3,4], as earlier shown in Fig. 1. Consequently, this has the effect of deforming the material, causing an internal strain which results in a change in the refractive index. Thereafter, the strain is transmitted to the acousto-optic medium which is mechanically coupled to the transducer. An incident light on the acousto-optic medium will scatter off (diffract) the variation of the refractive index - compression and rarefaction [5]. According to Nath and Raman [9], among other things, the width of piezo-electric transducer width plays a vital role in the amount of light diffraction orders and the operation regime. Similarly, a parameter Q , also referred to as quality factor, determines the interaction regime, with Raman-Nath regime (i.e., $Q \ll 1$) and Bragg regime (i.e., $Q \gg 1$) [6] specified. As observed in Fig. 3 for a relatively low acoustic frequency-Nath-Raman regime[21], the main lobe gets wider as the transducer length L decreases and gets narrower (more directional/focused) as the transducer length increases.

Interestingly, the simple description above has metamorphosized into a purely mathematical one over the years. In order to establish the various notations used in this research work, the principles of acousto-optics [2, 9] shall be reviewed briefly. Table 1 lists and defines various fundamental parameters and standard assumptions as evaluated

Table 1. Fundamental Parameters (After Pieper et al. [14, 21])

Name of parameters	Acoustic	Relation	Optical
Wavelength	Λ	\gg	λ
Wave speed	V_s	\ll	c
Radian frequency	Ω	\ll	ω
Wave number	K	\ll	k

within the acoustic medium in this analysis. The uppercase and lowercase parameters have been reserved for acoustic and optical parameters respectively.

From the knowledge of elementary optical physics [12], the radian frequency ω and hertz frequency f are connected as:

$$\omega = 2\pi f. \quad (2.1)$$

whereas, light speed c and wavelength λ are related by:

$$c = f\lambda. \quad (2.2)$$

Besides, the following sound and optical wave relationships respectively exist between wave numbers K, k ; wavelengths Λ, λ ; and radian frequencies Ω, ω :

$$K = \frac{2\pi}{\Lambda} = \frac{\Omega}{V_s} \quad (2.3)$$

$$k = \frac{2\pi}{\lambda} = \frac{\omega}{c}. \quad (2.4)$$

Here, it is reaffirmed that the standard assumption employed is in the regime where

$$K \ll k. \quad (2.5)$$

The magnitude of the diffraction angle, otherwise known as the Bragg angle (ϕ_B), can be predicted based on a conservation of momentum diagram which, as seen in Fig. 1, is exactly one half of the angle between the adjacent diffracted orders as given by

$$\phi_B = \sin^{-1}\left(\frac{K}{2k}\right). \quad (2.6)$$

With the consistency in (2.5), and as predicted from Fig. 2, it follows that

$$\phi_B \approx \frac{K}{2k} = \frac{\lambda}{2\Lambda} = \frac{\Omega}{2kV_s}. \quad (2.7)$$

The diffraction angles ϕ_n for various diffracted orders can be expressed in terms of a 0-order. Angle ϕ_0 defined between a horizontal reference (z -axis) and the 0-order light ray trajectory, which satisfies the physical requirement of momentum and energy conservation between photons and phonons, as seen in Fig. 1, and is given by

$$\phi_n = \phi_0 + 2n\phi_B, \quad (2.8)$$

where, for the problem involving four diffracted orders,

$$-2 \leq n \leq +1. \quad (2.9)$$

Although Debye and Sears worked out criteria for operation in the Bragg regime, Klein and Cook, in 1967 [12], discovered a better quantitative criterion which is defined by a quality factor Q after some numerical computer simulations were

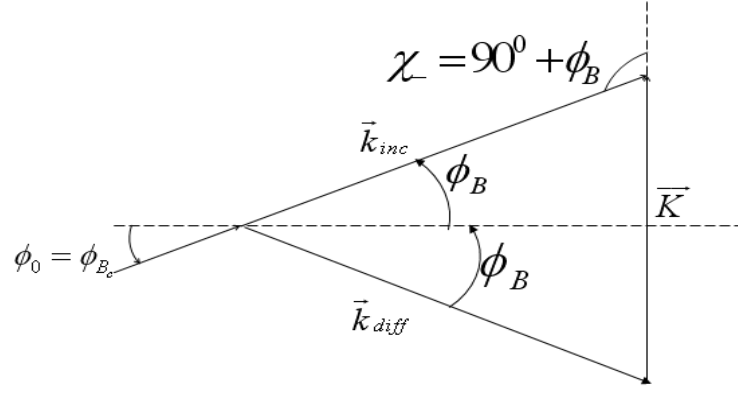


Figure 2. Conservation of momentum triangle for downshift

performed. It was confirmed that for operation in the Bragg regime [21], over 90% of the 0-order incident power, where $\phi_{inc} = \phi_0$, is diverted into the first diffracted order of the spectrum orders, i.e. for $n = -1$. This requires that two Bragg regime conditions were met:

$$\Delta\phi \equiv \phi_0 - \phi_B \approx 0 \quad (2.10)$$

and

$$Q \equiv 2\pi L \frac{\lambda}{\Lambda^2} > 2\pi, \quad (2.11)$$

where

$$\text{Debye-Sears ratio} = L \frac{\lambda}{\Lambda^2} \gg 1, \quad (2.12)$$

and Q is the Klein-Cook parameter [12, 14]. It is worth mentioning that spurious

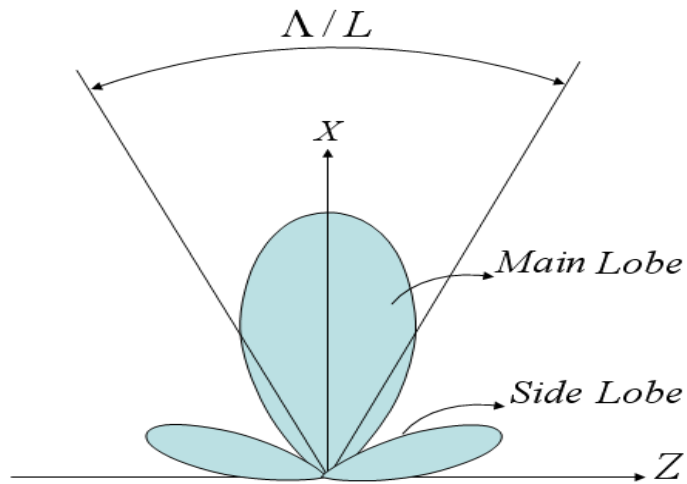


Figure 3. Sound angular spectrum profile

orders, other than 0 and -1, are generated from the acoustic sidelobes [14] if the sound field amplitude is too high.

2.2 AO Analysis based on Korpel Plane Wave Formalism

Generally, in order to proceed with the numerical analysis, a formalism for strong AO interaction, proposed in 1979 by Korpel, is introduced [8]. The following differential equation formalism couples electric field phasors between adjacent diffracted orders ψ_n , ψ_{n-1} , and ψ_{n+1} :

$$\Delta\psi_n(z) = -ja(S_{n+1}^-(z)\psi_{n+1}(z) + S_{n-1}^+(z)\psi_{n-1}(z))\Delta z, \quad (2.13)$$

where

$$a = \frac{kC}{4}. \quad (2.14)$$

Here C is a constant that measures the strain-optic sensitivity [2]. A time-dependent acoustic field $S(\rho, t)$ introduces compression and rarefaction on index of refraction n , which changes according to

$$\delta n(\rho, t) = CS(\rho, t). \quad (2.15)$$

Note that $\rho = (x, z)$ identifies the coordinates for a point in the sound field i.e. position vector, as shown in Fig. 4. The sound field is assumed to be time harmonic at the sound frequency Ω , and accordingly the sound phasor, $\tilde{S}(\rho) \equiv \tilde{S}(x, z)$ can be defined through the engineering convention as

$$S(\rho, t) = \text{Re}\{\tilde{S}(\rho)e^{j\Omega t}\}. \quad (2.16)$$

Similarly, the electric field phasors, i.e., $\tilde{\psi}(\rho) \equiv \tilde{\psi}(x, z)$, are defined according to an engineering convention as

$$\psi(\rho, t) = \text{Re}\{\tilde{\psi}(\rho, t)e^{j\omega t}\}, \quad (2.17)$$

with Doppler shifted harmonics,

$$\omega_n = \omega + n\Omega, \quad (2.18)$$

and the phase referenced back to the origin at the cell entrance $z = 0$. The sound coefficients $S_{n-1}^+(z)$ and $S_{n+1}^-(z)$ in (2.13) are then obtained after defining the x component of the bisectors (dashed lines) for the diffracted orders:

$$x_n^\pm \equiv z \tan(\phi_n \pm \phi_B) \approx z(\phi_n \pm \phi_B). \quad (2.19)$$

Considering Fig. 4, these bisectors (dashed lines) are known as Bragg lines [14] while the solid lines represents the trajectories for the diffracted orders. Approximation of (2.19) is valid, assuming small angles for all diffracted orders, which gives

$$S_{n-1}^+(z) \equiv \tilde{S}(z, x_{n-1}^+) \approx \tilde{S}(z, z(\phi_{n-1} + \phi_B)), \quad (2.20a)$$

$$S_{n+1}^-(z) \equiv \tilde{S}^*(z, x_{n+1}^-) \approx \tilde{S}^*(z, z(\phi_{n+1} - \phi_B)), \quad (2.20b)$$

where the superscript * indicates the complex conjugate.

For the bounded sound column plane-wave model, the dependence of the sound phasor on the (x, z) variation is taken to be separable according to

$$\tilde{S}(z, x) = \begin{cases} |\tilde{S}(z)| e^{-jKx + j\theta(z)} & z[0, L] \\ 0 & \text{otherwise} \end{cases} \quad (2.21)$$

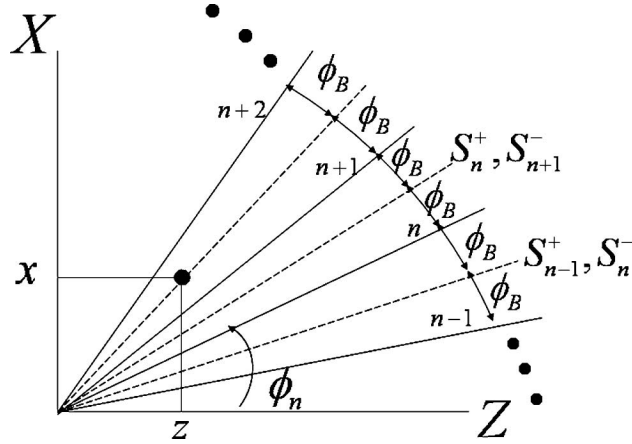


Figure 4. General AO interaction diagram showing (dashed) Bragg lines (after Pieper et al. [14,21])

where $\theta(z)$, in an ad hoc manner, accounts for any special related z -dependent phase shift along the transducer. This would, for example, be non-zero in the case that the design of the transducer employs phased-array techniques [15]. The combination of (2.8), (2.20) and (2.21) yields

$$S_{n-1}^+(z) = \tilde{S}(z) e^{(-jKz(\phi_0 + (2n-1)\phi_B) + j\theta(z))}, \quad (2.22a)$$

$$S_{n+1}^-(z) \equiv \tilde{S}^*(z, x_{n+1}^-) \approx \tilde{S}^*(z, z(\phi_{n+1} - \phi_B)). \quad (2.22b)$$

The AO transducer manufacturer will typically provide specifications on the operating power limits and a center frequency of operation, Ω_c . The existence of a center frequency permits a normalization in many of the predominant AO parameters, including frequency, Bragg angle, and incident angle, as outlined in Table 2.

In addition, as described in Table 2, the space coordinate z can be included in the normalization scheme. Subscript "c" indicates being evaluated at center frequency.

Table 2. Normalized Parameters^a (Pieper et al. [20])

Normalized Variable	Defining Relation
z coordinate	$\xi \equiv z/L$
Acoustic frequency	$\bar{\Omega} \equiv \Omega/\Omega_c$
Incident angle of light	$\bar{\phi}_0 \equiv \phi_o/\phi_{Bc}$
Klein-Cook Parameter	$Q_c \equiv LK_c^2/k$

[a] Subscript ‘c’ indicates evaluated at center frequency

In the context of normalization described, the sound coefficients in (2.22) can be recast in the following forms:

$$S_{n-1}^+(\xi) = \tilde{S}(\xi) e^{\left(-j\frac{1}{2}Q_c\bar{\Omega}^2\left(\frac{\bar{\phi}_0}{\bar{\Omega}}+(2n-1)\right)\xi+j\theta(\xi)\right)}, \quad (2.23a)$$

$$S_{n+1}^-(\xi) = \tilde{S}^*(\xi) e^{\left(+j\frac{1}{2}Q_c\bar{\Omega}^2\left(\frac{\bar{\phi}_0}{\bar{\Omega}}+(2n+1)\right)\xi-j\theta(\xi)\right)}, \quad (2.23b)$$

and the original coupled equation (2.13) is given in a normalized form by

$$\Delta\psi_n(\xi) = -jaL\left(S_{n-1}^+(\xi)\psi_{n-1}(\xi) + S_{n+1}^-(\xi)\psi_{n+1}(\xi)\right)\Delta\xi. \quad (2.24)$$

2.3 An Exact Four-Order Analysis with Restriction

From the prior work [20], special cases considered are identified according to the following conditions:

$$\theta(\xi) = 0 \quad (\text{No design phase shift}), \quad (2.25a)$$

$$S(\xi) = |\tilde{S}| \quad (\text{Uniform sound field}), \quad (2.25b)$$

$$\bar{\Omega} = 1 \quad (\text{Operating at the center frequency}), \quad (2.25c)$$

$$\bar{\phi}_0 = 1 \quad (\text{Exact Bragg condition } \Delta\phi = 0). \quad (2.25d)$$

The uniform sound field assumption is commonly used due to consistency with typical Bragg cell conditions. However, advantages of going with anon-uniform sound field have been studied [15]. In situations in which phased arrays (which require concatenated Bragg cells) the assumption of zero design phase shift cannot be used. [14]. Back substitution of (2.25) will lead to a special case for (2.23) as follows:

$$\frac{S_{n-1}^+(\xi)}{|\tilde{S}|} = e^{-jnQ_c\xi}, \quad (2.26a)$$

$$\frac{S_{n+1}^-(\xi)}{|\tilde{S}|} = e^{+j(n+1)Q_c\xi}. \quad (2.26b)$$

And the following subsequent simplification of (2.24) using (2.26) leads to

$$\Delta\psi_n(\xi) = -j\alpha \left(e^{-jnQ_c\xi}\psi_{n-1}(\xi) + e^{j(n+1)Q_c\xi}\psi_{n+1}(\xi) \right) \Delta\xi \quad (2.27)$$

where the sound factor,

$$\alpha \equiv a|\tilde{S}|L, \quad (2.28)$$

is typically selected to be $\pi/2$ in order to achieve a maximum in the efficiency of diffraction from the 0-order into the -1-order [3]. For the four orders:

$$\Psi^T(\xi) = (\psi_{+1}(\xi), \psi_0(\xi), \psi_{-1}(\xi), \psi_{-2}(\xi)). \quad (2.29)$$

The coupled differential equation (2.27) can be placed into matrix form:

$$\frac{d\Psi(\xi)}{d\xi} = -j\alpha A(\xi)\Psi(\xi), \quad (2.30)$$

where

$$A = \begin{pmatrix} 0 & e^{-jQ_c\xi} & 0 & 0 \\ e^{+jQ_c\xi} & 0 & 1 & 0 \\ 0 & 1 & 0 & e^{+jQ_c\xi} \\ 0 & 0 & e^{-jQ_c\xi} & 0 \end{pmatrix}. \quad (2.31)$$

The special case here leads to a Hermitian operator matrix (2.31), and therefore it has four real eigenvalues [5]. It was observed that the eigenvalues are either equal in magnitude to the Divine Proportion [7] or equal in magnitude to the reciprocal of this constant.

2.4 Solutions for the Four-Order Problem

Starting from (2.30), it can be shown, see appendix A, that the solution for the -2 diffracted order satisfies a 4th-order linear homogeneous constant coefficient differential equation as follows:

$$\frac{d^4\psi_{-2}(\xi)}{d\xi^4} + 2jQ_c \frac{d^3\psi_{-2}(\xi)}{d\xi^3} + (3\alpha^2 - Q_c^2) \frac{d^2\psi_{-2}(\xi)}{d\xi^2} + 2jQ_c\alpha^2 \frac{d\psi_{-2}(\xi)}{d\xi} + \alpha^4\psi_{-2}(\xi) = 0. \quad (2.32)$$

The form for (2.32) suggests four independent solutions of the form

$$\psi_{-2}(\xi) = e^{jr\xi}. \quad (2.33)$$

Backsubstitution into (2.33) leads to a quartic polynomial in root r :

$$r^4 + 2Q_c r^3 + (Q_c^2 - 3\alpha^2)r^2 - 2Q_c \alpha^2 r + \alpha^4 = 0, \quad (2.34)$$

and the roots obtained are

$$r_1 = -\frac{1}{2} \left(Q_c + \alpha + (Q_c^2 + 2Q_c \alpha + 5\alpha^2)^{1/2} \right), \quad (2.35a)$$

$$r_2 = -\frac{1}{2} \left(Q_c + \alpha - (Q_c^2 + 2Q_c \alpha + 5\alpha^2)^{1/2} \right), \quad (2.35b)$$

$$r_3 = -\frac{1}{2} \left(Q_c - \alpha + (Q_c^2 - 2Q_c \alpha + 5\alpha^2)^{1/2} \right), \quad (2.35c)$$

$$r_4 = -\frac{1}{2} \left(Q_c - \alpha - (Q_c^2 - 2Q_c \alpha + 5\alpha^2)^{1/2} \right), \quad (2.35d)$$

which are consistent with the results previously found [7]. It can be confirmed that all the roots are real as seen from

$$Q_c^2 \pm 2Q_c \alpha + 5\alpha^2 = (Q_c \pm \alpha)^2 + 4\alpha^2. \quad (2.36)$$

From a substitution of (2.36) into (2.35) two roots (r_2 and r_4) are identified to be positive and the other two roots (r_1 and r_3) are negative. The general solution to (2.32) is a superposition of four homogeneous solutions,

$$\psi_{-2}(\xi) = Ae^{j r_1 \xi} + Be^{j r_2 \xi} + Ce^{j r_3 \xi} + De^{j r_4 \xi}, \quad (2.37a)$$

and the coupling back to the other orders can be shown to lead to a consistent solution form for all orders given as follows:

$$\psi_{+1}(\xi) = Ae^{j r_1 \xi} + Be^{j r_2 \xi} - Ce^{j r_3 \xi} - De^{j r_4 \xi}, \quad (2.37b)$$

$$\psi_0(\xi) = -\frac{1}{\alpha} \left\{ r_1 A e^{j(r_1+Q_c)\xi} + r_2 B e^{j(r_2+Q_c)\xi} - r_3 C e^{j(r_3+Q_c)\xi} - r_4 D e^{j(r_4+Q_c)\xi} \right\}, \quad (2.37c)$$

$$\psi_{-1}(\xi) = -\frac{1}{\alpha} \left\{ r_1 A e^{j(r_1+Q_c)\xi} + r_2 B e^{j(r_2+Q_c)\xi} + r_3 C e^{j(r_3+Q_c)\xi} + r_4 D e^{j(r_4+Q_c)\xi} \right\}. \quad (2.37d)$$

In a special case, an evaluation of (2.37) at $\xi = 0$ links initial conditions from the left-hand side of (2.37) to unknown coefficients $\{A, B, C, D\}$ appearing on the right-hand side of (2.37). Solving $\{A, B, C, D\}$ at $\xi = 0$ results in a set of prediction rules for the unknown coefficients which are:

$$A = \frac{1}{2(r_2 - r_1)} \left\{ r_2 \psi_{+1}(0) + \alpha \psi_0(0) + \alpha \psi_{-1}(0) + r_2 \psi_{-2}(0) \right\}, \quad (2.38a)$$

$$B = \frac{1}{2(r_2 - r_1)} \{-r_1\psi_{+1}(0) - \alpha\psi_0(0) - \alpha\psi_{-1}(0) - r_1\psi_{-2}(0)\}, \quad (2.38b)$$

$$C = \frac{1}{2(r_3 - r_4)} \{r_4\psi_{+1}(0) + \alpha\psi_0(0) - \alpha\psi_{-1}(0) - r_4\psi_{-2}(0)\}, \quad (2.38c)$$

$$D = \frac{1}{2(r_3 - r_4)} \{-r_3\psi_{+1}(0) - \alpha\psi_0(0) + \alpha\psi_{-1}(0) + r_3\psi_{-2}(0)\}. \quad (2.38d)$$

Substituting (2.38) into (2.37) leads to

$$\psi_{+1}(\xi) = \frac{1}{2} [(\sigma + \tau)\psi_{+1}(0) + \alpha(\mu - \rho)\psi_0(0) + \alpha(\mu + \rho)\psi_{-1}(0) + (\sigma - \tau)\psi_{-2}(0)], \quad (2.39a)$$

$$\psi_0(\xi) = \frac{1}{2} e^{iQ_0\xi} [\alpha(\mu - \rho)\psi_{+1}(0) + (\theta + \gamma)\psi_0(0) + (\theta - \gamma)\psi_{-1}(0) + \alpha(\mu + \rho)\psi_{-2}(0)], \quad (2.39b)$$

$$\psi_{-1}(\xi) = \frac{1}{2} e^{iQ_0\xi} [\alpha(\mu + \rho)\psi_{+1}(0) + (\theta - \gamma)\psi_0(0) + (\theta + \gamma)\psi_{-1}(0) + \alpha(\mu - \rho)\psi_{-2}(0)], \quad (2.39c)$$

$$\psi_{-2}(\xi) = \frac{1}{2} [(\sigma - \tau)\psi_{+1}(0) + \alpha(\mu + \rho)\psi_0(0) + \alpha(\mu - \rho)\psi_{-1}(0) + (\sigma + \tau)\psi_{-2}(0)]. \quad (2.39d)$$

where

$$\mu \equiv \frac{e^{jr_1\xi} - e^{jr_2\xi}}{r_2 - r_1}, \quad (2.40a)$$

$$\rho \equiv \frac{e^{jr_3\xi} - e^{jr_4\xi}}{r_3 - r_4}, \quad (2.40b)$$

$$\sigma \equiv \frac{r_2 e^{jr_1\xi} - r_1 e^{jr_2\xi}}{r_2 - r_1}, \quad (2.40c)$$

$$\tau \equiv \frac{-r_4 e^{jr_3\xi} + r_3 e^{jr_4\xi}}{r_3 - r_4}, \quad (2.40d)$$

$$\theta \equiv \frac{-r_1 e^{jr_1\xi} + r_2 e^{jr_2\xi}}{r_2 - r_1}, \quad (2.40e)$$

$$\gamma \equiv \frac{r_3 e^{jr_3\xi} - r_4 e^{jr_4\xi}}{r_3 - r_4}. \quad (2.40f)$$

Equations (2.39) can be written more compactly in matrix form as

$$\Psi(\xi) = G(\xi)\Psi(0) \quad (2.41)$$

where

$$\Psi(\xi) = \begin{pmatrix} \psi_{+1}(\xi) \\ \psi_0(\xi) \\ \psi_{-1}(\xi) \\ \psi_{-2}(\xi) \end{pmatrix}, \quad (2.42a)$$

$$G(\xi) \equiv \frac{1}{2} \begin{bmatrix} \sigma + \tau & \alpha(\mu - \rho) & \alpha(\mu + \rho) & \sigma - \tau \\ \alpha(\mu - \rho)e^{jQ_c\xi} & (\theta + \gamma)e^{jQ_c\xi} & (\theta - \gamma)e^{jQ_c\xi} & \alpha(\mu + \rho)e^{jQ_c\xi} \\ \alpha(\mu + \rho)e^{jQ_c\xi} & (\theta - \gamma)e^{jQ_c\xi} & (\theta + \gamma)e^{jQ_c\xi} & \alpha(\mu - \rho)e^{jQ_c\xi} \\ \sigma - \tau & \alpha(\mu + \rho) & \alpha(\mu - \rho) & \sigma + \tau \end{bmatrix}, \quad (2.42b)$$

$$\Psi(0) = \begin{pmatrix} \psi_{+1}(0) \\ \psi_0(0) \\ \psi_{-1}(0) \\ \psi_{-2}(0) \end{pmatrix}. \quad (2.42c)$$

It is important to note that $G(\xi)$ has the following property:

$$G(G^T)^\dagger = GG^\dagger = G^\dagger G = I \quad (2.43)$$

where I is the identity matrix. The adjoint operator, also known as the Hermitian conjugate, of a tensor quantity M is designated M^\dagger and is defined [5] by two specific order-independent successive operations, i.e., complex conjugation- and transpose. As seen from (2.43), the adjoint of the transition matrix G is the matrix inverse or more succinctly G is the unitary [9]. The unitary property, applicable to the AO transition matrix, for any number of orders considered, is sufficient to guarantee the physical property of energy conservation. To illustrate the implementation of (2.42b), the following cases, with identified initial condition, have been considered.

$$\Psi^T(0) \equiv (0, 1, 0, 0) \Rightarrow \Psi^T(\xi) = \frac{1}{2}(\alpha(\mu - \rho), (\theta + \gamma)e^{jQ_c\xi}, (\theta - \gamma)e^{jQ_c\xi}, \alpha(\mu + \rho)), \quad (2.44a)$$

$$\Psi^T(0) \equiv (0, 0, 1, 0) \Rightarrow \Psi^T(\xi) = \frac{1}{2}(\alpha(\mu + \rho), (\theta - \gamma)e^{jQ_c\xi}, (\theta + \gamma)e^{jQ_c\xi}, \alpha(\mu - \rho)), \quad (2.44b)$$

$$\Psi^T(0) \equiv (1, 0, 0, 0) \Rightarrow \Psi^T(\xi) = \frac{1}{2}(\sigma + \tau, \alpha(\mu - \rho)e^{jQ_c\xi}, \alpha(\mu + \rho)e^{jQ_c\xi}, \sigma - \tau), \quad (2.44c)$$

$$\Psi^T(0) \equiv (0, 0, 0, 1) \Rightarrow \Psi^T(\xi) = \frac{1}{2}(\sigma - \tau, \alpha(\mu + \rho)e^{jQ_c\xi}, \alpha(\mu - \rho)e^{jQ_c\xi}, \sigma + \tau). \quad (2.44d)$$

Each of the four conditions represents 100% of the energy in one of the four rays incident on the sound cell from the left as shown in Fig. 1.

The space variation simulation figures from the prior work [20] have been added such that the solid lines, obtained from the numerical predictions, (2.26) and (2.27), and the data plots, generated from analytical solutions, (2.41) and (2.42b), are both represented. As a check for both the numerical and the analytical solutions, the total intensity, I_T ,

$$I_T = I_{+1} + I_0 + I_{-1} + I_{-2} = \sum_{i=-1}^{-2} |\psi_i(\xi)|^2, \quad (2.45)$$

is also computed. In a clearer context, Fig. 5 shows the numerical and analytical ξ - dependent predicted results when 100% of the incident light is in the 0th order [see (2.44b)]. As seen at the right-hand side of the plot, approximately 90% of the power is transferred to the -1-order via phonon emission and related photon frequency down conversion [14]. Relatively low percentages remain in the other orders. Agreement between numerical and analytical solutions is excellent with a confirming check shown for the total intensities according to (2.45).

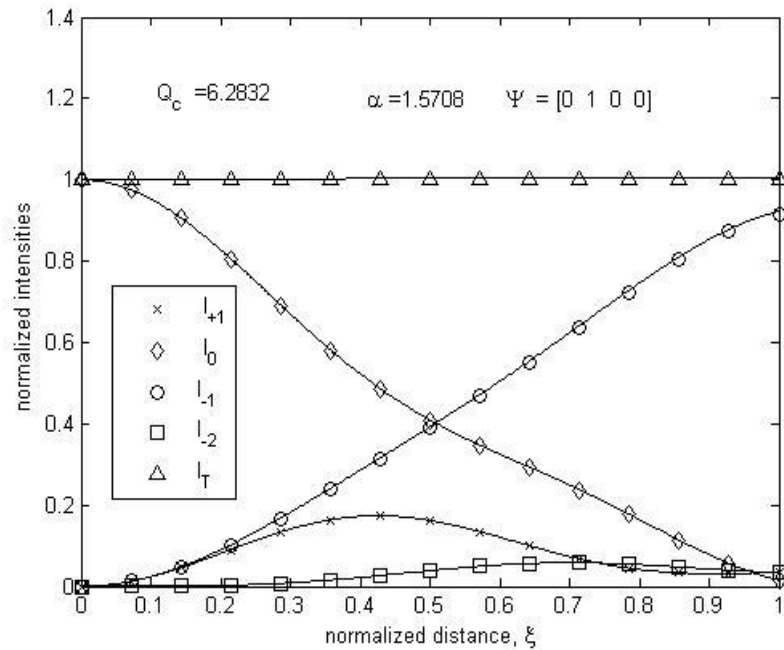


Figure 5. Comparison for four-order numerical and analytical solutions; all power is initially in the 0-order [20]

Fig. 6 shows numerical and analytical predicted results when 100% of the incident light is in the -1 order [see (2.44c)]. It can be observed that the curves both

numerically and analytically appear shapewise identical to those observed in Fig. 5, however, the orders have been swapped. Specifically, for relatively alike figs., the swap follows the path:

$$I_0 \Leftrightarrow I_{-1}, \quad (2.46a)$$

$$I_{+1} \Leftrightarrow I_{-2}. \quad (2.46b)$$

From a physical viewpoint this provides a validation of the accuracy of the solution. It is known that the Bragg conservation of momentum triangle engenders a fundamental symmetry in the phonon-assisted transfer of energy between orders [14]. Fig. 6 is then explained in terms of a sound phonon absorbed with a corresponding photon frequency upshift. Again, the level of agreement between numerical and analytical solutions is complete.

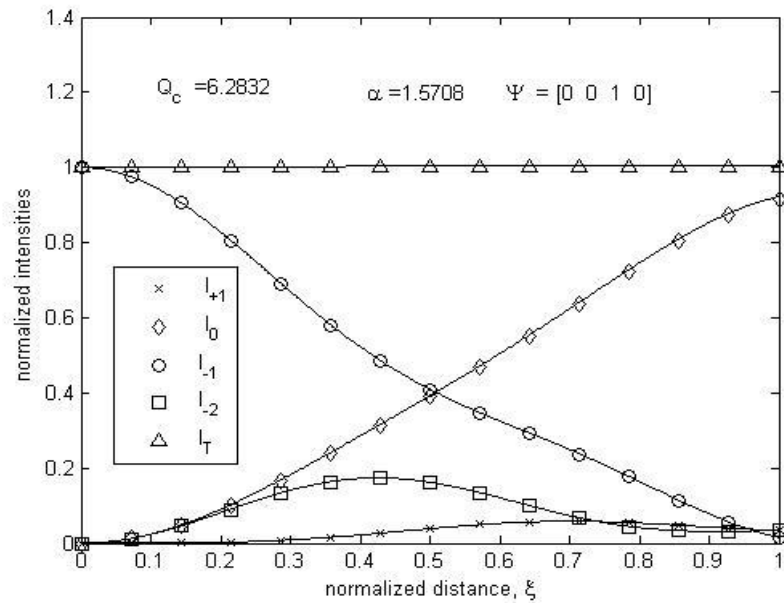


Figure 6. Comparison for four-order numerical and analytical solutions; all power is initially in the -1-order [20]

Fig. 7 shows the numerical and analytical predicted results when 100% of the incident light is in the +1 order [see (2.44a)]. Both numerical and analytical results as before are in complete agreement.

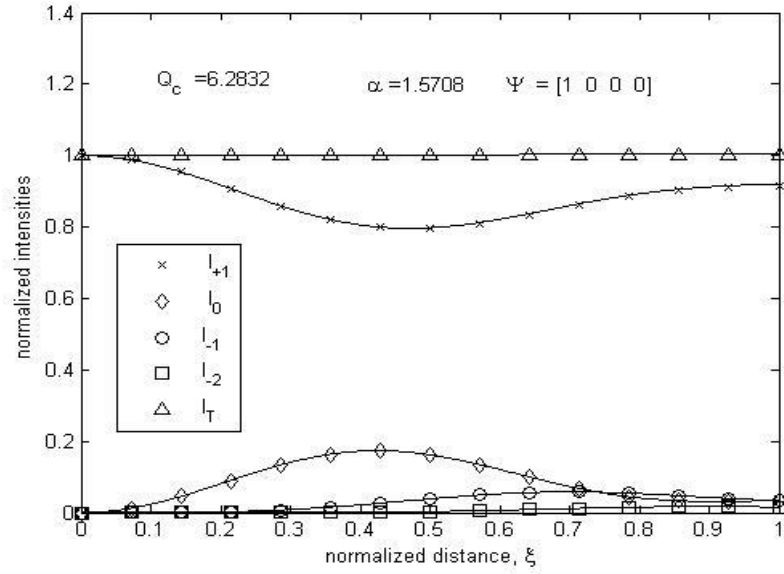


Figure 7. Comparison for four-order numerical and analytical solutions; all power is initially in the +1-order [20]

The case of 100% of the light in the -2-order [see (3.49d)], was also tested and compared. Curves were again shapewise identical to those in Fig. 7 with a repeated pattern [refer to (2.46)]. There is a complete agreement between numerical and analytical predictions.

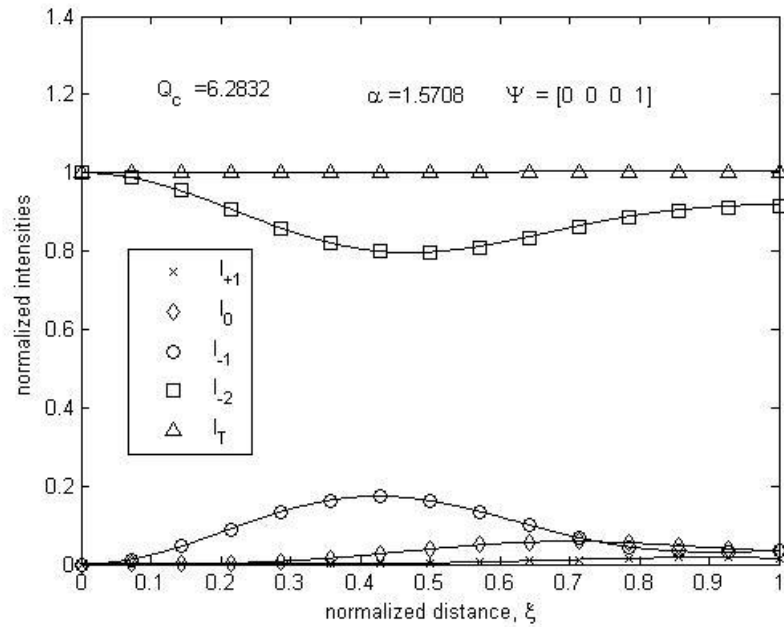


Figure 8. Comparison for four-order numerical and analytical solutions; all power is initially in the -2-order [20]

The plots show that not much power at the end of the cell is coupled out of the ψ_{+1} order. A qualitative observation is that the angular spectrum of the sound field is not broad enough in width to generate higher levels of energy transfer for this order. The power coupled into the cell in the +1 order, ψ_{+1} , is physically coupled to the higher ψ_{+2} , but this order is not being included in the formalism.

2.5 Ferrari Approach in Determining the Quartic Roots (2.35)

The quartic solutions obtained in (2.35) can be generated using the Ferrari method. The steps used to predict the quartic roots in (2.35) shall be presented sequentially. Starting from the characteristic quartic equation in (2.34):

$$r^4 + 2Q_c r^3 + (Q_c^2 - 3\alpha^2)r^2 - 2Q_c \alpha^2 r + \alpha^4 = 0 \quad (2.47)$$

by using in (2.47),

$$r = y - \frac{2Q_c}{4}, \quad (2.48)$$

results in

$$y^4 - \frac{1}{2}Q_c^2 y^2 - 3\alpha^2 y^2 + \alpha^2 Q_c y + \frac{1}{4}\alpha^2 Q_c^2 + \frac{1}{16}Q_c^4 + \alpha^4 = 0. \quad (2.49)$$

Re-grouping of (2.49) is a standard depressed quartic form which is expressed as

$$y^4 + py^2 + qy + dr = 0, \quad (2.50)$$

where

$$p = -\frac{1}{2}Q_c^2 - 3\alpha^2, \quad (2.51a)$$

$$q = \alpha^2 Q_c, \quad (2.51b)$$

$$dr = \frac{1}{4}\alpha^2 Q_c^2 + \frac{1}{16}Q_c^4 + \alpha^4, \quad (2.51c)$$

(2.50) is made a perfect square after adding $y^2 z + \frac{z^2}{4}$ to both sides, thus,

$$\left(y^2 + \frac{z}{2}\right)^2 = (z-p)y^2 - qy + \left(\frac{z^2}{4} - dr\right) \equiv (my+k)^2, \quad (2.52)$$

where m and k are to be determined. As observed, (2.52) is quadratic in y such that

$$\left(y^2 + \frac{z}{2}\right) = \pm(my+k). \quad (2.53)$$

Now, considering a quadratic equation,

$$ax^2 + bx + c = 0, \quad (2.54)$$

then (2.54) is a perfect square when its discriminant is zero, thus,

$$b^2 - 4ac = 0, \quad (2.55)$$

and when the constant coefficients of (2.54) is compared with that of the middle expression in (2.52), and thereafter, paralleled in (2.55) gives

$$q^2 - 4(z-p)\left(\frac{z^2}{4} - dr\right) = 0. \quad (2.56)$$

Simplification of (2.56) results in resolvent cubic:

$$z^3 - pz^2 - 4drz + (4pdr - q^2) = 0. \quad (2.57)$$

Back substitution of (2.51) in (2.57) leads to

$$z^3 + \left(\frac{1}{2}Q_c^2 + 3\alpha^2\right)z^2 - \left(\alpha^2Q_c^2 + \frac{1}{4}Q_c^4 + 4\alpha^4\right)z - \frac{1}{8}Q_c^6 - \frac{5}{4}Q_c^4\alpha^2 - 6Q_c^2\alpha^4 - 12\alpha^6 = 0. \quad (2.58)$$

the resolvent cubic roots after solving for z in (2.58) are

$$z_1 = -\frac{1}{2}Q_c^2 - 2\alpha^2, \quad (2.59a)$$

$$z_2 = -\frac{1}{2}\alpha^2 + \frac{1}{2}\sqrt{Q_c^4 + 6\alpha^2Q_c^2 + 25\alpha^4}, \quad (2.59b)$$

$$z_3 = -\frac{1}{2}\alpha^2 - \frac{1}{2}\sqrt{Q_c^4 + 6\alpha^2Q_c^2 + 25\alpha^4}. \quad (2.59c)$$

It then follows that, m and k in (2.52) can be determined after equating the expanded RHS with the middle expression as

$$m^2y^2 + 2mky + k^2 = (z-p)y^2 - qy + \left(\frac{z^2}{4} - dr\right), \quad (2.60)$$

such that, the conclusion drawn, following the comparison of the LHS and RHS (2.60) are

$$m = \pm\sqrt{(z-p)} \quad (2.61a)$$

and

$$k = -\frac{q}{2m}. \quad (2.61b)$$

More explicitly, backsubstitution of (2.51a) and (2.59a) after choosing m in (2.61a) as

$$m = -\sqrt{(z_1-p)} = -\alpha. \quad (2.62a)$$

Invariably, using (2.51) and (2.62a) in (2.61b) yields

$$k = \frac{q}{2\sqrt{z_1-p}} = \frac{1}{2}Q_c\alpha. \quad (2.62b)$$

Also, (2.53) implies that

$$y^2 - my - \left(k - \frac{z}{2}\right) = 0 \quad (2.63a)$$

and

$$y^2 + my + \left(k + \frac{z}{2}\right) = 0. \quad (2.63b)$$

Using the quadratic formula, (2.63) has the solutions:

$$y_{1,3} = \frac{m}{2} \pm \frac{1}{2} \sqrt{m^2 + 4 \left(k - \frac{z}{2}\right)} \quad (2.64a)$$

and

$$y_{2,4} = -\frac{m}{2} \pm \frac{1}{2} \sqrt{m^2 - 4 \left(k + \frac{z}{2}\right)}. \quad (2.64b)$$

Combining (2.62) and (2.54a) in (2.64) and thereafter, substituted back in (2.48) gives the characteristic quartic roots in (2.35) as:

$$r_1 = -\frac{1}{2}Q_c - \frac{1}{2}\alpha - \frac{1}{2}\sqrt{Q_c^2 + 2Q_c\alpha + 5\alpha^2}, \quad (2.65a)$$

$$r_2 = -\frac{1}{2}Q_c + \frac{1}{2}\alpha - \frac{1}{2}\sqrt{Q_c^2 - 2Q_c\alpha + 5\alpha^2}, \quad (2.65b)$$

$$r_3 = -\frac{1}{2}Q_c - \frac{1}{2}\alpha + \frac{1}{2}\sqrt{Q_c^2 + 2Q_c\alpha + 5\alpha^2}, \quad (2.65c)$$

$$r_4 = -\frac{1}{2}Q_c + \frac{1}{2}\alpha + \frac{1}{2}\sqrt{Q_c^2 - 2Q_c\alpha + 5\alpha^2}. \quad (2.65d)$$

2.6 Overview of Chapter Two

In this chapter, prior work has been explored. The fundamental principles of AO have been discussed. Following this, the AO analysis based on Korpel plane wave formalism was presented. Thereafter, an exact four order analysis with restriction was addressed. A system of differential equations was resolved into a 4th order DE. The solution of a four order problem led to a state of transition matrix, having the unitary property. Lastly, the matlab space variation simulations, for both analytical and numerical results was discussed.

Chapter Three

A Comprehensive Four-Order Exact Solution Analysis of Acousto-Optic

This chapter begins with the derivation of the mathematical system of 1st order coupled DE which consequently led to a generalized 4th order linear DE. Afterwards, the solution of characteristic quartic equations will be presented. The homogeneous solution of all coupling orders which diffused to the development of transition matrix will also be discussed.

3.1 Translating the Physical Four-Order AO Problem to Mathematical System of First Order Linear Homogenous Coupled Differential Equations in Field Terms

$$\{\psi_1, \psi_0, \psi_{-1}, \psi_{-2}\}$$

Since this research is based on non-phased-array techniques and uniform sound field, imposing the condition in (2.25) to (2.23) results in

$$S_{n-1}^+(\bar{\phi}_0, \bar{\Omega}, \xi) = |\tilde{S}| e^{-j\frac{1}{2}Q_c \bar{\Omega}^2 \left(\frac{\bar{\phi}_0}{\bar{\Omega}} + (2n-1)\right) \xi}, \quad (3.1a)$$

$$S_{n+1}^-(\bar{\phi}_0, \bar{\Omega}, \xi) = |\tilde{S}| e^{+j\frac{1}{2}Q_c \bar{\Omega}^2 \left(\frac{\bar{\phi}_0}{\bar{\Omega}} + (2n+1)\right) \xi}. \quad (3.1b)$$

Manipulation of (3.1) using the knowledge of elementary algebra leads to

$$S_{n-1}^+(\bar{\phi}_0, \bar{\Omega}, \xi) = |\tilde{S}| e^{-j\frac{1}{2}Q_c \bar{\Omega}^2 \left(\frac{\bar{\phi}_0 - \bar{\Omega}}{\bar{\Omega}} + 2n\right) \xi}, \quad (3.2a)$$

$$S_{n+1}^-(\bar{\phi}_0, \bar{\Omega}, \xi) = |\tilde{S}| e^{+j\frac{1}{2}Q_c \bar{\Omega}^2 \left(\frac{\bar{\phi}_0 - \bar{\Omega}}{\bar{\Omega}} + 2(n+1)\right) \xi}. \quad (3.2b)$$

Furthermore, (3.2) can be written again in terms of $\bar{\delta\phi}$ as

$$S_{n-1}^+(\bar{\delta\phi}, \xi) = |\tilde{S}| e^{-jQ_c \bar{\Omega}^2 \left(\frac{\bar{\delta\phi}}{2} + n\right) \xi}, \quad (3.3a)$$

$$S_{n+1}^-(\bar{\delta\phi}, \xi) = |\tilde{S}| e^{+jQ_c \bar{\Omega}^2 \left(\frac{\bar{\delta\phi}}{2} + (n+1)\right) \xi}, \quad (3.3b)$$

where

$$\overline{\delta\phi} = \left(\frac{\overline{\phi_0} - \overline{\Omega}}{\overline{\Omega}} \right). \quad (3.4)$$

In notation wise, (3.3) can also be re-written in terms of x and b as

$$S_{n-1}^+(x, b, \xi) = \left| \tilde{S} \right| e^{-j(x+bn)\xi}, \quad (3.5a)$$

$$S_{n+1}^-(x, b, \xi) = \left| \tilde{S} \right| e^{+j(x+b(n+1))\xi}, \quad (3.5b)$$

where

$$b = Q_c \overline{\Omega}^2, \quad (3.6a)$$

$$x = b \frac{\overline{\delta\phi}}{2}. \quad (3.6b)$$

Generally, with (3.4), both normalized angle ($\overline{\phi_0}$) and normalized frequency ($\overline{\Omega}$) enveloped in the x term [see (3.6b)], (3.5) forms the landmark of possible variations in terms of normalized space, angle and frequency after considering that for any order, the sound coefficient is susceptible to a change by either varying at least one of the three parameters - normalized space (ξ), normalized angle ($\overline{\phi_0}$) and normalized frequency ($\overline{\Omega}$), rather than having the transducer operate at the center frequency (i.e. $\overline{\Omega} = 1$) and light always entering at the Bragg angle (i.e., $\overline{\phi_0} = 1$) as demonstrated in the examples considered in previous work [20].

Basically, in order to proceed with the derivation of a generalized system of differential equations, the sound coefficients of all four orders is first obtained by using (2.9) in (3.5) as follows:

$$n = +1,$$

$$S_0^+(x, b, \xi) = \left| \tilde{S} \right| e^{-j(x+b)\xi}, \quad (3.7a)$$

$$S_{+2}^-(x, b, \xi) \text{ not used (+2 order excluded in analysis)}. \quad (3.7b)$$

$$n = 0,$$

$$S_{-1}^+(x, \xi) = \left| \tilde{S} \right| e^{-jx\xi}, \quad (3.8a)$$

$$S_{+1}^-(x, b, \xi) = \left| \tilde{S} \right| e^{+j(x+b)\xi}. \quad (3.8b)$$

$$n = -1,$$

$$S_{-2}^+(x, b, \xi) = |\tilde{S}| e^{-j(x-b)\xi}, \quad (3.9a)$$

$$S_0^-(x, \xi) = |\tilde{S}| e^{+jx\xi}. \quad (3.9b)$$

$$n = -2,$$

$$S_{-3}^+(x, b, \xi) \text{ not used } (-2 \text{ order excluded in analysis}), \quad (3.10a)$$

$$S_{-1}^-(x, b, \xi) = |\tilde{S}| e^{+j(x-b)\xi}. \quad (3.10b)$$

Since orders of -3 and $+2$ are outside the limit after considering (2.9), this gives justification for why both (3.7b) and (3.10a) were excluded. Following substitution of (3.5) on (2.24), the coupled equation is

$$\Delta \psi_n(\xi) = -j\alpha \left(e^{-j(x+bn)\xi} \psi_{n-1}(\xi) + e^{+j(x+b(n+1))\xi} \psi_{n+1}(\xi) \right) \Delta \xi, \quad (3.11)$$

where $\alpha \equiv a|\tilde{S}|L$ is the sound factor. For the four orders:

$$\Psi^T(\xi) = (\psi_{+1}(\xi), \psi_0(\xi), \psi_{-1}(\xi), \psi_{-2}(\xi)). \quad (3.12)$$

The coupled differential equation in (3.11) can be re-written as

$$\frac{d\Psi(\xi)}{d\xi} = -j\alpha A(\xi) \Psi(\xi) \quad (3.13)$$

where

$$\frac{d\Psi(\xi)}{d\xi} = \frac{\Delta \psi_n(\xi)}{\Delta \xi}, \quad (3.14)$$

$$A(\xi) \Psi(\xi) = e^{-j(x+bn)\xi} \psi_{n-1}(\xi) + e^{+j(x+b(n+1))\xi} \psi_{n+1}(\xi). \quad (3.15)$$

By placing the coupled sound coefficients in (3.7) - (3.10) in matrix location to pattern with (3.15) leads to

$$A(\xi) \Psi(\xi) = \begin{pmatrix} 0 & s_0^+ & 0 & 0 \\ s_{+1}^- & 0 & s_{-1}^+ & 0 \\ 0 & s_0^- & 0 & s_{-2}^+ \\ 0 & 0 & s_{-1}^- & 0 \end{pmatrix} \begin{pmatrix} \psi_{+1}(\xi) \\ \psi_0(\xi) \\ \psi_{-1}(\xi) \\ \psi_{-2}(\xi) \end{pmatrix}, \quad (3.16)$$

or equivalently,

$$A(\xi)\Psi(\xi) = -j\alpha \begin{pmatrix} 0 & e^{-j(x+b)\xi} & 0 & 0 \\ e^{+j(x+b)\xi} & 0 & e^{-jx\xi} & 0 \\ 0 & e^{+jx\xi} & 0 & e^{-j(x-b)\xi} \\ 0 & 0 & e^{+j(x-b)\xi} & 0 \end{pmatrix} \begin{pmatrix} \psi_{+1}(\xi) \\ \psi_0(\xi) \\ \psi_{-1}(\xi) \\ \psi_{-2}(\xi) \end{pmatrix}. \quad (3.17)$$

As a check for correctness of this current research, using (2.55c) and (2.55d) in (3.4), and back substitution to $A(\xi)$ in (3.17) reduces to (2.31). Besides, the generalized case here shows that $A(\xi)$ could lead to a Hermitian operator matrix, and therefore it has four real eigenvalues [28]. Similarly, the eigenvalues are observed to be either equal in magnitude to the Divine Proportion [29] or equal in magnitude to the reciprocal of this constant; Appendix B shows the details. Using (3.12) and (3.17) to construct (3.13) generates

$$\frac{d}{d\xi} \begin{pmatrix} \psi_{+1}(\xi) \\ \psi_0(\xi) \\ \psi_{-1}(\xi) \\ \psi_{-2}(\xi) \end{pmatrix} = -j\alpha \begin{pmatrix} 0 & e^{-j(x+b)\xi} & 0 & 0 \\ e^{+j(x+b)\xi} & 0 & e^{-jx\xi} & 0 \\ 0 & e^{+jx\xi} & 0 & e^{-j(x-b)\xi} \\ 0 & 0 & e^{+j(x-b)\xi} & 0 \end{pmatrix} \begin{pmatrix} \psi_{+1}(\xi) \\ \psi_0(\xi) \\ \psi_{-1}(\xi) \\ \psi_{-2}(\xi) \end{pmatrix}. \quad (3.19)$$

Finally, simplification of (3.19) gives a system of linear differential equations as

$$\frac{d\psi_{+1}(\xi)}{d\xi} = -j\alpha e^{-j(x+b)\xi} \psi_0(\xi), \quad (3.20a)$$

$$\frac{d\psi_0(\xi)}{d\xi} = -j\alpha \left(e^{+j(x+b)\xi} \psi_{+1}(\xi) + e^{-jx\xi} \psi_{-1}(\xi) \right), \quad (3.20c)$$

$$\frac{d\psi_{-1}(\xi)}{d\xi} = -j\alpha \left(e^{+jx\xi} \psi_0(\xi) + e^{-j(x-b)\xi} \psi_{-2}(\xi) \right), \quad (3.20c)$$

$$\frac{d\psi_{-2}(\xi)}{d\xi} = -j\alpha e^{+j(x-b)\xi} \psi_{-1}(\xi). \quad (3.20d)$$

3.2 Steps taken to remove Coupling and generate the 4th Order Homogenous Linear Differential Equation for $\psi_{-2}(\xi)$

Starting from (3.20) it can be shown, through a lengthy substitution process, that the solution for the -2 diffracted order satisfies a more generalized 4th-order linear homogeneous constant-coefficient differential equation as follows:

$$\begin{aligned} & \frac{d^4\psi_{-2}(\xi)}{d\xi^4} + j(2b-6x)\frac{d^3\psi_{-2}(\xi)}{d\xi^3} + (3\alpha^2 - 11x^2 + 9bx - b^2)\frac{d^2\psi_{-2}(\xi)}{d\xi^2} \\ & + j(6x^3 - 9bx^2 + (3b^2 - 9\alpha^2)x + 2\alpha^2b)\frac{d\psi_{-2}(\xi)}{d\xi} + (3\alpha^2bx - 6\alpha^2x^2 + \alpha^4)\psi_{-2}(\xi) = 0. \end{aligned} \quad (3.21)$$

The salient features of this derivation are retained in Appendix C. To support the validity of (3.21), the underlying assumptions, i.e., (2.25c) and (2.25d), if imposed on (3.21), after substitution in (3.4) reduces to (2.32).

3.3 Generating the Characteristic Equation (Quartic) for the Fourth Order Differential Equation of $\psi_{-2}(\xi)$

The form for (3.1) suggests four independent solutions of the form

$$\psi_{-2}(\xi) = e^{jr\xi}. \quad (3.22)$$

By taking the 1st - 4th derivative of (3.22) as:

$$\frac{d\psi_{-2}(\xi)}{d\xi} = jre^{jr\xi}, \quad (3.23a)$$

$$\frac{d^2\psi_{-2}(\xi)}{d\xi^2} = -r^2e^{jr\xi}, \quad (3.23b)$$

$$\frac{d^3\psi_{-2}(\xi)}{d\xi^3} = -jr^3e^{jr\xi}, \quad (3.23c)$$

$$\frac{d^4\psi_{-2}(\xi)}{d\xi^4} = r^4e^{jr\xi}, \quad (3.23d)$$

and backsubstitution of (3.22) and (3.23) into (3.21) leads to a characteristic quartic equation in r as:

$$\begin{aligned} r^4 + (2b-6x)r^3 + (-3\alpha^2 + 11x^2 - 9bx + b^2)r^2 + (-6x^3 + 9bx^2 - (3b^2 - 9\alpha^2)x - 2\alpha^2b)r \\ + (3\alpha^2bx - 6\alpha^2x^2 + \alpha^4) = 0. \end{aligned} \quad (3.24)$$

3.4 Predicting the Four Roots for the Quartic Characteristic Equation

The " r " is then solved for in (3.24) by using the Ferrari method. Ferrari's approach, with details in appendix C, firstly reduces the quartic polynomial to what is termed depressed quartic, and thereafter, resolvent cubic polynomial respectively before the roots are generated [35-38] as

$$r_1 = -\frac{1}{2}P - \frac{1}{2}Q + \frac{1}{2}R, \quad (3.25a)$$

$$r_2 = -\frac{1}{2}P + \frac{1}{2}Q + \frac{1}{2}S, \quad (3.25b)$$

$$r_3 = -\frac{1}{2}P - \frac{1}{2}Q - \frac{1}{2}R, \quad (3.25c)$$

$$r_4 = -\frac{1}{2}P + \frac{1}{2}Q - \frac{1}{2}S, \quad (3.25d)$$

where

$$P = (b - 3x), \quad (3.26a)$$

$$Q = \left(\frac{1}{6}w^{1/3} + 2H + \frac{1}{3}b^2 + \frac{5}{3}x^2 + 2\alpha^2 \right)^{1/2}, \quad (3.26b)$$

$$R = \left[\left(-\frac{1}{6}w^{1/3} - 2H + \frac{2}{3}b^2 + \frac{10}{3}x^2 + 4\alpha^2 \right) + (2\alpha^2b - 4bx^2)Q^{-1} \right]^{1/2}, \quad (3.26c)$$

$$S = \left[\left(-\frac{1}{6}w^{1/3} - 2H + \frac{2}{3}b^2 + \frac{10}{3}x^2 + 4\alpha^2 \right) - (2\alpha^2b - 4bx^2)Q^{-1} \right]^{1/2}, \quad (3.26d)$$

$$H = \left(8\alpha^2x^2 + 2\alpha^2b^2 - \frac{5}{3}x^2b^2 + \frac{1}{3}b^4 + \frac{13}{3}x^4 + 7\alpha^4 \right)w^{-1/3}, \quad (3.26e)$$

$$w = w_1 + w_2 + 12(w_3 + w_4 + w_5 + w_6 + w_7)^{1/2}. \quad (3.26f)$$

All the "w" elements in (3.26f) are placed in two categories: the "non-square root" components (w_1 and w_2), and the "bracketed square root" components (w_3, w_4, w_5, w_6 and w_7). Noticeably, for all the parameters (α, b and x) used to describe the system, x^2 is common in w_1 , whereas, w_2 has no x term. Thus,

$$w_1 = \left(-864b^2\alpha^2 + 36(16x^2 + 23\alpha^2)\alpha^2 - 12(x^2 + 5b^2)b^2 + 280x^4 \right)x^2, \quad (3.26g)$$

$$w_2 = 72(b^2 + 5\alpha^2)b^2\alpha^2 + 8(b^6 + 81\alpha^6), \quad (3.26h)$$

$$w_3 = (-3162\alpha^2 x^2 - 9420\alpha^4 + 4110\alpha^2 b^2)\alpha^2 x^4 b^2, \quad (3.26i)$$

$$w_4 = (-4848\alpha^4 - 936\alpha^2 b^2 + 684x^2 b^2 - 648x^4)\alpha^2 x^2 b^4, \quad (3.26j)$$

$$w_5 = (-108\alpha^2 b^6 - 648\alpha^2 x^6 - 8760\alpha^8 - 27(x^2 b^6 - 10x^4 b^4 + 33b^2 x^6 - 40x^8))x^2 b^2, \quad (3.26k)$$

$$w_6 = (-3(4824\alpha^4 x^4 + 3064\alpha^2 x^6 + 4609\alpha^6 x^2 + 1056x^8 + 2220\alpha^8)\alpha^2 - 432x^{10})x^2, \quad (3.26l)$$

$$w_7 = -48(\alpha^6 b^2 + 6\alpha^8)\alpha^2 b^2 - 1200\alpha^{12}. \quad (3.26m)$$

Although, $\alpha^2 x^2$ and b^2 are all common to both w_3 and w_4 , however, w_3 and w_4 , have x^4 and b^4 as a highest common factor respectively. The common terms in w_5 are x^2 and b^2 , whereas in w_6 there is only x^2 . In w_7 , no x term is found.

3.5 A General Form of Solution for $\{\psi_1(\xi), \psi_0(\xi), \psi_{-1}(\xi), \psi_{-2}(\xi)\}$ in Terms of Four Undetermined Coefficients $\{A, B, C, D\}$

A proposed general solution to (3.21) is taken as a superposition of the four homogenous solutions,

$$\psi_{-2}(\xi) = Ae^{j r_1 \xi} + Be^{j r_2 \xi} + Ce^{j r_3 \xi} + De^{j r_4 \xi}. \quad (3.27a)$$

The coupling back to the other orders can be shown, in appendix F, to lead to a consistent solution form for all orders given as follows:

$$\psi_{-1}(\xi) = -\frac{1}{\alpha} e^{-j(x-b)\xi} (r_1 A e^{j r_1 \xi} + r_2 B e^{j r_2 \xi} + r_3 C e^{j r_3 \xi} + r_4 D e^{j r_4 \xi}), \quad (3.27b)$$

$$\begin{aligned} \psi_0(\xi) = \frac{1}{\alpha^2} e^{-j(2x-b)\xi} & \left((r_1^2 - (x-b)r_1 - \alpha^2) A e^{j r_1 \xi} + (r_2^2 - (x-b)r_2 - \alpha^2) B e^{j r_2 \xi} \right. \\ & \left. + (r_3^2 - (x-b)r_3 - \alpha^2) C e^{j r_3 \xi} + (r_4^2 - (x-b)r_4 - \alpha^2) D e^{j r_4 \xi} \right), \end{aligned} \quad (3.27c)$$

$$\begin{aligned}
\psi_{+1}(\xi) = & -\frac{1}{\alpha^3} e^{-j3x\xi} \left(r_1^3 - (3x-2b)r_1^2 + (2x^2 - 3bx + b^2 - 2\alpha^2)r_1 + \alpha^2(2x-b) \right) A e^{j\eta_1\xi} \\
& + \left(r_2^3 - (3x-2b)r_2^2 + (2x^2 - 3bx + b^2 - 2\alpha^2)r_2 + \alpha^2(2x-b) \right) B e^{j\eta_2\xi} \\
& + \left(r_3^3 - (3x-2b)r_3^2 + (2x^2 - 3bx + b^2 - 2\alpha^2)r_3 + \alpha^2(2x-b) \right) C e^{j\eta_3\xi} \\
& + \left(r_4^3 - (3x-2b)r_4^2 + (2x^2 - 3bx + b^2 - 2\alpha^2)r_4 + \alpha^2(2x-b) \right) D e^{j\eta_4\xi}.
\end{aligned} \tag{3.27d}$$

Equivalently, (3.27) can be more compactly written by placing in matrix form

$$\begin{pmatrix} \psi_{+1}(\xi) \\ \psi_0(\xi) \\ \psi_{-1}(\xi) \\ \psi_{-2}(\xi) \end{pmatrix} = \begin{pmatrix} -\frac{\kappa_1 t_1 e^{-j3x\xi}}{\alpha^3} & -\frac{\kappa_2 t_2 e^{-j3x\xi}}{\alpha^3} & -\frac{\kappa_3 t_3 e^{-j3x\xi}}{\alpha^3} & -\frac{\kappa_4 t_4 e^{-j3x\xi}}{\alpha^3} \\ \frac{\eta_1 t_1 e^{-j(2x-b)\xi}}{\alpha^2} & \frac{\eta_2 t_2 e^{-j(2x-b)\xi}}{\alpha^2} & \frac{\eta_3 t_3 e^{-j(2x-b)\xi}}{\alpha^2} & \frac{\eta_4 t_4 e^{-j(2x-b)\xi}}{\alpha^2} \\ -\frac{r_1 t_1 e^{-j(x-b)\xi}}{\alpha} & -\frac{r_2 t_2 e^{-j(x-b)\xi}}{\alpha} & -\frac{r_3 t_3 e^{-j(x-b)\xi}}{\alpha} & -\frac{r_4 t_4 e^{-j(x-b)\xi}}{\alpha} \\ t_1 & t_2 & t_3 & t_4 \end{pmatrix} \begin{pmatrix} A \\ B \\ C \\ D \end{pmatrix}, \tag{3.28}$$

where, for $i = 1, 4$, the notation implies

$$t_i \equiv e^{j\eta_i\xi}, \tag{3.29a}$$

$$\eta_i \equiv r_i^2 - (x-b)r_i - \alpha^2, \tag{3.29b}$$

$$\kappa_i \equiv r_i^3 - (3x-2b)r_i^2 + (2x^2 - 3bx + b^2 - 2\alpha^2)r_i + \alpha^2(2x-b). \tag{3.29c}$$

In a special case, however, an evaluation of (3.27) at $\xi = 0$ links initial conditions from the left-hand side of (3.27) to unknown coefficients $\{A, B, C, D\}$ appearing on the right-hand side of (3.27) as:

$$\psi_{-2}(0) = A + B + C + D, \tag{3.30a}$$

$$\psi_{-1}(0) = -\frac{1}{\alpha} (r_1 A + r_2 B + r_3 C + r_4 D), \tag{3.30b}$$

$$\begin{aligned}
\psi_0(0) = & \frac{1}{\alpha^2} \left((r_1^2 - (x-b)r_1 - \alpha^2) A + (r_2^2 - (x-b)r_2 - \alpha^2) B \right. \\
& \left. + (r_3^2 - (x-b)r_3 - \alpha^2) C + (r_4^2 - (x-b)r_4 - \alpha^2) D \right),
\end{aligned} \tag{3.30c}$$

$$\begin{aligned}
\psi_{+1}(0) = & -\frac{1}{\alpha^3} \left(r_1^3 - (3x-2b)r_1^2 + (2x^2-3bx+b^2-2\alpha^2)r_1 + \alpha^2(2x-b) \right) A \\
& + \left(r_2^3 - (3x-2b)r_2^2 + (2x^2-3bx+b^2-2\alpha^2)r_2 + \alpha^2(2x-b) \right) B \\
& + \left(r_3^3 - (3x-2b)r_3^2 + (2x^2-3bx+b^2-2\alpha^2)r_3 + \alpha^2(2x-b) \right) C \\
& + \left(r_4^3 - (3x-2b)r_4^2 + (2x^2-3bx+b^2-2\alpha^2)r_4 + \alpha^2(2x-b) \right) D.
\end{aligned} \tag{3.30d}$$

Solving for $\{A, B, C, D\}$ in either (3.30) at $\xi = 0$, or by the matrix inversion of the $\xi = 0$ version of (3.28), results in a set of prediction rules for the unknown coefficients,

$$\begin{pmatrix} A \\ B \\ C \\ D \end{pmatrix} = \begin{pmatrix} \frac{\alpha^3}{a} & \frac{\alpha^2 S_\delta}{a} & \frac{\alpha U_\delta}{a} & \frac{\alpha^2 N_\delta}{a} \\ \frac{\alpha^3}{b} & \frac{\alpha^2 S_\gamma}{b} & \frac{\alpha U_\gamma}{b} & \frac{\alpha^2 N_\gamma}{b} \\ \frac{\alpha^3}{c} & \frac{\alpha^2 S_\lambda}{c} & \frac{\alpha U_\lambda}{c} & \frac{\alpha^2 N_\lambda}{c} \\ \frac{\alpha^3}{d} & \frac{\alpha^2 S_\rho}{d} & \frac{\alpha U_\rho}{d} & \frac{\alpha^2 N_\rho}{d} \end{pmatrix} \begin{pmatrix} \psi_{+1}(0) \\ \psi_0(0) \\ \psi_{-1}(0) \\ \psi_{-2}(0) \end{pmatrix}, \tag{3.30d}$$

where,

$$a = -(r_1 - r_2)(r_1 - r_3)(r_1 - r_4) \tag{3.32a1}$$

$$b = (r_1 - r_2)(r_2 - r_3)(r_2 - r_4) \tag{3.32b2}$$

$$c = -(r_1 - r_3)(r_2 - r_3)(r_3 - r_4) \tag{3.32c3}$$

$$d = (r_1 - r_4)(r_2 - r_4)(r_3 - r_4) \tag{3.32d4}$$

$$\delta = r_2 + r_3 + r_4 \tag{3.33a1}$$

$$\gamma = r_1 + r_3 + r_4 \tag{3.33b2}$$

$$\lambda = r_1 + r_2 + r_4 \tag{3.33c3}$$

$$\rho = r_1 + r_2 + r_3 \tag{3.33d4}$$

$$U_\delta = x(x-2b-\delta) + b(b+\delta) + r_2 r_3 + r_2 r_4 + r_3 r_4 + 2\alpha^2 \tag{3.34a1}$$

$$U_\gamma = x(x-2b-\gamma) + b(b+\gamma) + r_1r_3 + r_1r_4 + r_3r_4 + 2\alpha^2 \quad (3.34b2)$$

$$U_\lambda = x(x-2b-\lambda) + b(b+\lambda) + r_1r_2 + r_1r_4 + r_2r_4 + 2\alpha^2 \quad (3.34c3)$$

$$U_\rho = x(x-2b-\rho) + b(b+\rho) + r_1r_2 + r_1r_3 + r_2r_3 + 2\alpha^2 \quad (3.34d4)$$

$$N_\delta = (b-x+\delta) + \frac{r_2r_3r_4}{\alpha^2} \quad (3.35a1)$$

$$N_\gamma = (b-x+\gamma) + \frac{r_1r_3r_4}{\alpha^2} \quad (3.35b2)$$

$$N_\lambda = (b-x+\lambda) + \frac{r_1r_2r_4}{\alpha^2} \quad (3.35c3)$$

$$N_\rho = (b-x+\rho) + \frac{r_1r_2r_3}{\alpha^2} \quad (3.35d4)$$

$$S_\delta = 2b-3x+\delta \quad (3.36a1)$$

$$S_\gamma = 2b-3x+\gamma \quad (3.36b2)$$

$$S_\lambda = 2b-3x+\lambda \quad (3.36c3)$$

$$S_\rho = 2b-3x+\rho. \quad (3.36d4)$$

In clearer terms, (3.31) can be re-written after backsubstitution of (3.32) - (3.36), as

$$A = -\frac{\alpha^3\psi_{+1}(0) + \alpha^2S_\delta\psi_0(0) + \alpha U_\delta\psi_{-1}(0) + (\alpha^2T_\delta + r_2r_3r_4)\psi_{-2}(0)}{(r_1-r_2)(r_1-r_3)(r_1-r_4)}, \quad (3.37a)$$

$$B = \frac{\alpha^3\psi_{+1}(0) + \alpha^2S_\gamma\psi_0(0) + \alpha U_\gamma\psi_{-1}(0) + (\alpha^2Y_\gamma + r_1r_3r_4)\psi_{-2}(0)}{(r_1-r_2)(r_2-r_3)(r_2-r_4)}, \quad (3.37b)$$

$$C = -\frac{(\alpha^3\psi_{+1}(0) + \alpha^2S_\lambda\psi_0(0) + \alpha U_\lambda\psi_{-1}(0) + (\alpha^2L_\lambda + r_1r_2r_4)\psi_{-2}(0))}{(r_1-r_3)(r_2-r_3)(r_3-r_4)}, \quad (3.37c)$$

$$D = \frac{\alpha^3 \psi_{+1}(0) + \alpha^2 S_\rho \psi_0(0) + \alpha U_\rho \psi_{-1}(0) + (\alpha^2 R_\rho + r_1 r_2 r_3) \psi_{-2}(0)}{(r_1 - r_4)(r_2 - r_4)(r_3 - r_4)}, \quad (3.37d)$$

such that

$$T_\delta = b - x + \delta \quad (3.38a)$$

$$Y_\gamma = b - x + \gamma \quad (3.38b)$$

$$L_\lambda = b - x + \lambda \quad (3.38c)$$

$$R_\rho = b - x + \rho. \quad (3.38d)$$

3.6 The Development of a Transition Matrix Solution

The progress on finding a transition matrix for the problem is facilitated by switching to a matrix symbolic formalism,

$$\Psi(\xi) \equiv \begin{pmatrix} \psi_{+1}(\xi) \\ \psi_0(\xi) \\ \psi_{-1}(\xi) \\ \psi_{-2}(\xi) \end{pmatrix} \quad \mathbf{V} = \begin{pmatrix} A \\ B \\ C \\ D \end{pmatrix}, \quad (3.39)$$

in which case (3.28) defines a matrix $\mathbf{H}(\xi)$

$$\Psi(\xi) \equiv \mathbf{H}(\xi) \cdot \mathbf{V} \quad (3.40)$$

while (3.31) defines the matrix $\mathbf{H}^{-1}(0)$

$$\mathbf{V} = \mathbf{H}^{-1}(0) \cdot \Psi(0). \quad (3.41)$$

Combination of (3.41) and (3.40) implies

$$\Psi(\xi) \equiv \mathbf{H}(\xi) \cdot \mathbf{H}^{-1}(0) \cdot \Psi(0) \equiv \mathbf{\Gamma}(\xi) \cdot \Psi(0). \quad (3.42)$$

This provides a matrix recipe for the transition matrix for the AO problem, namely

$$\mathbf{\Gamma}(\xi) = \mathbf{H}(\xi) \cdot \mathbf{H}^{-1}(0). \quad (3.43)$$

To compactly represent the transition matrix $\mathbf{\Gamma}(\xi)$ solution define row vectors for

$\mathbf{H}(\xi)$ shown in (3.28),

$$\mathbf{a}_{r1} = \left(-\frac{\kappa_1 t_1 e^{-j3x\xi}}{\alpha^3}, -\frac{\kappa_2 t_2 e^{-j3x\xi}}{\alpha^3}, -\frac{\kappa_3 t_3 e^{-j3x\xi}}{\alpha^3}, -\frac{\kappa_4 t_4 e^{-j3x\xi}}{\alpha^3} \right), \quad (3.44a)$$

$$\mathbf{b}_{r2} = \left(\frac{\eta_1 t_1 e^{-j(2x-b)\xi}}{\alpha^2}, \frac{\eta_2 t_2 e^{-j(2x-b)\xi}}{\alpha^2}, \frac{\eta_3 t_3 e^{-j(2x-b)\xi}}{\alpha^2}, \frac{\eta_4 t_4 e^{-j(2x-b)\xi}}{\alpha^2} \right), \quad (3.44b)$$

$$\mathbf{c}_{r3} = \left(-\frac{r_1 t_1 e^{-j(x-b)\xi}}{\alpha}, -\frac{r_2 t_2 e^{-j(x-b)\xi}}{\alpha}, -\frac{r_3 t_3 e^{-j(x-b)\xi}}{\alpha}, -\frac{r_4 t_4 e^{-j(x-b)\xi}}{\alpha} \right), \quad (3.44c)$$

$$\mathbf{d}_{r4} = (t_1, t_2, t_3, t_4). \quad (3.44d)$$

Now, as seen in (3.31), the column vectors for $\mathbf{H}^{-1}(0)$ are

$$\mathbf{e}_{c1} = \left(\frac{\alpha^3}{a}, \frac{\alpha^3}{b}, \frac{\alpha^3}{c}, \frac{\alpha^3}{d} \right)^T, \quad (3.45a)$$

$$\mathbf{f}_{c2} = \left(\frac{\alpha^2 S_\delta}{a}, \frac{\alpha^2 S_\gamma}{b}, \frac{\alpha^2 S_\lambda}{c}, \frac{\alpha^2 S_\rho}{d} \right)^T, \quad (3.45b)$$

$$\mathbf{g}_{c3} = \left(\frac{\alpha U_\delta}{a}, \frac{\alpha U_\gamma}{b}, \frac{\alpha U_\lambda}{c}, \frac{\alpha U_\rho}{d} \right)^T, \quad (3.45c)$$

$$\mathbf{h}_{c4} = \left(\frac{\alpha^2 N_\delta}{a}, \frac{\alpha^2 N_\gamma}{b}, \frac{\alpha^2 N_\lambda}{c}, \frac{\alpha^2 N_\rho}{d} \right)^T. \quad (3.45d)$$

It follows from (3.43) that in terms of vector sets (3.44) and (3.45), the transition matrix can be placed into the following form.

$$\Gamma(\xi) \equiv \begin{pmatrix} \mathbf{a}_{11} & \mathbf{a}_{12} & \mathbf{a}_{13} & \mathbf{a}_{14} \\ \mathbf{a}_{21} & \mathbf{a}_{22} & \mathbf{a}_{23} & \mathbf{a}_{24} \\ \mathbf{a}_{31} & \mathbf{a}_{32} & \mathbf{a}_{33} & \mathbf{a}_{34} \\ \mathbf{a}_{41} & \mathbf{a}_{42} & \mathbf{a}_{43} & \mathbf{a}_{44} \end{pmatrix} = \begin{pmatrix} \mathbf{a}_{r1} \cdot \mathbf{e}_{c1} & \mathbf{a}_{r1} \cdot \mathbf{f}_{c2} & \mathbf{a}_{r1} \cdot \mathbf{g}_{c3} & \mathbf{a}_{r1} \cdot \mathbf{h}_{c4} \\ \mathbf{b}_{r2} \cdot \mathbf{e}_{c1} & \mathbf{b}_{r2} \cdot \mathbf{f}_{c2} & \mathbf{b}_{r2} \cdot \mathbf{g}_{c3} & \mathbf{b}_{r2} \cdot \mathbf{h}_{c4} \\ \mathbf{c}_{r3} \cdot \mathbf{e}_{c1} & \mathbf{c}_{r3} \cdot \mathbf{f}_{c2} & \mathbf{c}_{r3} \cdot \mathbf{g}_{c3} & \mathbf{c}_{r3} \cdot \mathbf{h}_{c4} \\ \mathbf{d}_{r4} \cdot \mathbf{e}_{c1} & \mathbf{d}_{r4} \cdot \mathbf{f}_{c2} & \mathbf{d}_{r4} \cdot \mathbf{g}_{c3} & \mathbf{d}_{r4} \cdot \mathbf{h}_{c4} \end{pmatrix} \quad (3.46)$$

All the elements in (3.46) can be illustrated after the implementation of the method for translating dot product rules on (3.44) and (3.45) as follows:

$$\mathbf{a}_{11} \equiv \mathbf{a}_{r1} \cdot \mathbf{e}_{c1} = -e^{-j3x\xi} \left(\frac{\kappa_1 t_1}{a} + \frac{\kappa_2 t_2}{b} + \frac{\kappa_3 t_3}{c} + \frac{\kappa_4 t_4}{d} \right) \quad (3.47a1)$$

$$\mathbf{a}_{12} \equiv \mathbf{a}_{r1} \cdot \mathbf{f}_{c2} = -\frac{e^{-j3x\xi}}{\alpha} \left(\frac{\kappa_1 t_1 S_\delta}{a} + \frac{\kappa_2 t_2 S_\gamma}{b} + \frac{\kappa_3 t_3 S_\lambda}{c} + \frac{\kappa_4 t_4 S_\rho}{d} \right) \quad (3.47a2)$$

$$\mathbf{a}_{13} \equiv \mathbf{a}_{r1} \cdot \mathbf{g}_{c3} = -\frac{e^{-j3x\xi}}{\alpha^2} \left(\frac{\kappa_1 t_1 U_\delta}{a} + \frac{\kappa_2 t_2 U_\gamma}{b} + \frac{\kappa_3 t_3 U_\lambda}{c} + \frac{\kappa_4 t_4 U_\rho}{d} \right) \quad (3.47a3)$$

$$\mathbf{a}_{14} \equiv \mathbf{a}_{r1} \cdot \mathbf{h}_{c4} = -\frac{e^{-j3x\xi}}{\alpha} \left(\frac{\kappa_1 t_1 N_\delta}{a} + \frac{\kappa_2 t_2 N_\gamma}{b} + \frac{\kappa_3 t_3 N_\lambda}{c} + \frac{\kappa_4 t_4 N_\rho}{d} \right) \quad (3.47a4)$$

$$\mathbf{a}_{21} \equiv \mathbf{b}_{r2} \cdot \mathbf{e}_{c1} = \alpha e^{-j(2x-b)\xi} \left(\frac{\eta_1 t_1}{a} + \frac{\eta_2 t_2}{b} + \frac{\eta_3 t_3}{c} + \frac{\eta_4 t_4}{d} \right) \quad (3.47b1)$$

$$\mathbf{a}_{22} \equiv \mathbf{b}_{r2} \cdot \mathbf{f}_{c2} = e^{-j(2x-b)\xi} \left(\frac{\eta_1 t_1 S_\delta}{a} + \frac{\eta_2 t_2 S_\gamma}{b} + \frac{\eta_3 t_3 S_\lambda}{c} + \frac{\eta_4 t_4 S_\rho}{d} \right) \quad (3.47b2)$$

$$\mathbf{a}_{23} \equiv \mathbf{b}_{r2} \cdot \mathbf{g}_{c3} = \frac{e^{-j(2x-b)\xi}}{\alpha} \left(\frac{\eta_1 t_1 U_\delta}{a} + \frac{\eta_2 t_2 U_\gamma}{b} + \frac{\eta_3 t_3 U_\lambda}{c} + \frac{\eta_4 t_4 U_\rho}{d} \right) \quad (3.47b3)$$

$$\mathbf{a}_{24} \equiv \mathbf{b}_{r2} \cdot \mathbf{h}_{c4} = e^{-j(2x-b)\xi} \left(\frac{\eta_1 t_1 N_\delta}{a} + \frac{\eta_2 t_2 N_\gamma}{b} + \frac{\eta_3 t_3 N_\lambda}{c} + \frac{\eta_4 t_4 N_\rho}{d} \right) \quad (3.47b4)$$

$$\mathbf{a}_{31} \equiv \mathbf{c}_{r3} \cdot \mathbf{e}_{c1} = -\alpha^2 e^{-j(x-b)\xi} \left(\frac{r_1 t_1}{a} + \frac{r_2 t_2}{b} + \frac{r_3 t_3}{c} + \frac{r_4 t_4}{d} \right) \quad (3.47c1)$$

$$\mathbf{a}_{32} \equiv \mathbf{c}_{r3} \cdot \mathbf{f}_{c2} = -\alpha e^{-j(x-b)\xi} \left(\frac{r_1 t_1 S_\delta}{a} + \frac{r_2 t_2 S_\gamma}{b} + \frac{r_3 t_3 S_\lambda}{c} + \frac{r_4 t_4 S_\rho}{d} \right) \quad (3.47c2)$$

$$\mathbf{a}_{33} \equiv \mathbf{c}_{r3} \cdot \mathbf{g}_{c3} = -e^{-j(x-b)\xi} \left(\frac{r_1 t_1 U_\delta}{a} + \frac{r_2 t_2 U_\gamma}{b} + \frac{r_3 t_3 U_\lambda}{c} + \frac{r_4 t_4 U_\rho}{d} \right) \quad (3.47c3)$$

$$\mathbf{a}_{34} \equiv \mathbf{c}_{r3} \cdot \mathbf{h}_{c4} = -\alpha e^{-j(x-b)\xi} \left(\frac{r_1 t_1 N_\delta}{a} + \frac{r_2 t_2 N_\gamma}{b} + \frac{r_3 t_3 N_\lambda}{c} + \frac{r_4 t_4 N_\rho}{d} \right) \quad (3.47c4)$$

$$\mathbf{a}_{41} \equiv \mathbf{d}_{r4} \cdot \mathbf{e}_{c1} = \alpha^3 \left(\frac{t_1}{a} + \frac{t_2}{b} + \frac{t_3}{c} + \frac{t_4}{d} \right) \quad (3.47d1)$$

$$\mathbf{a}_{42} \equiv \mathbf{d}_{r4} \cdot \mathbf{f}_{c2} = \alpha^2 \left(\frac{t_1 S_\delta}{a} + \frac{t_2 S_\gamma}{b} + \frac{t_3 S_\lambda}{c} + \frac{t_4 S_\rho}{d} \right) \quad (3.47d2)$$

$$\mathbf{a}_{43} \equiv \mathbf{d}_{r4} \cdot \mathbf{g}_{c3} = \alpha \left(\frac{t_1 U_\delta}{a} + \frac{t_2 U_\gamma}{b} + \frac{t_3 U_\lambda}{c} + \frac{t_4 U_\rho}{d} \right) \quad (3.47d3)$$

$$\mathbf{a}_{44} \equiv \mathbf{d}_{r4} \cdot \mathbf{h}_{c2} = \alpha^2 \left(\frac{t_1 N_\delta}{a} + \frac{t_2 N_\gamma}{b} + \frac{t_3 N_\lambda}{c} + \frac{t_4 N_\rho}{d} \right). \quad (3.47d4)$$

It is important to note that (3.46) has the following property:

$$\mathbf{\Gamma}(\mathbf{\Gamma}^T)^* = \mathbf{\Gamma}\mathbf{\Gamma}^\dagger = \mathbf{\Gamma}^\dagger\mathbf{\Gamma} = \mathbf{I} \quad (3.48)$$

where \mathbf{I} is the identity matrix. The adjoint operator, also known as the Hermitian conjugate, of a tensor quantity \mathbf{M} is designated \mathbf{M}^\dagger and is defined [33] by two specific order-independent successive operations, i.e., complex conjugation- and transpose. As seen from (3.48), the adjoint of the transition matrix $\mathbf{\Gamma}$ is the matrix inverse or more succinctly $\mathbf{\Gamma}$ is the unitary [39]. It shall be demonstrated in Chapter 5 that the unitary property being satisfied, and applicable to the AO transition matrix, for any number of orders considered, is sufficient to guarantee the physical property of energy conservation.

3.7 The General Solution and Selected Sample Cases

The general solution follows after the backsubstitution of (3.46) into (3.42) which consistently leads to

$$\psi_{+1}(\xi) = \mathbf{a}_{11}\psi_{+1}(0) + \mathbf{a}_{12}\psi_0(0) + \mathbf{a}_{13}\psi_{-1}(0) + \mathbf{a}_{14}\psi_{-2}(0) \quad (3.49a)$$

$$\psi_0(\xi) = \mathbf{a}_{21}\psi_{+1}(0) + \mathbf{a}_{22}\psi_0(0) + \mathbf{a}_{23}\psi_{-1}(0) + \mathbf{a}_{24}\psi_{-2}(0) \quad (3.49b)$$

$$\psi_{-1}(\xi) = \mathbf{a}_{31}\psi_{+1}(0) + \mathbf{a}_{32}\psi_0(0) + \mathbf{a}_{33}\psi_{-1}(0) + \mathbf{a}_{34}\psi_{-2}(0) \quad (3.49c)$$

$$\psi_{-2}(\xi) = \mathbf{a}_{41}\psi_{+1}(0) + \mathbf{a}_{42}\psi_0(0) + \mathbf{a}_{43}\psi_{-1}(0) + \mathbf{a}_{44}\psi_{-2}(0). \quad (3.49d)$$

Besides, the following selected sample cases with identified initial condition shall be considered from (3.49). It is reiterated that while the incoming light is patterned according to $(\psi_{+1}(0), \psi_0(0), \psi_{-1}(0), \psi_{-2}(0))$, the diffraction order, in all cases considered here, is consistent with $(\psi_{+1}(\xi), \psi_0(\xi), \psi_{-1}(\xi), \psi_{-2}(\xi))$. So when the light comes in 100% in +1-order. i.e., $\mathbf{\Psi}^T(0) \equiv (1, 0, 0, 0)$, then it follows from (3.49) that the optical is diffracted according to

$$\mathbf{\Psi}^T(\xi) \equiv (\mathbf{a}_{11}, \mathbf{a}_{21}, \mathbf{a}_{31}, \mathbf{a}_{41}) = (\mathbf{a}_{r1} \cdot \mathbf{e}_{c1}, \mathbf{b}_{r2} \cdot \mathbf{e}_{c1}, \mathbf{c}_{r3} \cdot \mathbf{e}_{c1}, \mathbf{d}_{r4} \cdot \mathbf{e}_{c1}). \quad (3.50a)$$

The expressions for plotting all the four diffracted light in (3.50a) are (3.47a1), (3.47b1), (3.47c1) and (3.47d1).

Likewise, for light entering in 100% in the 0-order, i.e., $\Psi^T(0) \equiv (0, 1, 0, 0)$, the diffractions results in

$$\Psi^T(\xi) \equiv (\mathbf{a}_{12}, \mathbf{a}_{22}, \mathbf{a}_{32}, \mathbf{a}_{42}) = (\mathbf{a}_{r1} \cdot \mathbf{f}_{c2}, \mathbf{b}_{r2} \cdot \mathbf{f}_{c2}, \mathbf{c}_{r3} \cdot \mathbf{f}_{c2}, \mathbf{d}_{r4} \cdot \mathbf{f}_{c2}). \quad (3.50b)$$

More explicitly, plots for all the split light orders in (3.50b) were derived from (3.47a2), (3.47b2), (3.47c2) and (3.47d2), similarly, for 100% light incidence on -1-order, i.e., $\Psi^T(0) \equiv (0, 0, 1, 0)$, the scattering into four orders yields:

$$\Psi^T(\xi) \equiv (\mathbf{a}_{13}, \mathbf{a}_{23}, \mathbf{a}_{33}, \mathbf{a}_{43}) = (\mathbf{a}_{r1} \cdot \mathbf{g}_{c3}, \mathbf{b}_{r2} \cdot \mathbf{g}_{c3}, \mathbf{c}_{r3} \cdot \mathbf{g}_{c3}, \mathbf{d}_{r4} \cdot \mathbf{g}_{c3}), \quad (3.50c)$$

where, for (3.50c), the diffracted orders were plots generated from (3.47a3), (3.47b3), (3.47c3) and (3.47d3). Also considered is the entering of light in the -2-order, i.e., $\Psi^T(0) \equiv (0, 0, 0, 1)$. The scattered light into four order implies that

$$\Psi^T(\xi) \equiv (\mathbf{a}_{14}, \mathbf{a}_{24}, \mathbf{a}_{34}, \mathbf{a}_{44}) = (\mathbf{a}_{r1} \cdot \mathbf{h}_{c4}, \mathbf{b}_{r2} \cdot \mathbf{h}_{c4}, \mathbf{c}_{r3} \cdot \mathbf{h}_{c4}, \mathbf{d}_{r4} \cdot \mathbf{h}_{c4}). \quad (3.50d)$$

Precisely, the light diffraction plots in (3.50d) were obtained from (3.47a4), (3.47b4), (3.47c4) and (3.47d4). In clear context, each of the four above conditions represent 100% of the energy in one of the 4 rays incident on the sound cell from the left as shown in Fig. 1.

3.8 Overview of Chapter Three

In this chapter, a derived 4th order generalized homogenous linear DE from a mathematical system of first order linear coupled DE was accomplished. Thereafter, the roots of the quartic characteristic equation obtained from the fourth order linear DE was predicted using the Ferrari's method. Also presented is the homogeneous solution of all orders. Lastly, the development of the transition matrix solution and selected sample cases was considered.

Chapter Four

Matlab Simulations and Discussion of Results

4.1 Numerical and Analytical Simulation via Matlab yielding Confirmation of Four-Order AO Analytic Model

In this chapter, it will be shown how three methods- space variation, frequency variation, and angle variation are being used to confirm the level of agreement between numerical formalism and analytic predictions through matlab simulation. Basically, the numerical predictions were generated directly from (3.5) and (3.11), whereas, the corresponding four order analytical predictions are derived from (3.42) and (3.46). In Figs. 15 - 32, the solid line data identifies the numerical predictions from (3.5) and (3.11); the data using the analytical solution, (3.42) and (3.46), produced the diffraction order specific symbols. In all the examples considered, the combination of sound strength factor ($\alpha = \frac{\pi}{2}$) and normalized Klein-Cook parameter ($Q_c = 2\pi$) are constant. In all cases, normalized to unity, the intensity, $I_n = |\psi_n(k)|^2$, the total intensity, $I_T = \sum_{n=-2}^2 |\psi_n(k)|^2$, for the various test cases are also checked.

4.2 Flowchart Description for Implementation of Numerical and Analytical Methods

Starting from (3.5), each of the three methods used to present the numerical formalism implements at least one of the assumptions in (2.25c) or (2.25d). Typically, (3.5) forms the basis of all possible variations in terms of normalized space, normalized angle, and normalized frequency. The analysis is then discussed in subsection.

4.2.1 Numerical and Analytical Analysis of Space (ξ) Variation

The numerical space variation formalism implements both conditions specified in (2.25c) and (2.25d). In essence, subsequent backsubstitution of (2.25c)

and (2.25d) in (3.4), and later in (3.6b) makes the x term in (3.5) vanish, thus, (3.5) reduces to (2.26). This again ascertain the level of agreement between the current and previous work [20]. In clear context, Fig. 9 represents the flowchart of space variation numerical analysis. Typical values for the two parameters: sound strength factor ' α '

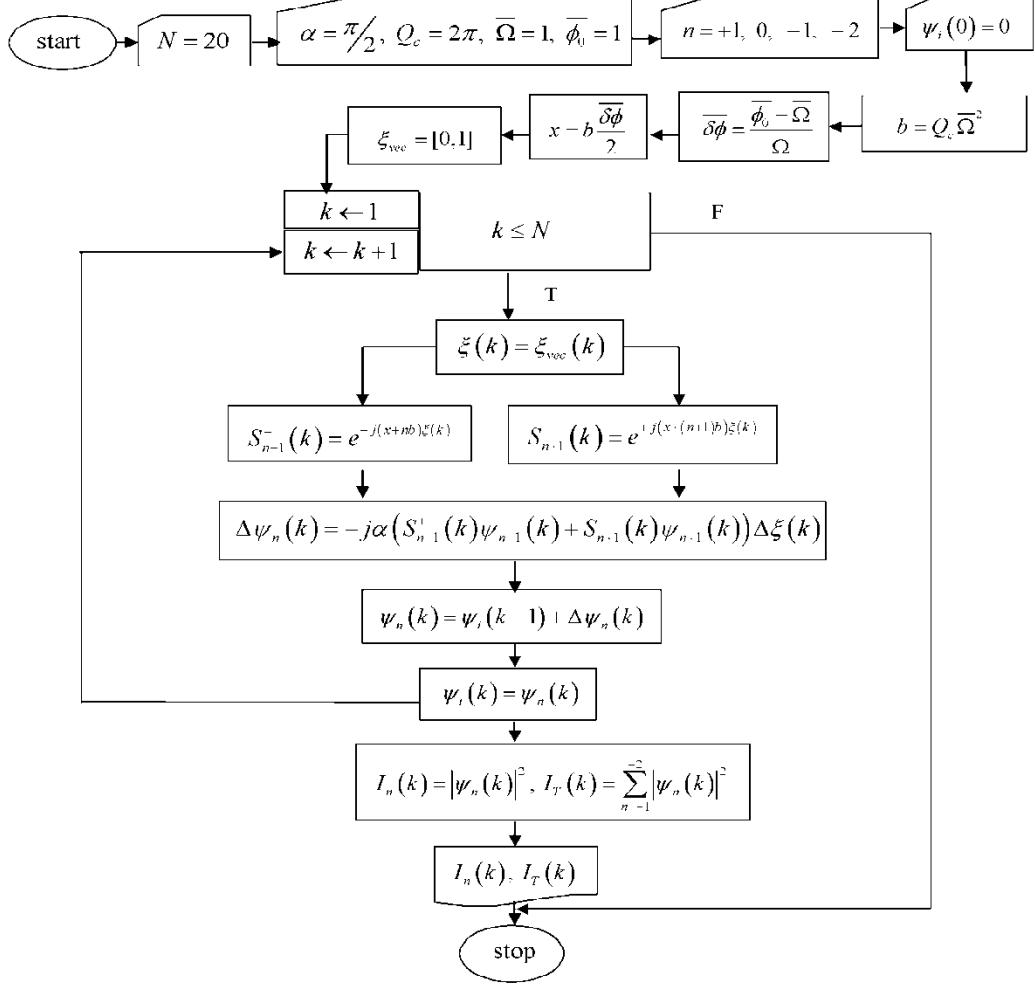


Figure 9. Flowchart of space variation numerical analysis

and Klein-Cook parameter ' Q_c ' have been specified. In all cases, the transducer operates at the center frequency, i.e. $\bar{\Omega} = 1$, and the light is incidence at the exact Bragg angle, $\bar{\phi}_0 = 1$. Obviously, both $\bar{\delta\phi}$ and x terms vanish, while $b = Q_c$, following the above conditions. The normalized distance is varied between 0 and 1 for a total number of points, i.e., $N = 20$. At each point (k), with both acoustic (S_i) and electric field (ψ_i) initialized, the sound coefficients, (S_{n+1}^- and S_{n-1}^+), coupling formalism, ($\Delta\psi_n$), the intensity of diffracted light, I_n , and the total intensity, I_T , for all the 4 orders (n) are then computed.

The flowchart of space variation analytical model is represented in Fig. 10. All the input parameters are consistent with the numerical model. However, the homogeneous solutions for all orders (n) are computed at every point (k) for a number of points (N). The diffracted light order, I_n , and total intensity, I_T , are estimated.

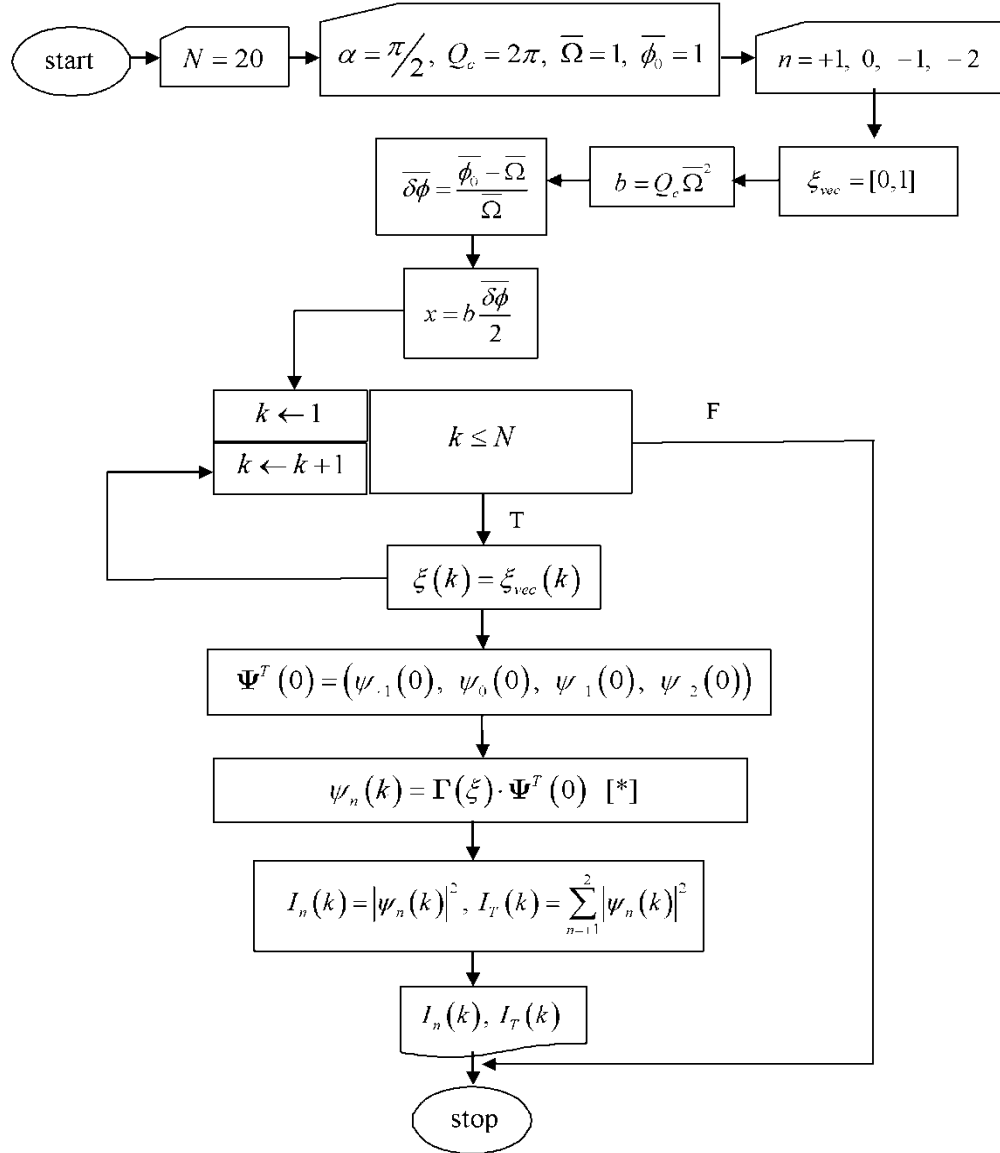


Figure 10. Flowchart of space variation analytical analysis

4.2.2 Numerical and Analytical Analysis of Frequency ($\bar{\Omega}$) Variation

The normalized frequency variation is conceived with the field referenced back at the cell exit, $z = L$. In the numerical formalism, frequency variation is achieved by varying both normalized frequency and normalized distance while

normalized angle is fixed, i.e., (2.25d). In other words, the sound coefficients in (3.5) are recast from (2.25d), (3.4) and (3.6) as

$$S_{n-1}^+(\bar{\Omega}, \xi) = |S| e^{-j \frac{Q_c \bar{\Omega}^2}{2} \left(\frac{1}{\bar{\Omega}} + (2n-1) \right) \xi}, \quad (4.1a)$$

$$S_{n+1}^-(\bar{\Omega}, \xi) = |S| e^{+j \frac{Q_c \bar{\Omega}^2}{2} \left(\frac{1}{\bar{\Omega}} + (2n+1) \right) \xi}. \quad (4.1b)$$

The flowchart in Fig. 11 presents the normalized frequency variation in the numerical model. With sound strength factor ' α ' and Klein-Cook parameter ' Q_c ' also

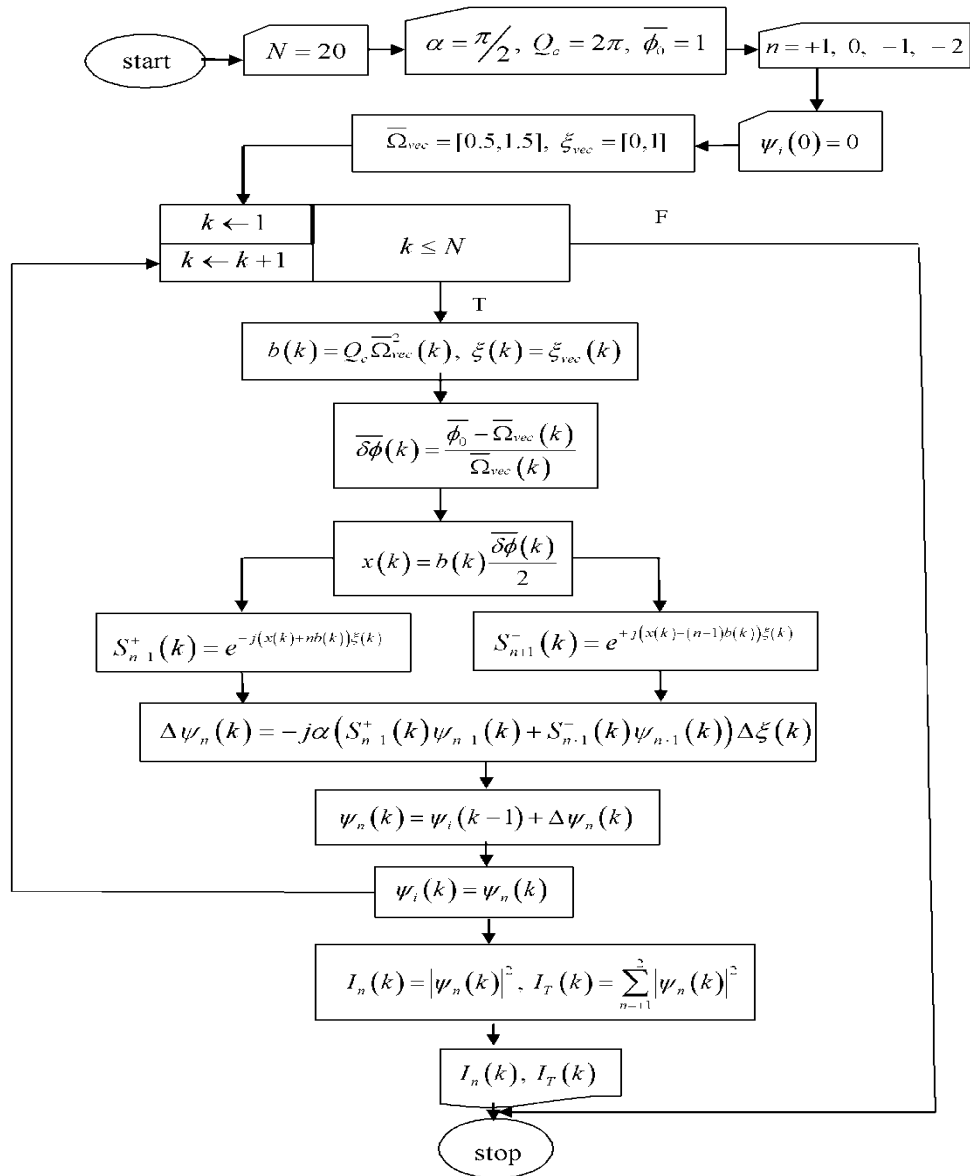


Figure 11. Flowchart of frequency variation numerical model

specified. The light is always incidence at the exact Bragg angle, $\bar{\phi}_0 = 1$. Obviously, for a number of points (i.e., $N = 20$), the acoustic frequency changes between 0.5 - 1.5, and the normalized distance varied between 0 and 1. As the acoustic frequency varies, b , $\bar{\delta\phi}$ and x terms vary simultaneously. At each points (k), with both acoustic (S_i) and electric field (ψ_i) initialized, the sound coefficients, (S_{n+1}^- and S_{n-1}^+), coupling formalism, ($\Delta\psi_n$), the intensity of diffracted light, I_n , and the total intensity, I_T , for all the 4 orders (n) are then computed at those points.

Fig. 12 shows the algorithm employed by normalized frequency variation analytical model. The analytical formalism input is consistent with the numerical

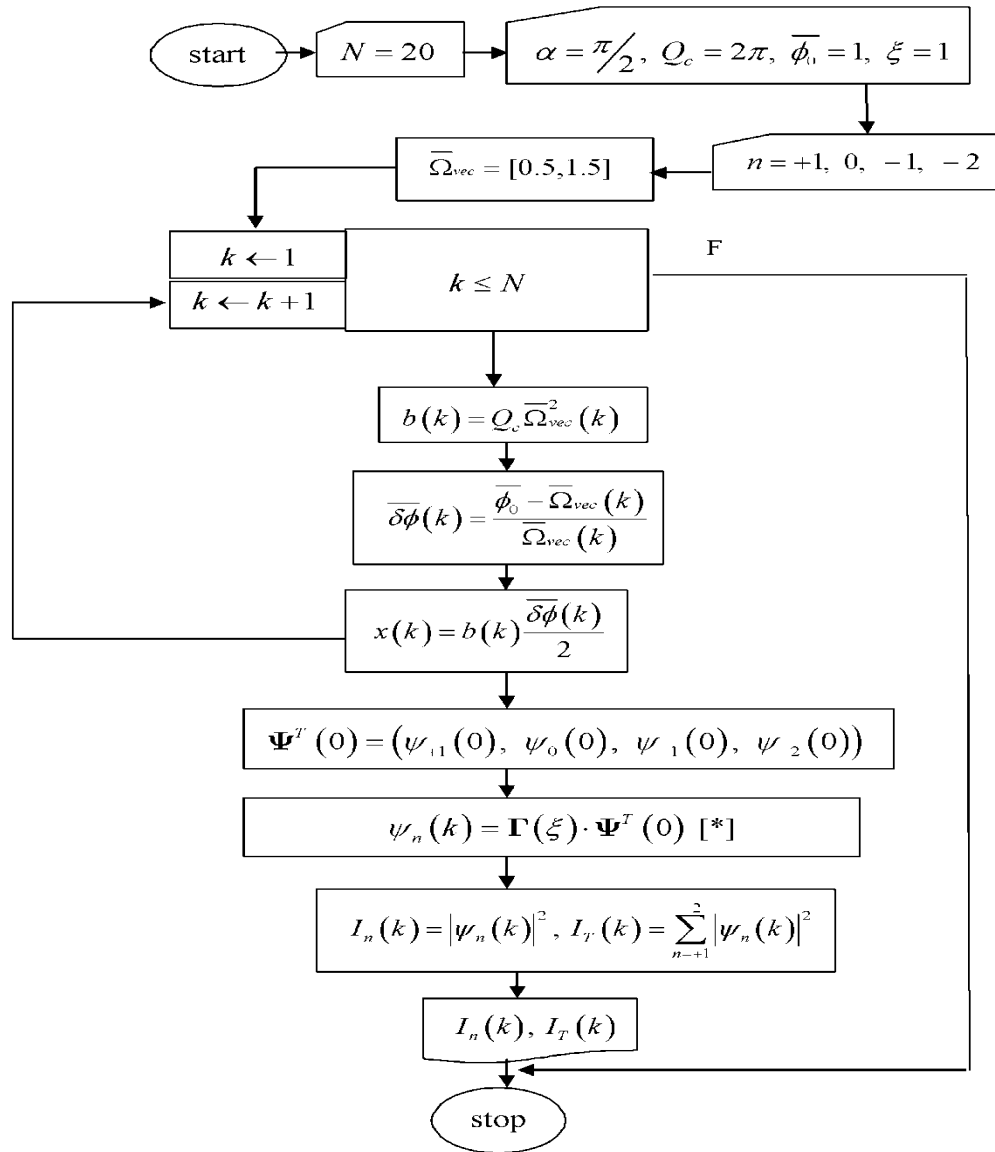


Figure 12. Flowchart of frequency variation analytical model

except for normalized distance which is fixed, i.e. $\xi = 1$. This explains that the measure of diffracted optical is taken with reference to the exit of the cell, for instance, $z = L$. For any degree of light incidence in any order, i.e., $\psi_n(0)$, the homogeneous solution, $\psi_n(k)$, at each point is calculated. Following this, the amount of diffracted light, and its overall estimate is computed. Practical applications of normalized frequency variation is found in acousto-optic deflectors.

4.2.3 Numerical and Analytical Analysis of Angle ($\bar{\phi}_0$) Variation

In the normalized angle variation, the field predicted is referenced back at the cell exit. Here, for every normalized angle of incident light, the transducer is made to operate at the center frequency. In clear terms, normalized frequency is fixed after implementing (2.25c), whereas, both the normalized angle and the normalized distance are varied. As observed from (3.5), the sound coefficients are recast from (3.5) after combining (2.25c), (3.4) and (3.6) as

$$S_{n-1}^+(\bar{\phi}_0, \xi) = |S| e^{-j \frac{Q_c}{2} (\bar{\phi}_0 + (2n-1)) \xi} \quad (4.2a)$$

$$S_{n+1}^-(\bar{\phi}_0, \xi) = |S| e^{+j \frac{Q_c}{2} (\bar{\phi}_0 + (2n+1)) \xi}. \quad (4.2b)$$

Fig. 13 shows the flowchart numerical angle variation. With sound strength factor ' α ' and Klein-Cook parameter ' Q_c ' specified, here, the transducer operates at the center frequency ($\bar{\Omega} = 1$) as the light travels through the transducer's length, for instance, normalized distance varied between 0 and 1. Similarly, at a number of points ($N = 20$), with incidence light angle referenced to a normal, the light is incidence at a range of 0.5 - 1.5. Variation in the incidence light angle would cause changes in b , $\bar{\delta\phi}$ and x terms simultaneously. At each point (k), with both acoustic (S_i) and electric field (ψ_i) initialized, the sound coefficients, (S_{n+1}^- and S_{n-1}^+), coupling formalism, ($\Delta\psi_n$), the intensity of diffracted light, I_n , and the total intensity, I_T , for all the 4 orders (n) are then computed at those points.

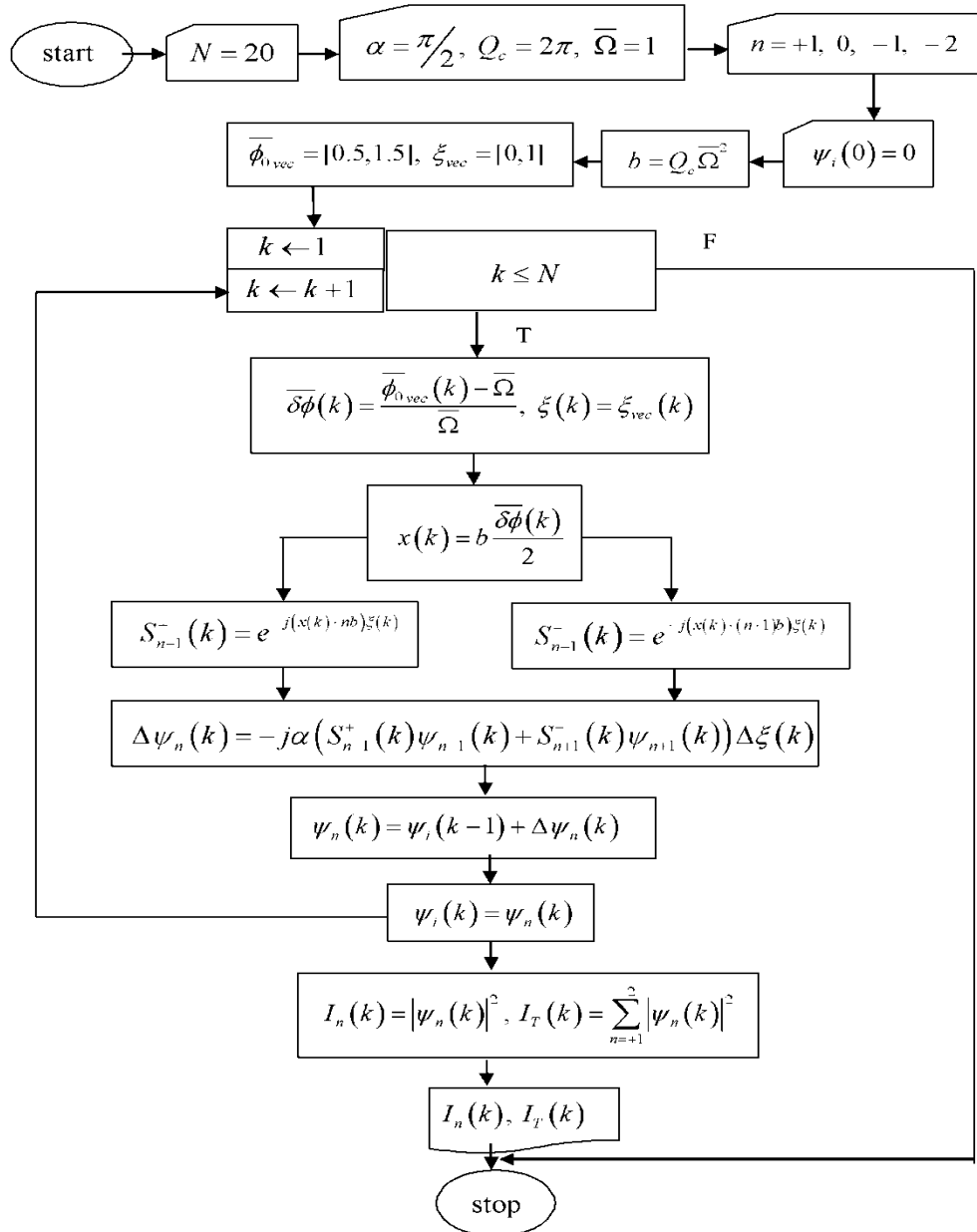


Figure 13. Flowchart of angle variation numerical model

Fig. 14 presents the methodology employed by a normalized angle variation analytical model. Again, there is consistency in the input parameters between the numerical and analytical except for normalized distance which is fixed, i.e., $\xi = 1$, in the analytical. This demonstrates that the measurement of diffractions is taken with reference to the exit of the cell, for instance, $z = L$. For any amount of light incidence in any order, i.e., $\psi_n(0)$, the homogeneous solution, $\psi_n(k)$, at each point is calculated. Consequently, the amount of diffracted light, and its overall estimate is

computed. Practical applications of normalized angle variation is found in acousto-optic modulator.

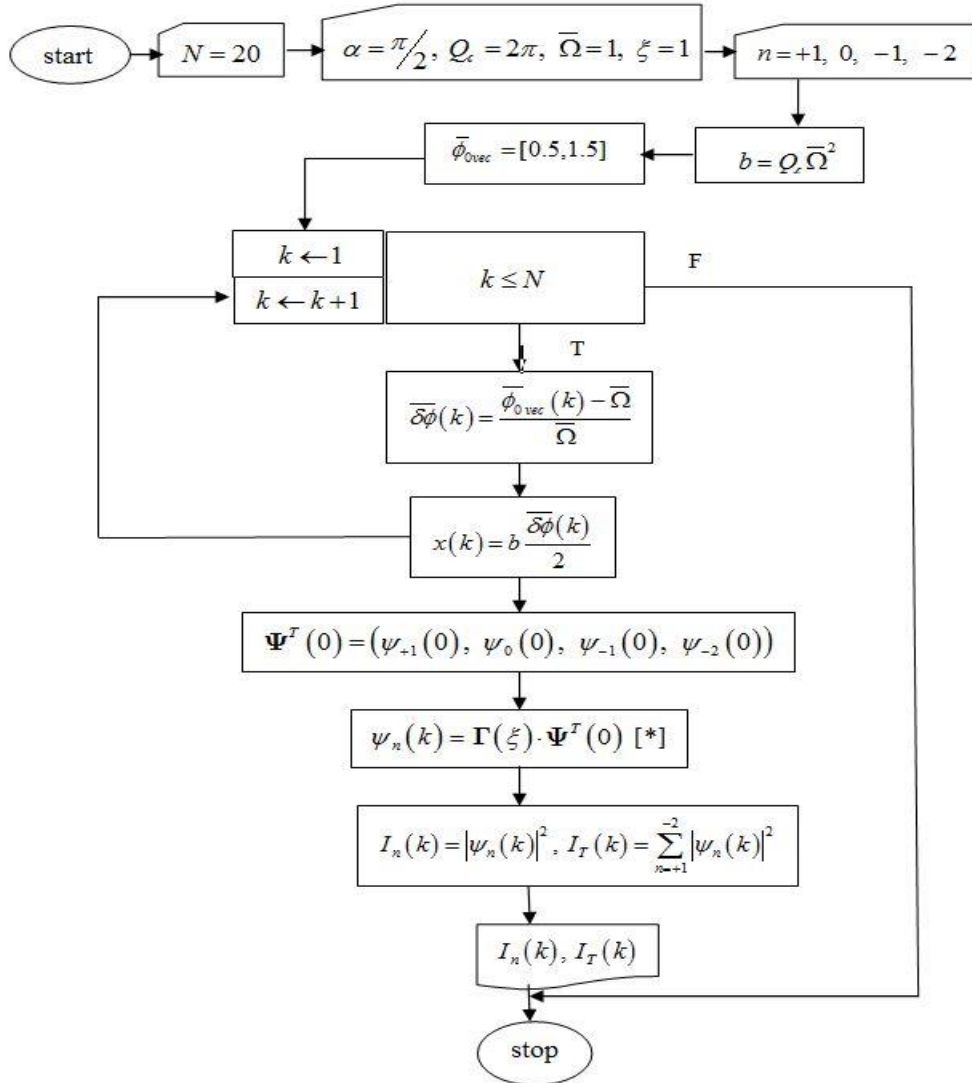


Figure 14. Flowchart of angle variation analytical model

4.3 Test Cases Demonstrating Variation in Normalized Space, Normalized Frequency, and Normalized Angle.

4.3.1 Test case(s) for normalized space variation

Now, Figs. 15-18 is the reproduction of figs. 5-8 in chapter 2, from both developed generalized analytical predictions, [see (3.42) and (3.46)], and the numerical model, [see (3.5) and (3.11)], in Chapter 3. Theoretical explanations of Figs. 15-18 can be found in chapter 2. Fig. 15 shows the numerical and analytical ξ - dependent predicted results when 100% of the incident light is in the 0th order [see (3.49b)].

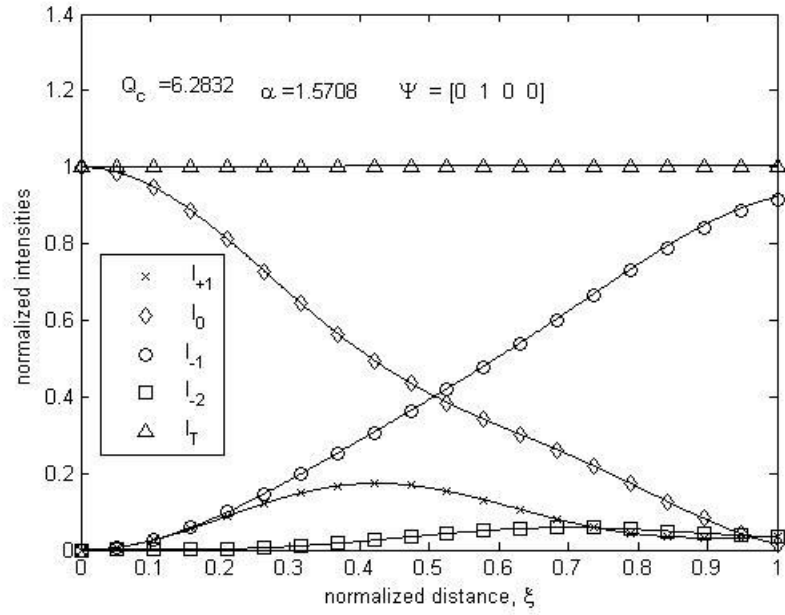


Figure 15. Comparison for four-order numerical and analytical solutions; all power is initially in the 0-order

Fig. 16 shows numerical and analytical predicted results when 100% of the incident light is in the -1 order [see (3.49c)]. As expected, with orders swapped [see (2.46)],

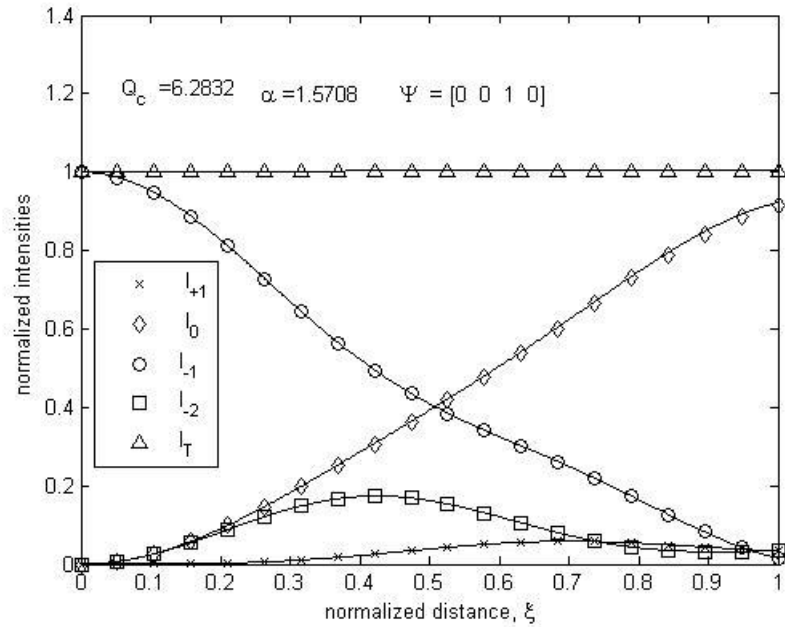


Figure 16. Comparison for four-order numerical and analytical solutions; all power is initially in the -1-order

Fig. 16, is identically shapewise as Fig. 15. Fig. 17 shows the numerical and analytical predicted results when 100% of the incident light is in the +1 order [see (3.49a)].

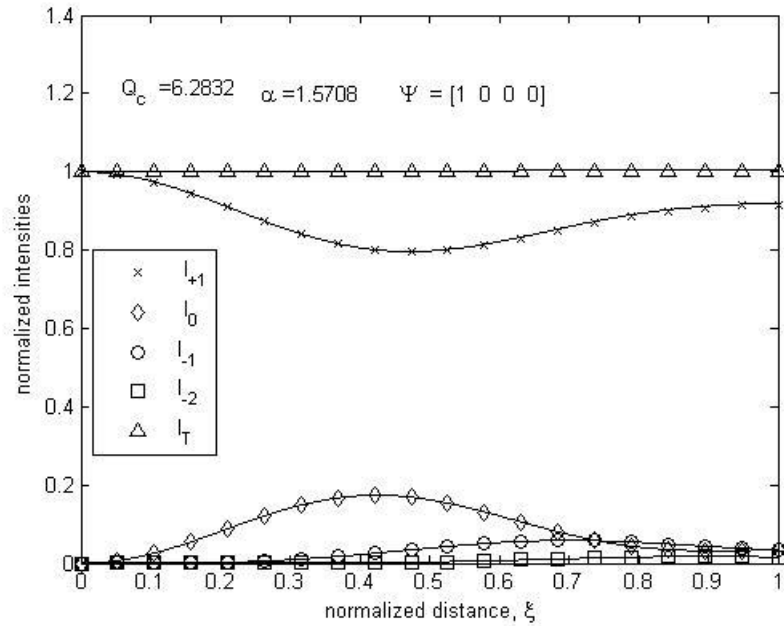


Figure 17. Comparison for four-order numerical and analytical solutions; all power is initially in the +1-order

The case of 100% of the light in the -2 order [see (3.49d)], was also tested and

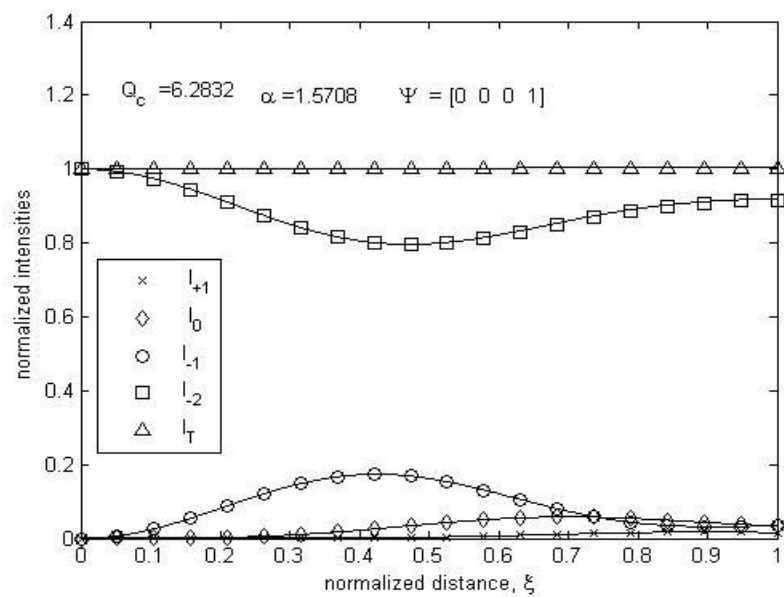


Figure 18. Comparison for four-order numerical and analytical solutions; all power is initially in the -2-order

compared as shown in Fig. 18. Curves were again shapewise identical to those in Fig. 17 with a repeated pattern [refer to (2.46)]. In addition, a demonstration of the robustness of the solution and its ability to accommodate a general combination of initial conditions was also performed. Specific initial conditions for this test case put equal amount of power in the 0th and -1 order. As can be seen in Fig. 19., the four-order analytical (symbols) and the four-order numerical (solid line) predictions are in perfect agreement.

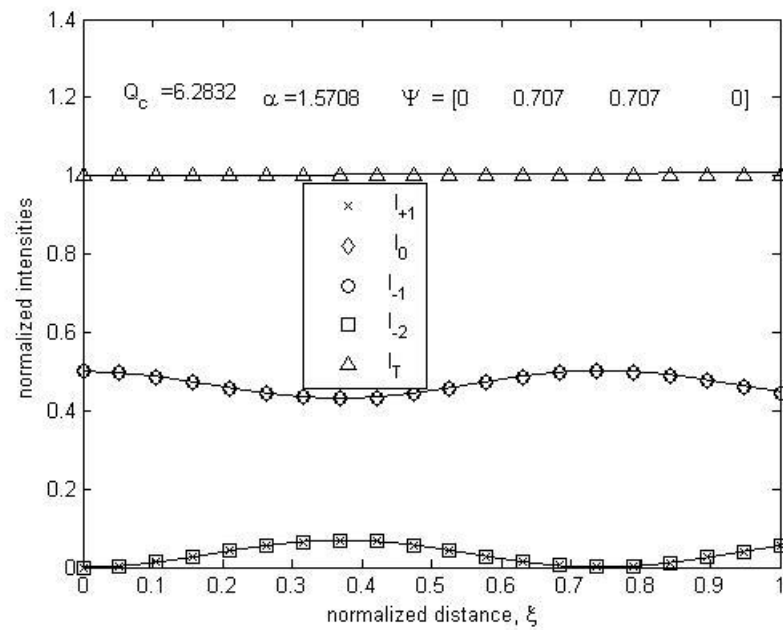


Figure 19. Comparison for four-order numerical and analytical solutions; power is initially 50% in both the 0th order and -1 order

Due to the physical symmetry for this test case created by the symmetry in the initial conditions it is expected that both the 0th order and the -1 order will overlay, and this can be confirmed from Fig. 19. This is also true, from the same symmetry argument, for the +1 order and -2 order. Note that, consistent with physical considerations, the exchange of energy is symmetric and less than 10% of the total energy is transferred from the Bragg regime combination of the +1 order and -2 order. The assumption made in Fig. 19 is that the two incident beams, 0th order and -1 order, are coherently related to the zero phase offset. If the two incident beams are phase incoherent then the appropriate method of solving would be to apply either analytical or numerical formalism for each incident light beam separately to predict the corresponding intensities at the output. Specifically, the intensities shown in Fig. 15 and 16 would

have to be scaled accordingly, and based on the principle of superposition of intensities for incoherent light, the results are added.

4.3.2 Test case(s) for normalized frequency variation

Fig. 20 shows the numerical and analytical $\bar{\Omega}$ -dependent predicted results when 100% of the incident light is in the 0th order [see (3.49b)].

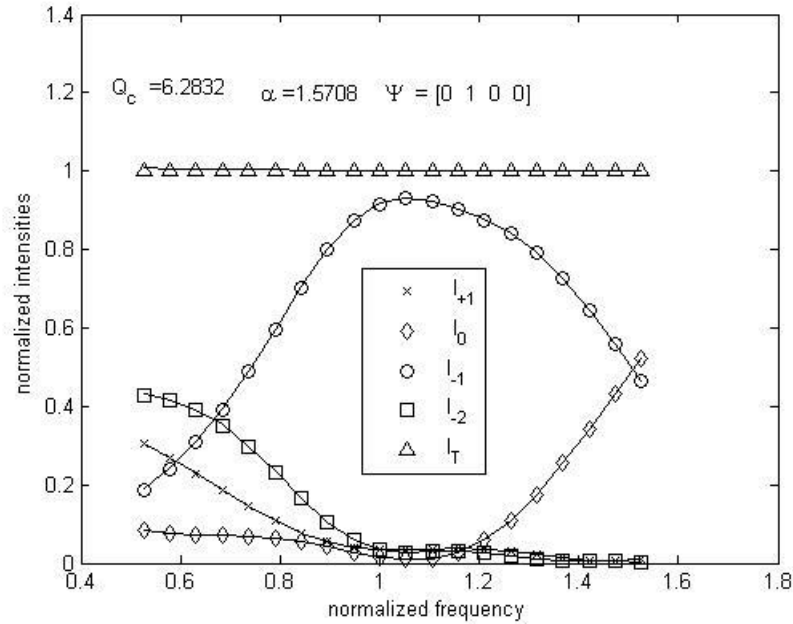


Figure 20. Comparison for four-order numerical and analytical solutions in terms of acoustic frequency, all power is initially in the 0-order

Agreement between numerical and analytical solutions is excellent with a confirming check shown for the total intensities according to (2.45). When all power is incidence in the 0 order, from the left toward the unity of the graph reveals a steady power rise in the -1 order, with its maximum at a shifted normalized frequency from unity, (i.e., $\bar{\Omega} \approx 1.05$). This explains that there are two competing effects impacting the normalized frequency response curve in the neighborhood of a normalized frequency of unity. Diffraction efficiency for the first order diffraction, i.e., $n = -1$, will decrease as the frequency increases from unity. This increase is creating a higher “Bragg angle” and therefore creates a mismatch between the incident light angle which fixed at unity (i.e., $\bar{\phi}_0 = 1$), and the increased frequency value (i.e., $\bar{\Omega} > 1$).

However, it is known that deeper conditions are driven into the “Bragg regime” when connected to higher Q_c values [see (2.11)], thus, the higher the

diffraction efficiency due to the angular spectrum being narrowed. This is consistent with less light spilling over into other orders due to the spread in angular spectrum of sound, thus, justifying why powers are negligible in the -2 and +1-order, as seen in Fig 20. The angular width of the main lobe in the angular spectrum of sound goes proportional to Λ/L [see Fig. 3]. When frequency of sound increases, its wavelength decreases so the shift to a higher frequency narrowed the spectrum of sound and therefore moved conditions deeper into or towards the “Bragg regime” of operation, hence increasing diffraction efficiency.

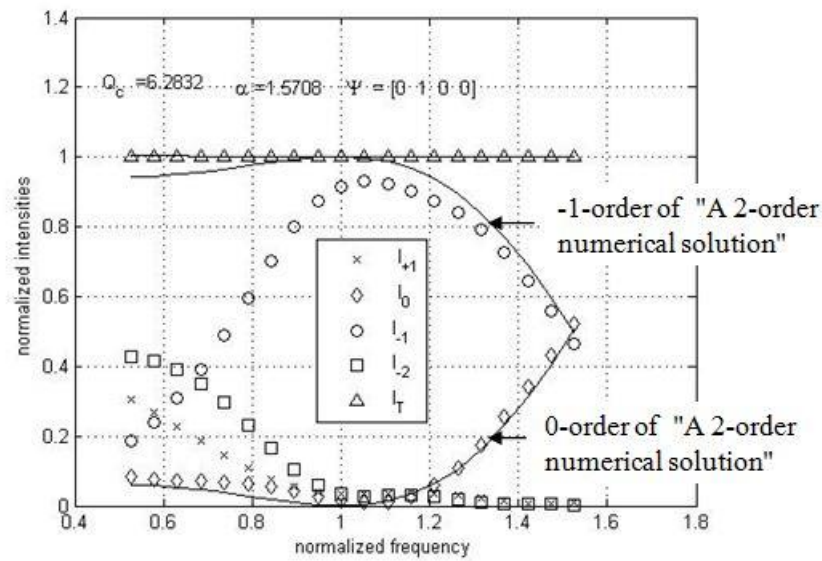


Figure 21. A two-order numerical solutions and a four-order analytical solution in terms of acoustic frequency, with all power is initially in the 0-order

Hence, the response curve continued to rise past the unity value until the first effect mentioned above takes over. It can be predicted as seen in Fig. 21, (i.e., comprising data plots of a 4-order analytical model and the solid line plots of a 2-order numerical formalism), that the frequency dependent curve anomaly should disappear if only using a two order numerical analysis model because this anomaly depends on reduction in diffraction efficiency due to the presence of orders other than the typical Bragg regime zero order and minus one order. Similarly, Fig. 22 shows numerical and analytical predicted results when 100% of the incident light is in the -1 order [see Eq. (3.49c)]. Although it can be observed that the curves, both numerically and analytically, relatively appear shapewise identical to those observed in Fig. 20, the orders have once again been swapped. Significantly,

steady transfer of power from -1 to 0-order is conspicuous towards the unity, with the maximum slightly shifted from the normalized frequency of unity, i.e., $\bar{\Omega} \approx 1.05$.

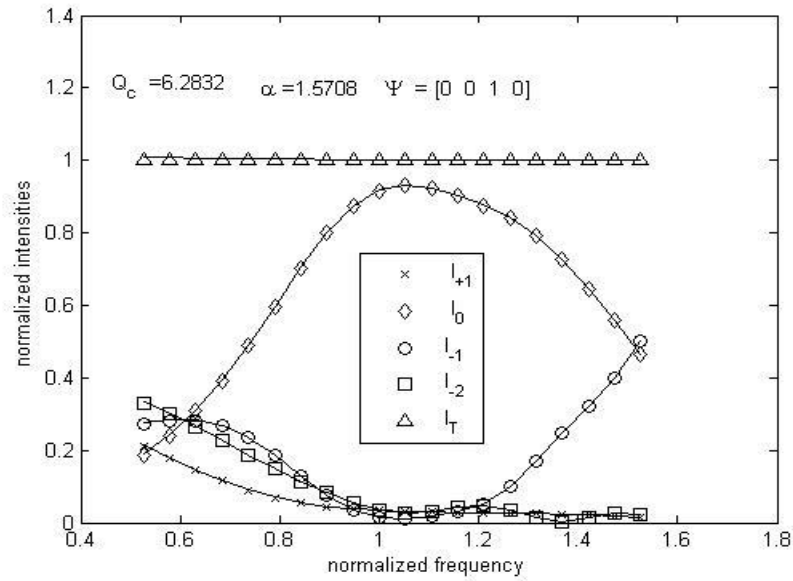


Figure 22. Comparison for four-order numerical and analytical solutions in terms of acoustic frequency, all power is initially in the -1-order

The same theory used to explain the shifted peak in Fig. 20, using Fig. 21, applies here. Meanwhile, little power is spilled over in the remaining order. Fig. 23 shows the numerical and analytical predicted results when 100% of the incident light is in +1-

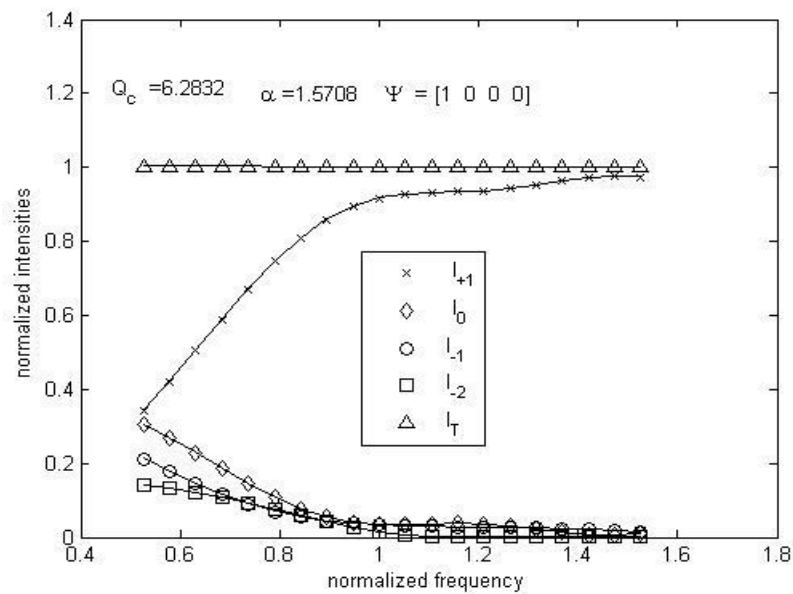


Figure 23. Comparison for four-order numerical and analytical solutions in terms of acoustic frequency, all power is initially in the +1-order

order [see (3.49a)]. Both numerical and analytical results, as before, are in complete agreement. Obviously, the plot shows that not much power at the end of the cell is coupled out of the ψ_{+1} order. Thus, dominant power is retained by +1-order. This justifies why power is minimal in the remaining orders. The idea is that the angular spectrum of the sound field is not broad enough in width to generate higher levels of energy transfer for this order. Meanwhile, a slight dip (also known as degeneracy) was suspected toward the right side of the plot.

The case of 100% of the light in the -2-order [see (3.49d)], was also tested and compared as shown in Fig. 24. Both numerical and analytical results as before are in complete agreement. Interestingly, the curve is completely different from Fig. 23. As easily seen, power rises steadily in the -2-order throughout, with a corresponding negligible energy in the remaining order.

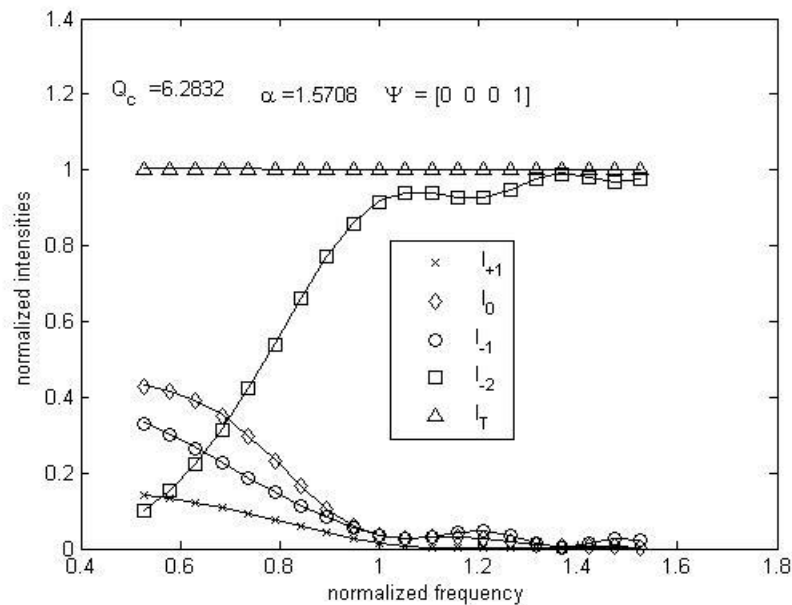


Figure 24. Comparison for four-order numerical and analytical solutions in terms of acoustic frequency, with all power is initially in the -1-order

Hence, not much power at the end of the cell is coupled out of the ψ_{-2} order. The logical reasoning is that the angular spectrum of the sound field is not wide enough to generate higher levels of energy transfer for this order. Similarly, beyond the normalized frequency of unity, a reoccurring dip (referred to as degeneracy) with an improvement toward the right side of the curve has been observed. Moreover, for the normalized frequency variation, the simplicity of the solution and its ability to

accommodate a general combination of initial conditions using a matlab simulation was also illustrated.

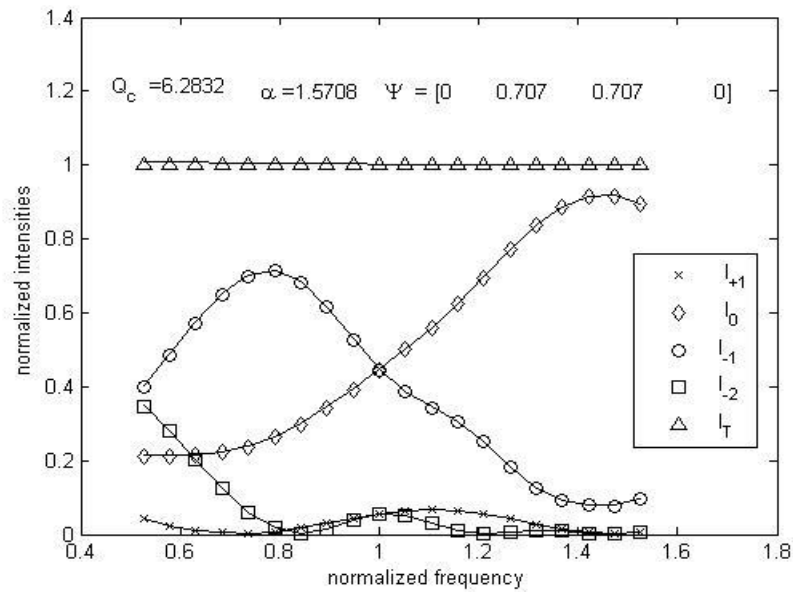


Figure 25. Comparison for four-order numerical and analytical solutions for normalized frequency variation; power is initially 50% in both the 0-order and -1-order

Both Figs. 25 and 26 successively put 50% of the power in the 0 and -1 order [see Fig. 25], and +1 order and -2 order [see Fig. 26] respectively.

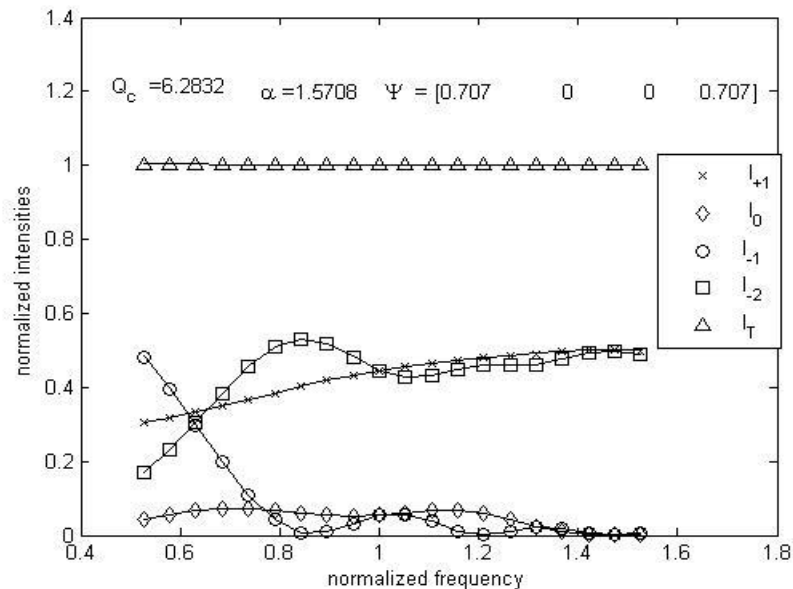


Figure 26. Comparison for four-order numerical and analytical solutions for normalized frequency variation; power is initially 50% in both the +1-order and -2-order

Notice that the four-order analytical (symbols) and the four-order numerical (solid

line) predictions are in perfect agreement.

4.3.3 Test cases for normalized angle variation

Fig. 27 shows the numerical and analytical $\bar{\phi}_0$ - dependent predicted results when 100% of the incident light is in the 0th order [see (3.49b)]. From the plot (left side to the normalized angle of unity), as expected, the incident light is mostly diffracted at the expense of other orders to -1 order, with its peak (about 90%) at unity (i.e., $\bar{\phi}_0 = 1$). Thus, confirming the Braggs condition. Theoretical explanation reveals that a higher percentage of the power is transferred to the -1 order via phonon emission and related photon frequency down conversion [14]. However, the power decreases steadily with a corresponding gradual power rise in the remaining orders when the normalized angle of unity is exceeded. As expected, agreement between numerical and analytical solutions is excellent, with a confirming check shown for the total intensities according to (2.45).

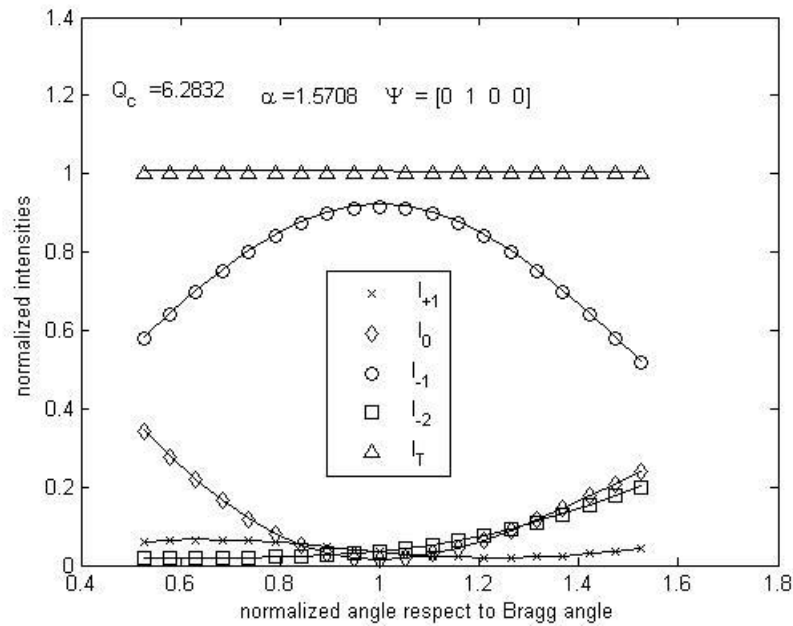


Figure 27. Comparison for four-order numerical and analytical solutions in terms of optical angle with all power is initially in the 0-order

Fig. 28 shows numerical and analytical predicted results when 100% of the incident light is in the -1-order [see (3.49c)]. It can be observed that the curves both numerically and analytically appear as a mirror image of those in Fig. 27, with the order swapped as (2.46). Likewise, both numerical and analytical results, as before,

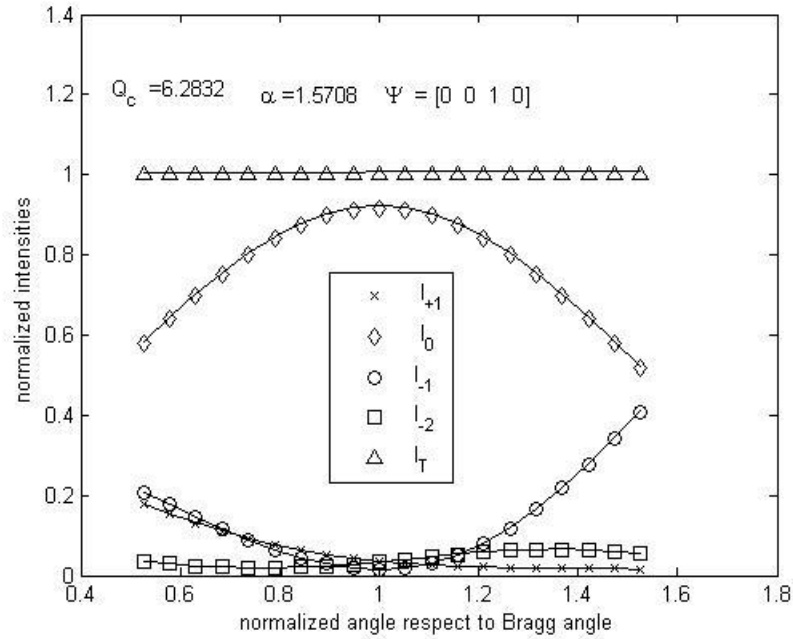


Figure 28. Comparison for four-order numerical and analytical solutions in terms of optical angle with all power is initially in the -1-order

are in complete agreement. From the plot (left side towards normalized angle of unity), comparison of all orders shows that entering light is greatly diverted (via phonon emission and related photon frequency down conversion [14]) to the 0-order with the maximum (about 90%) at normalized angle of unity, (i.e. $\bar{\phi}_0 = 1$), which satisfy the Bragg condition. From a physical viewpoint this provides a validation of the accuracy of the solution. It is known that the Bragg conservation of momentum triangle engenders a fundamental symmetry in the phonon-assisted transfer of energy between orders [14]. This is then explained in terms of a sound phonon absorbed with a corresponding photon frequency upshift. However, when the normalized angle of unity is exceeded, the transferred power in the 0-order reduces gradually. This give rise to more energy in the remaining order. Fig. 29 shows the numerical and analytical predicted results when 100% of the incident light is in the +1-order [see (3.49a)]. Both numerical and analytical results are in complete agreement. In Fig. 30, the case of 100% of the light in the -2 order [see Eq. (3.49d)], was also tested and compared with a perfect agreement between the analytical and numerical predictions.

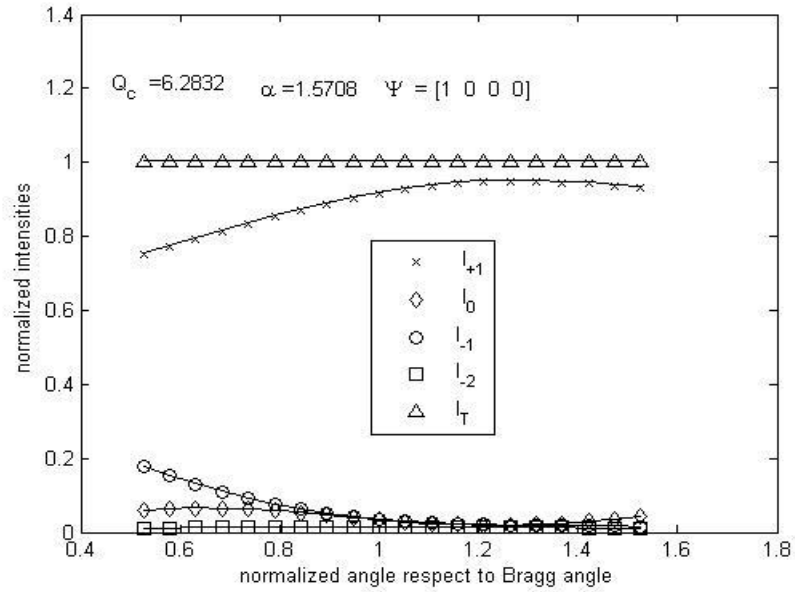


Figure 29. Comparison for four-order numerical and analytical solutions in terms of optical angle with all power is initially in the +1-order

Lastly, for the normalized angle variation, the flexibility of the solution and its ability to accommodate a general combination of initial conditions was also presented. As it is easily seen in both Figs. 31 and 32, specific initial conditions for

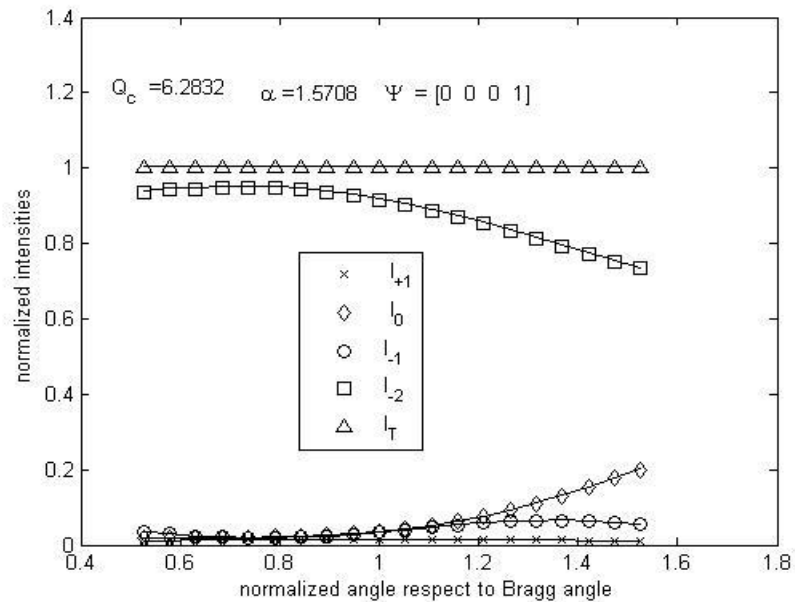


Figure 30. Comparison for four-order numerical and analytical solutions in terms of optical angle with all power is initially in the -1-order

this test case put 50% amount of power in both the 0th and -1 order, and similarly in

both the +1 and -2-order respectively.

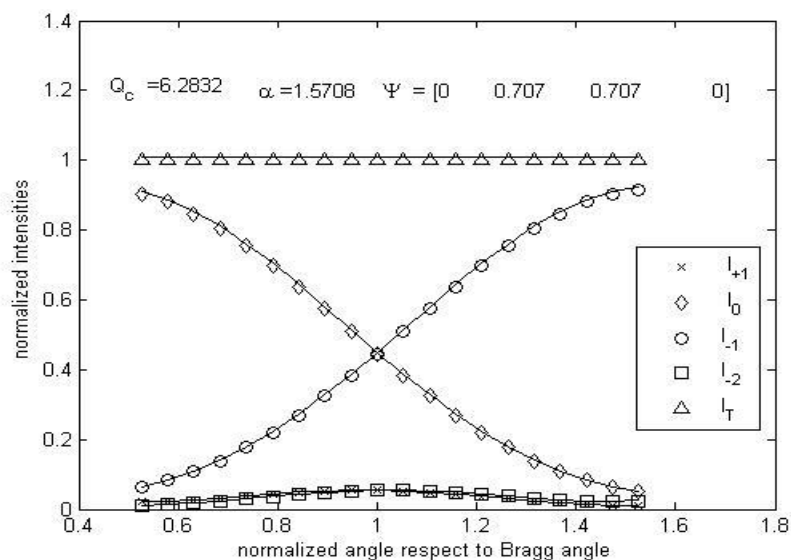


Figure 31. Comparison for four-order numerical and analytical solutions for normalized angle variation; power is initially 50% in both the 0-order and -1-order

The four-order analytical (symbols) and the four-order numerical (solid line) predictions are in perfect agreement.

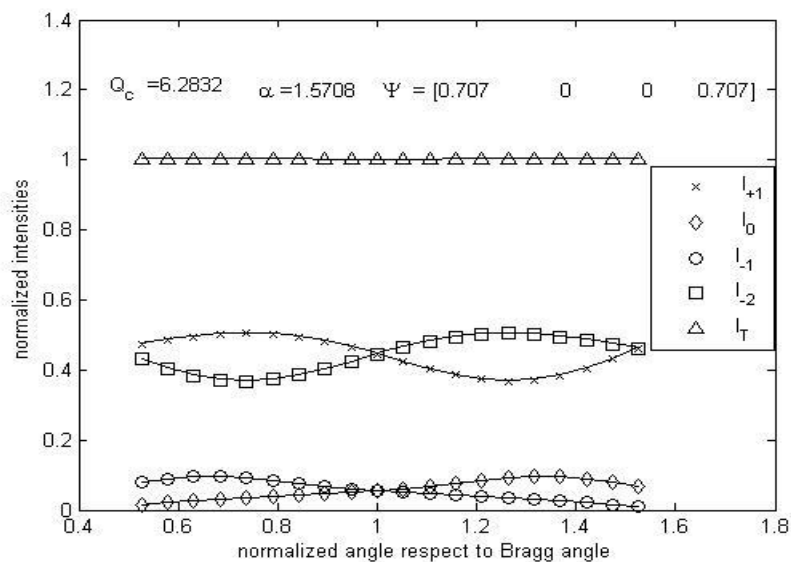


Figure 32. Comparison for four-order numerical and analytical solutions for normalized angle variation; power is initially 50% in both the +1-order and -2-order

4.4 Concluding Remarks for Chapter Four

In this chapter, the critical conditions employed by both numerical solutions and analytical predictions for variations in normalized space, normalized frequency, and normalized angle have been canvassed. Also presented are the outputs of their respective matlab simulations. The numerical model demonstrates validity of the four-order analytic model based on the level agreement between numerical formalism and analytical predictions for all space, frequency and angle variation.

Chapter Five

Additional Topics

As introductory remarks in this chapter, explanation on qualitative and listed topics including: divine proportion, energy conservation based on a unitary transition matrix, numerical evaluation for the roots to general 4th order characteristic equation being real, and numerical support for transition matrix being unitary shall be covered.

5.1 Divine Proportion Analysis

It can be recognized that (3.21) is a linear homogeneous first-order system of differential equations. If this system of differential equations also has constant coefficients, i.e., A , is a constant matrix, it would be possible to predict the state transition matrix from [39]

$$\Gamma(\xi, \xi_0) = e^{A(\xi - \xi_0)}, \quad (5.1)$$

where

$$\Psi(\xi) = \Gamma(\xi, \xi_0) \cdot \Psi(\xi_0), \quad (5.2)$$

and $\Psi(\xi_0)$ is the known initial condition at some specified location ξ_0 . Expanding the exponential of matrix (A1) into four additive matrix terms using the eigenvalues of A is then possible using Sylvester's theorem [39]. However, because A is not a constant matrix, the (5.1) approach is not applicable. Nonetheless, it was discovered that the matrix operator for A , taken from (3.13), did have four distinct eigenvalues, all of which are related to Euclid's Divine Proportion, also known as the Golden Ratio. Here, the appearance of the Divine Proportion constant, Φ , in the AO problem considered is demonstrated. Euclid's Divine Proportion is associated with the numerical constant [34],

$$\Phi = \frac{1 + \sqrt{5}}{2} = 1.6180. \quad (5.3)$$

Considering the differential equation

$$\frac{d\Psi(\xi)}{d\xi} = -j\alpha A(\xi)\Psi(\xi), \quad (5.4)$$

where

$$\alpha(\xi) = \alpha \in \mathbb{R}, \quad (5.5a)$$

$$\Psi(\xi) = \begin{pmatrix} \psi_{+1}(\xi) \\ \psi_0(\xi) \\ \psi_{-1}(\xi) \\ \psi_{-2}(\xi) \end{pmatrix}, \quad (5.5b)$$

$$A(\xi) = \begin{pmatrix} 0 & e^{-j(x+b)\xi} & 0 & 0 \\ e^{+j(x+b)\xi} & 0 & e^{-jx\xi} & 0 \\ 0 & e^{+jx\xi} & 0 & e^{-j(x-b)\xi} \\ 0 & 0 & e^{+j(x-b)\xi} & 0 \end{pmatrix}. \quad (5.5c)$$

The eigenvalues are generated by

$$|A(\xi) - \lambda \mathbf{I}| = \begin{vmatrix} -\lambda & e^{-j(x+b)\xi} & 0 & 0 \\ e^{+j(x+b)\xi} & -\lambda & e^{-jx\xi} & 0 \\ 0 & e^{+jx\xi} & -\lambda & e^{-j(x-b)\xi} \\ 0 & 0 & e^{+j(x-b)\xi} & -\lambda \end{vmatrix}, \quad (5.6)$$

where \mathbf{I} is an identity matrix. One method is to evaluate the determinant which leads to a quartic polynomial equation in λ :

$$\begin{aligned} &= -\lambda \begin{vmatrix} -\lambda & e^{-jx\xi} & 0 \\ e^{+jx\xi} & -\lambda & e^{-j(x-b)\xi} \\ 0 & e^{+j(x-b)\xi} & -\lambda \end{vmatrix} - e^{-j(x+b)\xi} \begin{vmatrix} e^{+j(x+b)\xi} & e^{-jx\xi} & 0 \\ 0 & -\lambda & e^{-j\beta(x-b)\xi} \\ 0 & e^{+j(x-b)\xi} & -\lambda \end{vmatrix} \\ &= -\lambda \left(-\lambda \begin{vmatrix} -\lambda & e^{-j(x-b)\xi} \\ e^{+j(x-b)\xi} & -\lambda \end{vmatrix} - e^{-jx\xi} \begin{vmatrix} e^{+jx\xi} & e^{-j(x-b)\xi} \\ 0 & -\lambda \end{vmatrix} \right) \\ &\quad - e^{-j(x+b)\xi} \begin{pmatrix} e^{+j(x+b)\xi} & -\lambda & e^{-j(x-b)\xi} \\ e^{+j(x-b)\xi} & -\lambda & -e^{-jx\xi} \end{pmatrix} \begin{vmatrix} 0 & e^{-j\beta(x-b)\xi} \\ 0 & -\lambda \end{vmatrix} \\ &= \lambda^2(\lambda^2 - 1) + \lambda(-\lambda) - (\lambda^2 - 1) \end{aligned}$$

$$= \lambda^4 - 3\lambda^2 + 1. \quad (5.7)$$

It is observed that (5.7) is biquadratic in λ^2 . The λ^2 is solved for by using the quadratic formula after equating (5.7) to zero. This results in

$$\lambda^2 = \frac{3 \pm \sqrt{9-4}}{2} = \frac{3 \pm \sqrt{5}}{2}. \quad (5.8)$$

Taking the square root of both sides of (5.8) gives

$$\lambda = \pm \sqrt{\frac{3 \pm \sqrt{5}}{2}}. \quad (5.9)$$

Finally, the four roots of the biquadratic equation (5.7) are

$$\lambda_{1,2} = \pm \sqrt{\frac{3 + \sqrt{5}}{2}} = \pm \sqrt{\frac{1 + 2\sqrt{5} + 5}{4}} = \pm \sqrt{\frac{(1 + \sqrt{5})^2}{4}} = \frac{1 + \sqrt{5}}{2} = \pm \Phi \quad (5.10a)$$

and

$$\lambda_{3,4} = \pm \sqrt{\frac{3 - \sqrt{5}}{2}} = \pm \sqrt{\frac{1 - 2\sqrt{5} + 5}{4}} = \pm \sqrt{\frac{(1 - \sqrt{5})^2}{4}} = \frac{1 - \sqrt{5}}{2} = -\frac{2}{1 + \sqrt{5}} = \mp \frac{1}{\Phi}. \quad (5.10b)$$

5.2 Energy Conservation for Unitary Transition Matrices

Starting from a row vector representation for the solution,

$$\Psi^T(\xi) \equiv (\psi_{+1}(\xi), \psi_0(\xi), \psi_{-1}(\xi), \psi_{-2}(\xi)), \quad (5.11)$$

the energy field is the sum of the magnitude squared of the incoherently [3] related orders:

$$\Psi^\dagger(\xi) \cdot \Psi(\xi) = \sum_{n=-1}^{-2} |\psi_n(\xi)|^2. \quad (5.12)$$

The first term on the left-hand side of (5.12) can be represented in terms of the adjoint operator of the transition matrix $\Gamma(\xi)$. After rearrangement of terms with reference to (3.42) produces

$$\Psi^T(\xi) = (\Gamma(\xi) \cdot \Psi(0))^\dagger = \Psi^\dagger(0) \cdot \Gamma^\dagger(\xi). \quad (5.13)$$

From the matrix property involving the identity matrix \mathbf{I} and arbitrary vector ν ,

$$\nu^\dagger \cdot \mathbf{I} \cdot \nu = \nu^\dagger \cdot \nu, \quad (5.14)$$

combined with (3.48) and (5.13) and the left-hand side of (5.12) results in

$$\Psi^\dagger(\xi) \cdot \Psi(\xi) = \Psi^\dagger(0) \cdot \Gamma^\dagger(\xi) \cdot \Gamma(\xi) \cdot \Psi(0) = \Psi^\dagger(0) \cdot \Psi(0). \quad (5.15)$$

Or equivalent from (5.12) returns

$$\sum_{n=-1}^{-2} |\psi_n(\xi)|^2 = \sum_{n=-1}^{-2} |\psi_n(0)|^2, \quad (5.16)$$

which completes the assertion that the solution is consistent with energy conservation. As a disclaimer, the specific limits on the number of orders could be generalized, and therefore, it can be concluded that the property that a transition matrix being unitary will guarantee AO energy conversion, which can be extended to any number of orders. Because of the simplicity of the conservation rule in (5.16), it is convenient to check on the accuracy of AO numerical tests.

5.3 Numerical Demonstration that Roots are Real

In this section, presentation of the claim that although roots were not symbolically proven to be real due to complexity of the quartic roots, numerical test taken, however, support the fact that they are. As a disclaimer, the limitations in Maple [40] in simplifying complicated expressions are probable. Certainly, all the quartic solutions in (3.25) are dependent on the parameters, $\bar{\phi}_0, \bar{\Omega}, Q_c$ and α .

Invariably, each of the quartic roots, for instance, these r_1, r_2, r_3 and r_4 , is susceptible to a change whenever any of the four parameters changes. Here, four different test cases shall be used to establish the claim that roots are real simply by varying one parameter at a time while others are held constant. Both Figs. 33 and 34, typically combine two constant parameters: sound factor, $\alpha = \frac{\pi}{2}$, and Klein-Cook normalized

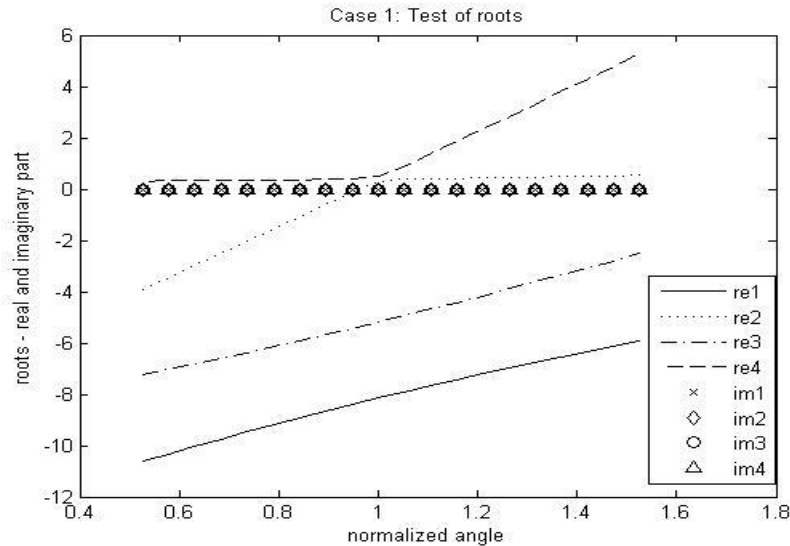


Figure 33. Test of roots with normalized angle variation

parameter, $Q_c = 2\pi$, as the inputs in order to test in computations if the imaginary parts of the quartic roots is making any significant contribution or not. After setting

the $\bar{\Omega} = 1$, the sensitivity of the roots (i.e., real and imaginary parts) as normalized angle changes has been observed from Fig. 33. Without mincing words, it is conspicuous that for all real plots, the graph is positive as lines slide upward from left to right. As expected, all the imaginary parts collapse at the zero margin throughout the normalized angle variation, thus confirming, that the imaginary part is negligible. On the other hand, Fig. 34 depicts that the graph is negative due to a downward slide in the curves from left to right for the real plots.

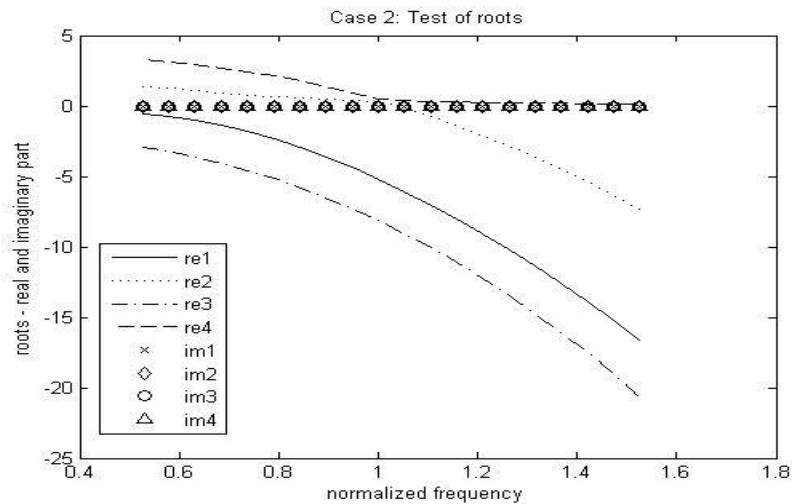


Figure 34. Test of roots with normalized frequency variation

Similarly, all the imaginary plots collide at the zero margin throughout the normalized frequency change after the normalized angle has been fixed, i.e., $\bar{\phi}_0 = 1$. This again assures that the imaginary parts makes no contribution in the computation. A variation in the sound factor, α , was also tested, as seen in Fig. 35.

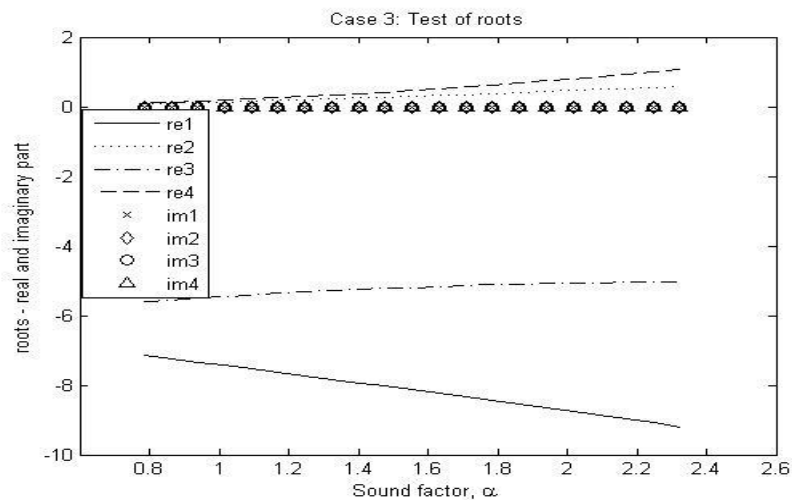


Figure 35. Test of roots with sound factor variation

While $\bar{\phi}_0$, $\bar{\Omega}$ and Q_c are fixed, the sound factor (α) variation has been selected between $\frac{\pi}{4}$ and $\frac{3\pi}{4}$. It was evident that as the real part varies, their respective imaginary counterparts, once again have been studied to align at zero, thus confirming all roots are real. Lastly, with $\bar{\phi}_0$, $\bar{\Omega}$ and α all kept constant, variation of the quality factor, Q_c , chosen between π and 4π , was also considered, see Fig. 36.

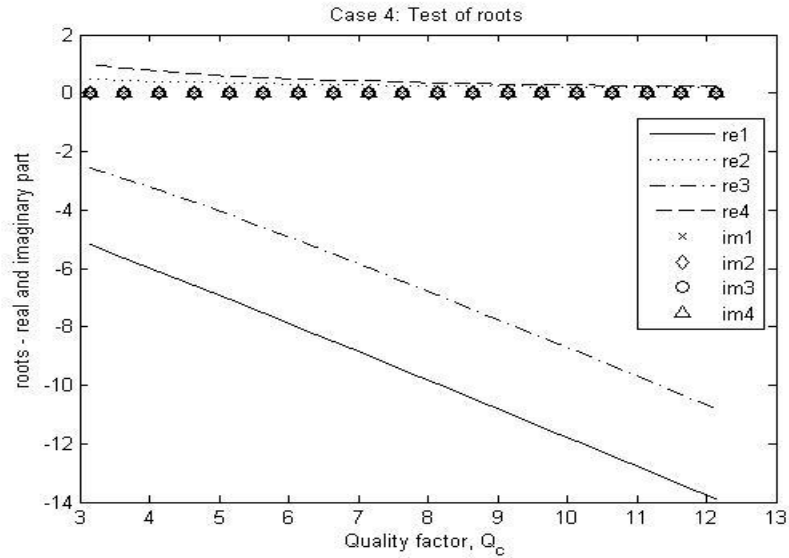


Figure 36. Test of roots with quality factor (Q_c) variation

As expected, all the imaginary parts overlap at the zero margin as the real parts vary. With these four test cases of numerical demonstrations, the conclusion can be drawn that the quartic roots are real.

5.4 Analysis and Demonstration for Consistency of Roots satisfying Vieta's Formulas [38]

This section recalls Vieta's rule as a measure to ascertain the level of accuracy for the quartic characteristic roots generated in (3.25). Vieta's theorem presents a correlation between the constant coefficient of a quartic polynomial and its generated roots. Thus, given a general quartic polynomial equation as,

$$r^4 + a_1r^3 + a_2r^2 + a_3r + a_4 = 0. \quad (5.17)$$

It then implies that the relationship between all four roots, r_1, r_2, r_3, r_4 , and their constant coefficients in (5.17) are as follows:

$$r_1 + r_2 + r_3 + r_4 = -a_1, \quad (5.18a)$$

$$r_1 r_2 + r_3 r_4 + r_2 r_3 + r_1 r_4 + r_1 r_3 + r_2 r_4 = a_2, \quad (5.18b)$$

$$r_1 r_2 r_3 + r_1 r_2 r_4 + r_1 r_3 r_4 + r_2 r_3 r_4 = -a_3, \quad (5.18c)$$

$$r_1 r_2 r_3 r_4 = a_4. \quad (5.18d)$$

Certainly, the analytic arguments support the first three rules. However, the fourth rule is only supported with numerical demonstration. See Appendix F for details.

5.5 Demonstration that Transition Matrix " $\Gamma(\xi)$ " is Unitary

The coefficients for the adjoint (complex conjugate transpose) of the transition matrix $\Gamma(\xi)$ in (3.46) are

$$\Gamma^\dagger(\xi) \equiv \begin{pmatrix} \mathbf{b}_{11} & \mathbf{b}_{12} & \mathbf{b}_{13} & \mathbf{b}_{14} \\ \mathbf{b}_{21} & \mathbf{b}_{22} & \mathbf{b}_{23} & \mathbf{b}_{24} \\ \mathbf{b}_{31} & \mathbf{b}_{32} & \mathbf{b}_{33} & \mathbf{b}_{34} \\ \mathbf{b}_{41} & \mathbf{b}_{42} & \mathbf{b}_{43} & \mathbf{b}_{44} \end{pmatrix} = \begin{pmatrix} \mathbf{a}_{r1}^* \cdot \mathbf{e}_{c1} & \mathbf{b}_{r2}^* \cdot \mathbf{e}_{c1} & \mathbf{c}_{r3}^* \cdot \mathbf{e}_{c1} & \mathbf{d}_{r4}^* \cdot \mathbf{e}_{c1} \\ \mathbf{a}_{r1}^* \cdot \mathbf{f}_{c2} & \mathbf{b}_{r2}^* \cdot \mathbf{f}_{c2} & \mathbf{c}_{r3}^* \cdot \mathbf{f}_{c2} & \mathbf{d}_{r4}^* \cdot \mathbf{f}_{c2} \\ \mathbf{a}_{r1}^* \cdot \mathbf{g}_{c3} & \mathbf{b}_{r2}^* \cdot \mathbf{g}_{c3} & \mathbf{c}_{r3}^* \cdot \mathbf{g}_{c3} & \mathbf{d}_{r4}^* \cdot \mathbf{g}_{c3} \\ \mathbf{a}_{r1}^* \cdot \mathbf{h}_{c4} & \mathbf{b}_{r2}^* \cdot \mathbf{h}_{c4} & \mathbf{c}_{r3}^* \cdot \mathbf{h}_{c4} & \mathbf{d}_{r4}^* \cdot \mathbf{h}_{c4} \end{pmatrix}, \quad (5.19)$$

where the complex conjugate transposes element notations in (5.19) represents

$$\mathbf{a}_{r1}^* \equiv \left(-\frac{\kappa_1 e^{+j3x\xi}}{t_1 \alpha^3}, -\frac{\kappa_2 e^{+j3x\xi}}{t_2 \alpha^3}, -\frac{\kappa_3 e^{+j3x\xi}}{t_3 \alpha^3}, -\frac{\kappa_4 e^{+j3x\xi}}{t_4 \alpha^3} \right), \quad (5.20a)$$

$$\mathbf{b}_{r2}^* \equiv \left(\frac{\eta_1 e^{+j(2x-b)\xi}}{t_1 \alpha^2}, \frac{\eta_2 e^{+j(2x-b)\xi}}{t_2 \alpha^2}, \frac{\eta_3 e^{+j(2x-b)\xi}}{t_3 \alpha^2}, \frac{\eta_4 e^{+j(2x-b)\xi}}{t_4 \alpha^2} \right), \quad (5.20b)$$

$$\mathbf{c}_{r3}^* \equiv \left(-\frac{r_1 e^{+j(x-b)\xi}}{t_1 \alpha}, -\frac{r_2 e^{+j(x-b)\xi}}{t_2 \alpha}, -\frac{r_3 e^{+j(x-b)\xi}}{t_3 \alpha}, -\frac{r_4 e^{+j(x-b)\xi}}{t_4 \alpha} \right), \quad (5.20c)$$

$$\mathbf{d}_{r4}^* \equiv \left(\frac{1}{t_1}, \frac{1}{t_2}, \frac{1}{t_3}, \frac{1}{t_4} \right). \quad (5.20d)$$

Each of the elements in (5.19) can be analyzed following the combination of (5.20) and (3.45) as:

$$\mathbf{b}_{11} \equiv \mathbf{a}_{r1}^* \cdot \mathbf{e}_{c1} = -e^{+j3x\xi} \left(\frac{\kappa_1}{t_1 a} + \frac{\kappa_2}{t_2 b} + \frac{\kappa_3}{t_3 c} + \frac{\kappa_4}{t_4 d} \right), \quad (5.21a1)$$

$$\mathbf{b}_{12} \equiv \mathbf{b}_{r2}^* \cdot \mathbf{e}_{c1} = \alpha e^{+j(2x-b)\xi} \left(\frac{\eta_1}{t_1 a} + \frac{\eta_2}{t_2 b} + \frac{\eta_3}{t_3 c} + \frac{\eta_4}{t_4 d} \right), \quad (5.21a2)$$

$$\mathbf{b}_{13} \equiv \mathbf{c}_{r3}^* \cdot \mathbf{e}_{c1} = -\alpha^2 e^{+j(x-b)\xi} \left(\frac{r_1}{t_1 a} + \frac{r_2}{t_2 b} + \frac{r_3}{t_3 c} + \frac{r_4}{t_4 d} \right), \quad (5.21a3)$$

$$\mathbf{b}_{14} \equiv \mathbf{d}_{r4}^* \cdot \mathbf{e}_{c1} = \alpha^3 \left(\frac{1}{t_1 a} + \frac{1}{t_2 b} + \frac{1}{t_3 c} + \frac{1}{t_4 d} \right), \quad (5.21a4)$$

$$\mathbf{b}_{21} \equiv \mathbf{a}_{r1}^* \cdot \mathbf{f}_{c2} = -\frac{e^{+j3x\xi}}{\alpha} \left(\frac{\kappa_1 S_\delta}{t_1 a} + \frac{\kappa_2 S_\gamma}{t_2 b} + \frac{\kappa_3 S_\lambda}{t_3 c} + \frac{\kappa_4 S_\rho}{t_4 d} \right), \quad (5.21b1)$$

$$\mathbf{b}_{22} \equiv \mathbf{b}_{r2}^* \cdot \mathbf{f}_{c2} = e^{+j(2x-b)\xi} \left(\frac{\eta_1 S_\delta}{t_1 a} + \frac{\eta_2 S_\gamma}{t_2 b} + \frac{\eta_3 S_\lambda}{t_3 c} + \frac{\eta_4 S_\rho}{t_4 d} \right), \quad (5.21b2)$$

$$\mathbf{b}_{23} \equiv \mathbf{c}_{r3}^* \cdot \mathbf{f}_{c2} = -\alpha e^{+j(x-b)\xi} \left(\frac{r_1 S_\delta}{t_1 a} + \frac{r_2 S_\gamma}{t_2 b} + \frac{r_3 S_\lambda}{t_3 c} + \frac{r_4 S_\rho}{t_4 d} \right), \quad (5.21b3)$$

$$\mathbf{b}_{24} \equiv \mathbf{d}_{r4}^* \cdot \mathbf{f}_{c2} = \alpha^2 \left(\frac{S_\delta}{t_1 a} + \frac{S_\gamma}{t_2 b} + \frac{S_\lambda}{t_3 c} + \frac{S_\rho}{t_4 d} \right), \quad (5.21b4)$$

$$\mathbf{b}_{31} \equiv \mathbf{a}_{r1}^* \cdot \mathbf{g}_{c3} = -\frac{e^{+j3x\xi}}{\alpha^2} \left(\frac{\kappa_1 U_\delta}{t_1 a} + \frac{\kappa_2 U_\gamma}{t_2 b} + \frac{\kappa_3 U_\lambda}{t_3 c} + \frac{\kappa_4 U_\rho}{t_4 d} \right), \quad (5.21c1)$$

$$\mathbf{b}_{32} \equiv \mathbf{b}_{r2}^* \cdot \mathbf{g}_{c3} = \frac{e^{+j(2x-b)\xi}}{\alpha} \left(\frac{\eta_1 U_\delta}{t_1 a} + \frac{\eta_2 U_\gamma}{t_2 b} + \frac{\eta_3 U_\lambda}{t_3 c} + \frac{\eta_4 U_\rho}{t_4 d} \right), \quad (5.21c2)$$

$$\mathbf{b}_{33} \equiv \mathbf{c}_{r3}^* \cdot \mathbf{g}_{c3} = -e^{+j(x-b)\xi} \left(\frac{r_1 U_\delta}{t_1 a} + \frac{r_2 U_\gamma}{t_2 b} + \frac{r_3 U_\lambda}{t_3 c} + \frac{r_4 U_\rho}{t_4 d} \right), \quad (5.21c3)$$

$$\mathbf{b}_{34} \equiv \mathbf{d}_{r4}^* \cdot \mathbf{g}_{c3} = \alpha \left(\frac{U_\delta}{t_1 a} + \frac{U_\gamma}{t_2 b} + \frac{U_\lambda}{t_3 c} + \frac{U_\rho}{t_4 d} \right), \quad (5.21c4)$$

$$\mathbf{b}_{41} \equiv \mathbf{a}_{r1}^* \cdot \mathbf{h}_{c4} = -\frac{e^{+j3x\xi}}{\alpha} \left(\frac{\kappa_1 N_\delta}{t_1 a} + \frac{\kappa_2 N_\gamma}{t_2 b} + \frac{\kappa_3 N_\lambda}{t_3 c} + \frac{\kappa_4 N_\rho}{t_4 d} \right), \quad (5.21d1)$$

$$\mathbf{b}_{42} \equiv \mathbf{b}_{r2}^* \cdot \mathbf{h}_{c4} = e^{+j(2x-b)\xi} \left(\frac{\eta_1 N_\delta}{t_1 a} + \frac{\eta_2 N_\gamma}{t_2 b} + \frac{\eta_3 N_\lambda}{t_3 c} + \frac{\eta_4 N_\rho}{t_3 d} \right), \quad (5.21d2)$$

$$\mathbf{b}_{43} \equiv \mathbf{c}_{r3}^* \cdot \mathbf{h}_{c4} = -\alpha e^{+j(x-b)\xi} \left(\frac{r_1 N_\delta}{t_1 a} + \frac{r_2 N_\gamma}{t_2 b} + \frac{r_3 N_\lambda}{t_3 c} + \frac{r_4 N_\rho}{t_4 d} \right), \quad (5.21d3)$$

$$\mathbf{b}_{44} \equiv \mathbf{d}_{r4}^* \cdot \mathbf{h}_{c4} = \alpha^2 \left(\frac{N_\delta}{t_1 a} + \frac{N_\gamma}{t_2 b} + \frac{N_\lambda}{t_3 c} + \frac{N_\rho}{t_4 d} \right). \quad (5.21d4)$$

With symbolic processing capability, it is possible to demonstrate, with reference to (3.46) and (5.19), that:

$$\mathbf{\Gamma} \cdot \mathbf{\Gamma}^\dagger \equiv \begin{pmatrix} \mathbf{c}_{11} & \mathbf{c}_{12} & \mathbf{c}_{13} & \mathbf{c}_{14} \\ \mathbf{c}_{21} & \mathbf{c}_{22} & \mathbf{c}_{23} & \mathbf{c}_{24} \\ \mathbf{c}_{31} & \mathbf{c}_{32} & \mathbf{c}_{33} & \mathbf{c}_{34} \\ \mathbf{c}_{41} & \mathbf{c}_{42} & \mathbf{c}_{43} & \mathbf{c}_{44} \end{pmatrix} = \mathbf{I} \Leftrightarrow (\mathbf{\Gamma} \cdot \mathbf{\Gamma}^\dagger)_y = \delta_y \quad (5.22)$$

where \mathbf{I} is the identity matrix, since all the non-leading diagonal elements (i.e., both real and imaginary parts) are approximately zero, and that δ_y is the Kronecker-Delta tensor. Therefore the adjoint of the transition matrix $\mathbf{\Gamma}$ is the matrix inverse or more succinctly $\mathbf{\Gamma}$ is unitary [39]. Expanded here are the diagonal elements in (5.22):

$$\mathbf{c}_{11} = \mathbf{a}_{11} \cdot \mathbf{b}_{11} + \mathbf{a}_{12} \cdot \mathbf{b}_{21} + \mathbf{a}_{13} \cdot \mathbf{b}_{31} + \mathbf{a}_{14} \cdot \mathbf{b}_{41}, \quad (5.23a)$$

$$\mathbf{c}_{22} = \mathbf{a}_{21} \cdot \mathbf{b}_{12} + \mathbf{a}_{22} \cdot \mathbf{b}_{22} + \mathbf{a}_{23} \cdot \mathbf{b}_{32} + \mathbf{a}_{24} \cdot \mathbf{b}_{42}, \quad (5.23b)$$

$$\mathbf{c}_{33} = \mathbf{a}_{31} \cdot \mathbf{b}_{13} + \mathbf{a}_{32} \cdot \mathbf{b}_{23} + \mathbf{a}_{33} \cdot \mathbf{b}_{33} + \mathbf{a}_{34} \cdot \mathbf{b}_{43}, \quad (5.23c)$$

$$\mathbf{c}_{44} = \mathbf{a}_{41} \cdot \mathbf{b}_{14} + \mathbf{a}_{42} \cdot \mathbf{b}_{24} + \mathbf{a}_{43} \cdot \mathbf{b}_{34} + \mathbf{a}_{44} \cdot \mathbf{b}_{44}. \quad (5.23d)$$

To support the matrix unitary condition argument, only the demonstrations of a limited set of numerical tests performed on the diagonal elements (i.e., real and imaginary parts) have been plotted. Apparently, the sensitivity of the leading diagonal elements of the unitary matrix with the normalized angle variation [see Fig. 37],

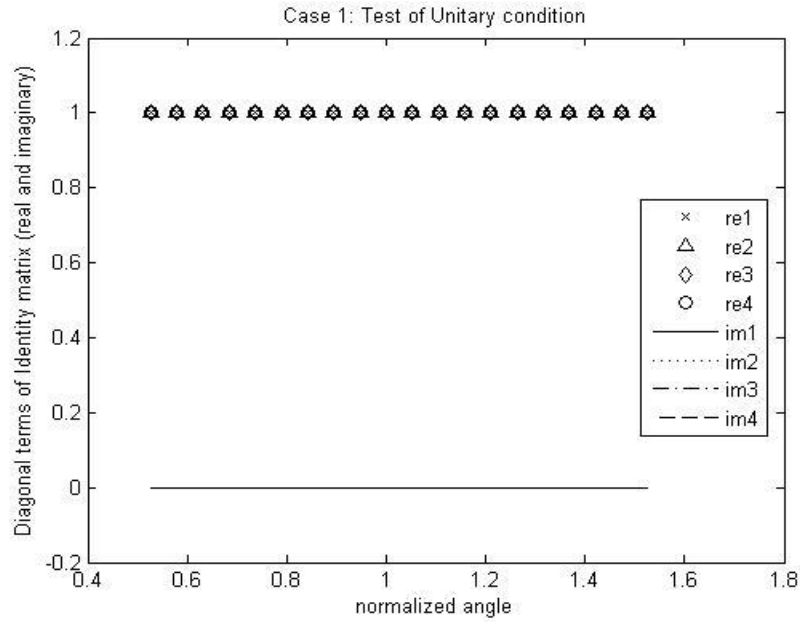


Figure 37. Demonstration of matrix unitary condition with normalized angle variation

and normalized frequency variation [see Fig. 38] respectively, is clarified after

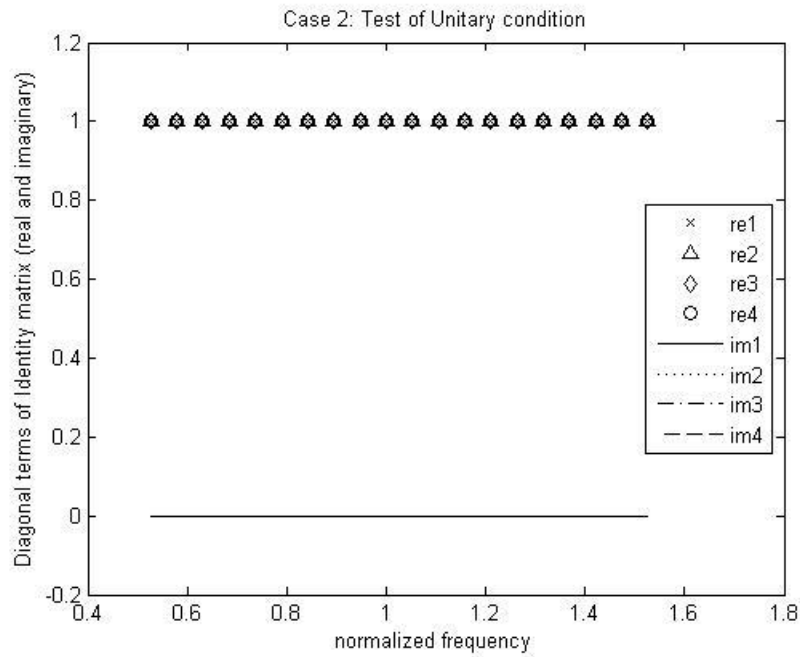


Figure 38. Demonstration of matrix unitary condition with normalized frequency variation

observing that all the real parts represented by the data plots coincide at one while the imaginary counterparts denoted by solid lines do overlap at zero. This again confirms that the imaginary parts are negligible.

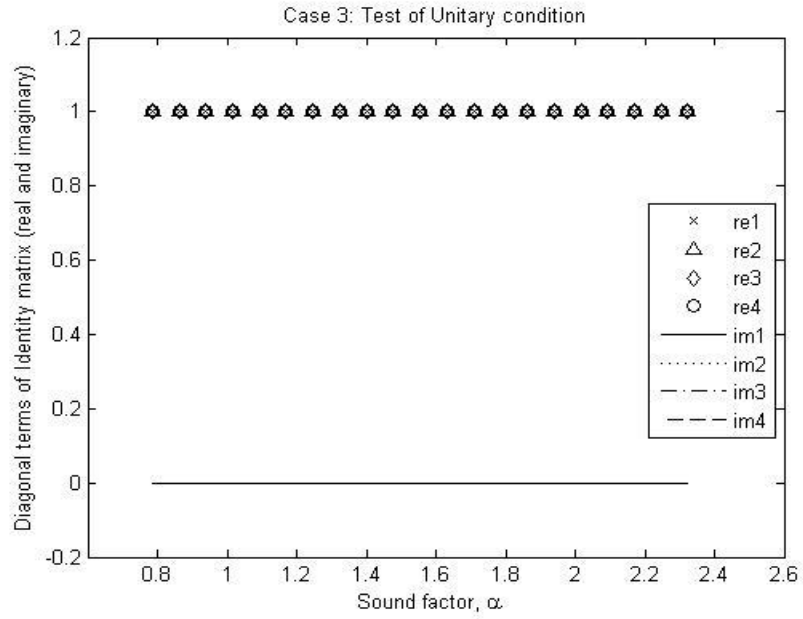


Figure 39. Demonstration of matrix unitary condition with sound factor variation

The variation of sound factor, α , was tested for unitary illustration. As seen graphically from Fig. 39, all the real roots (data plots), and their imaginary

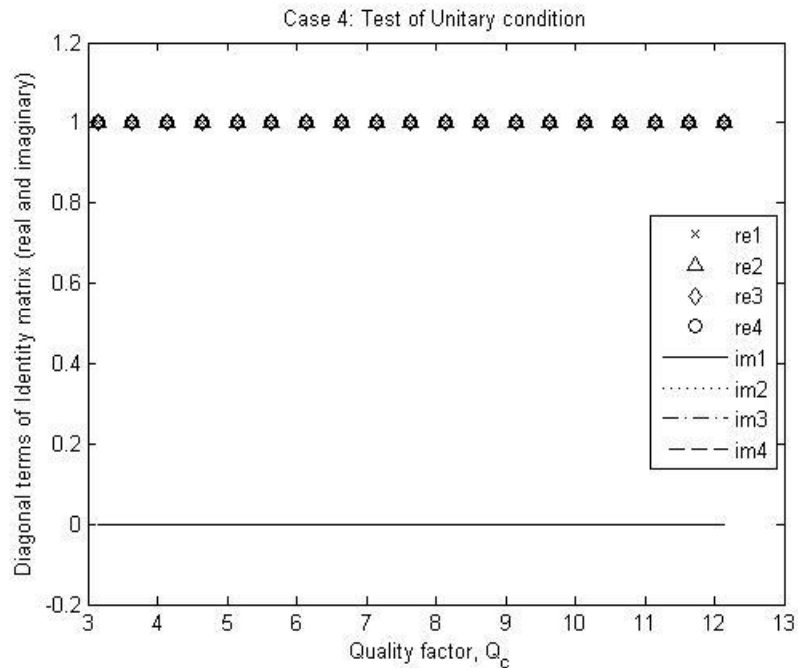


Figure 40. Demonstration of matrix unitary condition with quality factor variation

counterparts (solid lines), symmetrically overlapped on 1 and 0 respectively. Lastly, the variation of quality factor, Q_c , was also considered. The output, as seen from Fig.

40, was in complete agreement with the others. This contains the unitary condition of the transition matrix.

5.6 Concluding Remarks for Chapter Five

In this chapter, analysis of the divine proportion has been presented. Energy conservation analysis, based on a unitary transition matrix condition, was also discussed. The roots to general 4th order characteristic equation was numerically illustrated to be real, and that for every set of numerical conditions taken so far, the transition matrix, to within machine error, appears to be unitary.

Chapter Six

Conclusion and Future Work

The work presented in this thesis extends the prior exact analytic analysis for acousto-optic diffraction involving four orders of light which did not allow variation in normalized frequency and incident angle. With the uniform sound field and zero phase shifts design assumptions maintained throughout, an exact four-order analytic solution of a generalized 4th order DE which incorporates dependence on both input angle of light and sound frequency in an acousto-optic Bragg cell has been presented. The four-order DE analysis resulted in a quartic equation, and its characteristic roots, which were used in constructing the solution, have been obtained via the Ferrari approach. As demonstrated, the solution can be cast into the form of a transition matrix operator. Energy conservation for the four-order analytical solution was proven, assuming that the transition matrix is unitary. This assumption is consistent with numerical tests performed. Secondly, it was formally shown that the unitary matrix condition is a sufficient condition for the energy conservation rule applicable for all orders considered. Multiple comparisons of the analytical solution and numerically generated solutions which were made using three different parameter variations, for instance, normalized space variation, normalized frequency variation, and normalized angle variation served to validate the analytical solution. Finally, it was confirmed, as was established for the limited prior analysis, that within context for the more general analysis presented herein, acousto-optics can be included in the long list of physical, mathematical, and structural examples for which the ubiquitous Euclid's Divine Proportion appears.

It is suggested that further efforts with parameterization and possibly application of a second symbolic processing program may allow going beyond demonstration tests but lead to proofs that roots are real and that the transition matrix is unitary. The more general matrix formalism for four orders, allowing for variation in incident angles and frequency, should be potentially valuable for generating more accurate predictions for applications mentioned such as multi cell phased arrays and

recent interest in information transmission using chaotic systems which incorporate AO cells.

References

1. Rayleigh, L. (1885). "*Waves Propagated along the Plane Surfaces of an Elastic Solid*," Proc. London Math. Soc., 17, 4–11.
2. Korpel, A. (1997). "*Acousto-Optics*," 2nd ed. Marcel Dekker Inc, New York.
3. Brillouin, L. (1922). "*Diffusion de la lumiere et des rayons X par un corps transparent homogène*," Ann. Phys. (Paris), 17, 88-122.
4. Korpel, A. (1972). "*Acousto-optics*," in Applied Solid State Science, Vol. 3, R. Wolfe, Ed. New York: Academic Press, Ch. 2, 73-179.
5. Pieper, R., and Poon, T.-C. (Feb. 1985). "*An Acoustooptic FM Receiver Demonstrating Some Principles of Modern Signal Processing*," IEEE Transactions on Education, Vol. E-28, No. 1, 11-17.
6. Hereman, W., Mertens, R., Verheest, F., Leroy, O., Claeys, J. M. and Blomme, E. (1984). "*Interaction of light and ultrasound*," Phys. Mag. 6, 213-245.
7. Klein, W. R. and Cook, B.D. (1967). "*Unified approach to ultrasonic light diffraction*," IEEE Trans. Sonics Ultrason, SU-14,123-133.
8. Korpel, A. (May 1979). "*Two-dimensional plane wave theory of strong acousto-optic interaction in isotropic media*," J. Opt. Soc. Am., 69, 678-683.
9. Korpel, A. (Jan. 1981). "*Acousto-Optics - A Review of Fundamentals*," Proc. IEEE, 69, 48-53.
10. Lucas, R. and Biquard, P. (1932). "*Propriétés optiques des milieux solides et liquides soumis aux vibrations élastiques ultra sonores*," J. Phys. Rad., 3, 464-477.
11. Debye, P. and Sears, F.W. (Jun. 1932). "*On the scattering of light by supersonic waves*," Proc. Natl. Acad. Sci. (U.S.), 18, 409-414.
12. Bueche, F.J., and Hecht, E. (2006). *College Physics*, Schaum's Outline Series, McGraw-Hill, 10th Ed., 106, 221-222.
13. Collins, J. H., Lean, E. G. H. and Shaw, H.J. (Oct. 1967). "*Pulse Compression by Bragg Diffraction of Light with Microwave Sound*," Appl. Phys. Lett., 11,

242 - 242.

14. Pieper, R. J., Korpel, A. and Hereman, W. (Oct. 1986). "*Extension of the acoustic-optic Bragg regime through Hamming apodization of the sound field*," J. Opt. Soc. Am. A, 3, 1608-1619.
15. Pieper, R. and Korpel, A. (Sep. 1984). "*Comparison of phased-array Bragg cells operating in the second order*," *Applied Optics*, 23, 2921-2934.
16. Poon, T.-C. and Korpel, A. (Oct. 1981). "*Feynman diagram approach to acousto-optic scattering in the near-Bragg region*," J. Opt. Soc. Am., 71, 1202-1208.
17. Poon, T.-C. (1982). "*A Feynman diagram approach to multiple plane wave scattering in acousto-optic interactions*," Ph.D. dissertation (University of Iowa), 63-68.
18. Blomme, E. and Leroy, O. (1986). "*Diffraction of light by ultrasound at oblique incidence; An exact 4-order solution*," *Acustica* 59, 182-192.
19. Pieper, R. J. and Korpel, A. (Dec. 1983). "*Matrix formalism for the analysis of acoustooptic beam steering*," *Applied Optics*, 22, 4073-4081.
20. Pieper, R., Koslover, D. and Poon, T.-C. (2009). "*Exact solution for four-order acousto-optic Bragg diffraction with arbitrary initial conditions*," *Applied Optics*, 48, 141-150.
21. Pieper, R., Koslover, D. and Ndwata, H (Mar. 2009). "*Combining Phased Array and Hamming Sound Apodization Techniques to Improve the Acousto-Optic Diffraction Bandwidth*," 41st Southeastern Symposium on System Theory, TN, 311-316.
22. Korpel, A., Adler, R. Desmares, P., and Watson, W. (Oct. 1966). "*A Television Display Using Acoustic Deflection and Modulation of Coherent Light*," *Proc. IEEE*, 54,. 1429-1437.
23. Watson, W. H. and Adler, R. (Jun. 1969). "*Cascading Wide-Band Acousto-Optic Deflectors*," IEEE Conf. Laser Engineering and Applications, Washington D. C.
24. Schulz, M. B., Holland, M. G., and Davis Jr., (Oct. 1967). "*Optical Pulse Compression Using Bragg Scattering by Ultrasonic Waves*," *Appl. Phys. Lett.*, 11, 237-240.
25. Wenkoff, M. P., and Katchky, M. (Jan. 1970). "*An Improved Read-in Technique For Optical Delay Line Correlators*," *Applied Optics*, 9, 135-147.

26. Lambert, L. B. (Mar. 1962). "*Wide-Band, Instantaneous Spectrum Analyzers Employing Delay-Line Light Modulators*" *IRE Int. Conv. Rec.*, fit. 6, 10, 69-78.
27. Damon, R. W., Maloney, W. T. and McMahon, D. H. (1970). "*Interaction of Light with Ultrasound: Phenomena and Applications in Physical Acoustics*," Vol. VII, W. P. Mason and R. N. Thurston, Eds., Academic Press, New York.
28. Balakshy, V. I. and Voloshin, A. S. (Jun. 2016). "*Anisotropic acousto-optic interaction in tellurium crystal with acoustic walk-off*," *Applied Optics*, 55, 4542- 4549.
29. Romer, G.R.B.E., and Bechtold, P. (2014). "*Electro-optic and acousto-optic laser beam scanners, - invited paper*," 8th International Conference on Photonic Technologies LANE, Phy. Pro., 54, 29-39.
30. Shcherbakov, A. S., Arellanes, A. O. and Chavushyan, V. (Sep. 2013). "*Optical Spectrometer with Acousto-Optic Dynamic Grating for Guillermo Haro Astrophysical Observatory*," *International Journal of Astronomy and Astrophysics*, 3, 376-384.
31. Chatterjee, M. and Chaparala, S.M. (2016). "*Nonlinear Dynamics, Bifurcation Maps and Signal Encryption and Decryption Using Acousto-Optic Chaos Under a Variable Aperture Illumination*," *Frontiers in Optics*, OSA Technical Digest (CD), paper #JW4A.73, Rochester, NY.
32. Chatterjee, M. R. and Almeahmadi, F.S. (2015). "*Secure Transmission and Retrieval of Images in Conjunction with Steganography Using Chaos in Nonlinear Acousto-Optic Feedback*," *Nonlinear Optics*, OSA Technical Digest(CD), paper #NF1A.6, Kauai, Hawaii.
33. Nering, E. D. (1974). *Elementary Linear Algebra* , W. B. Saunders Company, Philadelphia, p. 297.
34. Hemenway, P. (2005). *Divine Proportion Φ (Phi) in Art, Nature and Science*, Sterling Publications, New York, 14.
35. Faucette, W. M. (1996). "*A Geometric Interpretation of the Solution of the General Quartic Polynomial*." *Amer. Math. Monthly* 103, 51-57.
36. Uspensky, J.V. (1948). *Theory of Equations*, NY: McGraw-Hill Book Co., 82-98.
37. Beachy, J. and Blair, W. (1966). *Abstract Algebra*, 2nd ed, Prospect Hts, IL:

Waveland Press, Inc., 396-403

38. Beyer, W. H. (1987). *Handbook of Mathematical Sciences*, 6th ed. Boca Raton, FL: CRC Press, 1987b.
39. De Russo, P. M., Roy, R. J. Close, C. M. and Desrochers, A. A. (1966). *State Variables for Engineers*, 2nd ed. John Wiley and Sons Inc., New York, p. 276-281, 356.
40. Garvan, F. (2001). *The Maple Book*, 1st ed. Chapman and Hall/CRC Press.
41. Chapra, S. C. (2012). *Applied Numerical Methods with Matlab for Engineers and Scientists*, 3rd ed. NY: McGraw-Hill Book Co., 555-583.
42. Kraus, A. D. (2002). *Matrices for Engineers*, Oxford University Press, New York, 274-275.

Appendix A: Obtaining the Fourth-Order Differential Equation [20]

From (2.27), a system of differential equations is written as follows:

$$\frac{d\psi_{+1}(\xi)}{d\xi} - j\alpha e^{-jQ_c\xi} \psi_0(\xi), \quad (\text{A1})$$

$$\frac{d\psi_0(\xi)}{d\xi} = -j\alpha e^{jQ_c\xi} \psi_{+1}(\xi) - j\alpha \psi_{-1}(\xi), \quad (\text{A2})$$

$$\frac{d\psi_{-1}(\xi)}{d\xi} = -j\alpha e^{jQ_c\xi} \psi_{-2}(\xi) - j\alpha \psi_0(\xi), \quad (\text{A3})$$

$$\frac{d\psi_{-2}(\xi)}{d\xi} = -j\alpha e^{-jQ_c\xi} \psi_{-1}(\xi). \quad (\text{A4})$$

Using (A1) and (A4), $\psi_0(\xi)$ and $\psi_{-1}(\xi)$ are solved for as

$$\psi_0(\xi) = \frac{j e^{jQ_c\xi}}{\alpha} \frac{d\psi_{+1}(\xi)}{d\xi}, \quad (\text{A5})$$

$$\psi_{-1}(\xi) = \frac{j e^{jQ_c\xi}}{\alpha} \frac{d\psi_{-2}(\xi)}{d\xi}. \quad (\text{A6})$$

Backsubstitution of (A5) and (A6) into (A2) leads to the 2nd-order differential equation given by

$$\frac{d^2\psi_{+1}(\xi)}{d\xi^2} + jQ_c \frac{d\psi_{+1}(\xi)}{d\xi} + \alpha^2 \psi_{+1}(\xi) = -j\alpha \frac{d\psi_{-2}(\xi)}{d\xi}. \quad (\text{A7})$$

Similarly, backsubstitution of (A5) and (A6) into (A3) leads to

$$\frac{d^2\psi_{-2}(\xi)}{d\xi^2} + jQ_c \frac{d\psi_{-2}(\xi)}{d\xi} + \alpha^2 \psi_{-2}(\xi) = -j\alpha \frac{d\psi_{+1}(\xi)}{d\xi}. \quad (\text{A8})$$

Differentiating (A7) once result in

$$\frac{d^3\psi_{+1}(\xi)}{d\xi^3} + jQ_c \frac{d^2\psi_{+1}(\xi)}{d\xi^2} + \alpha^2 \frac{d\psi_{+1}(\xi)}{d\xi} = -j\alpha \frac{d^2\psi_{-2}(\xi)}{d\xi^2}. \quad (\text{A9})$$

Then substitution of the right-hand side of (A8) into (A9) leads to the 4th-order ordinary differential equation; (2.32) in the main text.

Appendix B: Derivation of Fourth-Order Differential Equation

Starting from (3.11), the differential equation as a system of differential equations is presented as follows:

$$\frac{d\psi_{+1}(\xi)}{d\xi} = -j\alpha e^{-j(x+b)\xi} \psi_0(\xi), \quad (\text{B1})$$

$$\frac{d\psi_0(\xi)}{d\xi} = -j\alpha \left(e^{+j(x+b)\xi} \psi_{+1}(\xi) + e^{-jx\xi} \psi_{-1}(\xi) \right), \quad (\text{B2})$$

$$\frac{d\psi_{-1}(\xi)}{d\xi} = -j\alpha \left(e^{+jx\xi} \psi_0(\xi) + e^{-j(x-b)\xi} \psi_{-2}(\xi) \right), \quad (\text{B3})$$

$$\frac{d\psi_{-2}(\xi)}{d\xi} = -j\alpha e^{+j(x-b)\xi} \psi_{-1}(\xi). \quad (\text{B4})$$

From (B1) and (B4), $\psi_0(\xi)$ and $\psi_{-1}(\xi)$ is solved for respectively as:

$$\psi_0(\xi) = \frac{j e^{+j(x+b)\xi}}{\alpha} \frac{d\psi_{+1}(\xi)}{d\xi} \quad (\text{B5})$$

and

$$\psi_{-1}(\xi) = \frac{j e^{-j(x-b)\xi}}{\alpha} \frac{d\psi_{-2}(\xi)}{d\xi}. \quad (\text{B6})$$

The derivative of both sides of (B5) and (B6) is obtained as:

$$\frac{d\psi_0(\xi)}{d\xi} = \frac{j}{\alpha} \left(e^{+j(x+b)\xi} \frac{d^2\psi_{+1}(\xi)}{d\xi^2} + j(x+b) e^{+j(x+b)\xi} \frac{d\psi_{+1}(\xi)}{d\xi} \right) \quad (\text{B7})$$

and

$$\frac{d\psi_{-1}(\xi)}{d\xi} = \frac{j}{\alpha} \left(e^{-j(x-b)\xi} \frac{d^2\psi_{-2}(\xi)}{d\xi^2} - j(x-b) e^{-j(x-b)\xi} \frac{d\psi_{-2}(\xi)}{d\xi} \right). \quad (\text{B8})$$

Back substitution of (B6) and (B7) into (B2) leads to the 2nd-order differential equation

$$\frac{d^2\psi_{+1}(\xi)}{d\xi^2} + j(x+b) \frac{d\psi_{+1}(\xi)}{d\xi} + \alpha^2 \psi_{+1}(\xi) = -j\alpha e^{-j3x\xi} \frac{d\psi_{-2}(\xi)}{d\xi}. \quad (\text{B9})$$

Similarly back substitution of (B5) and (B8) into (B3) leads to:

$$\frac{d^2\psi_{-2}(\xi)}{d\xi^2} - j(x-b) \frac{d\psi_{-2}(\xi)}{d\xi} + \alpha^2 \psi_{-2}(\xi) = -j\alpha e^{+j3x\xi} \frac{d\psi_{+1}(\xi)}{d\xi}. \quad (\text{B10})$$

From (B10), $\frac{d\psi_{+1}(\xi)}{d\xi}$ is solved for as

Appendix B (Continued)

$$\frac{d\psi_{+1}(\xi)}{d\xi} = \frac{j}{\alpha} e^{-j3x\xi} \left(\frac{d^2\psi_{-2}(\xi)}{d\xi^2} - j(x-b) \frac{d\psi_{-2}(\xi)}{d\xi} + \alpha^2 \psi_{-2}(\xi) \right). \quad (\text{B11})$$

The 1st and 2nd derivative of (B11) is taken as:

$$\begin{aligned} \frac{d^2\psi_{+1}(\xi)}{d\xi^2} = \frac{1}{\alpha} e^{-j3x\xi} \left(j \left(\frac{d^3\psi_{-2}(\xi)}{d\xi^3} - j(x-b) \frac{d^2\psi_{-2}(\xi)}{d\xi^2} + \alpha^2 \frac{d\psi_{-2}(\xi)}{d\xi} \right) \right. \\ \left. + 3x \left(\frac{d^2\psi_{-2}(\xi)}{d\xi^2} - j(x-b) \frac{d\psi_{-2}(\xi)}{d\xi} + \alpha^2 \psi_{-2}(\xi) \right) \right), \end{aligned} \quad (\text{B12})$$

$$\begin{aligned} \frac{d^3\psi_{+1}(\xi)}{d\xi^3} = \frac{1}{\alpha} e^{-j3x\xi} \left(j \left(\frac{d^4\psi_{-2}(\xi)}{d\xi^4} - j(x-b) \frac{d^3\psi_{-2}(\xi)}{d\xi^3} + \alpha^2 \frac{d^2\psi_{-2}(\xi)}{d\xi^2} \right) \right. \\ \left. + 6x \left(\frac{d^3\psi_{-2}(\xi)}{d\xi^3} - j(x-b) \frac{d^2\psi_{-2}(\xi)}{d\xi^2} + \alpha^2 \frac{d\psi_{-2}(\xi)}{d\xi} \right) \right. \\ \left. - j9x^2 \left(\frac{d^2\psi_{-2}(\xi)}{d\xi^2} - j(x-b) \frac{d\psi_{-2}(\xi)}{d\xi} + \alpha^2 \psi_{-2}(\xi) \right) \right). \end{aligned} \quad (\text{B13})$$

By obtaining the differentiation of (B9) as

$$\frac{d^3\psi_{+1}(\xi)}{d\xi^3} + j(x+b) \frac{d^2\psi_{+1}(\xi)}{d\xi^2} + \alpha^2 \frac{d\psi_{+1}(\xi)}{d\xi} = -\alpha e^{-j3x\xi} \left(j \frac{d^2\psi_{-2}(\xi)}{d\xi^2} + 3x \frac{d\psi_{-2}(\xi)}{d\xi} \right) \quad (\text{B14})$$

and substitution (B11), (B12) and (B13) to the LHS of (B14) leads to the 4th-order DE

$$\begin{aligned} \frac{d^4\psi_{-2}(\xi)}{d\xi^4} + j(2b-6x) \frac{d^3\psi_{-2}(\xi)}{d\xi^3} + (3\alpha^2 - 11x^2 + 9bx - b^2) \frac{d^2\psi_{-2}(\xi)}{d\xi^2} \\ + j(6x^3 - 9bx^2 + (3b^2 - 9\alpha^2)x + 2\alpha^2b) \frac{d\psi_{-2}(\xi)}{d\xi} + (3\alpha^2bx - 6\alpha^2x^2 + \alpha^4) \psi_{-2}(\xi) = 0. \end{aligned} \quad (\text{B15})$$

Note that (B15) is a linear homogeneous constant coefficient differential equation suggests that the existence of 4 independent solutions all of the form

$$\psi_{-2}(\xi) \doteq e^{jr\xi}. \quad (\text{B16a})$$

The 1st - 4th derivative of (B16a) are

$$\frac{d\psi_{-2}(\xi)}{d\xi} \doteq jre^{jr\xi}, \quad (\text{B16b})$$

$$\frac{d^2\psi_{-2}(\xi)}{d\xi^2} \doteq -r^2 e^{jr\xi}, \quad (\text{B16c})$$

$$\frac{d^3\psi_{-2}(\xi)}{d\xi^3} \doteq -jr^3 e^{jr\xi}, \quad (\text{B16d})$$

Appendix B (Continued)

$$\frac{d^4 \psi_{-2}(\xi)}{d\xi^4} \doteq r^4 e^{jr\xi}. \quad (\text{B16e})$$

Backsubstitution of (B16a) - (B16e) into (B15) and canceling $e^{jr\xi}$ on both sides of the equation produces the 4th degree polynomial in coefficient 'r' as seen in the main text (3.24)

Appendix C: Obtaining the Quartic Roots using the Ferrari Approach

Starting from the characteristic quartic equation in (3.24),

$$r^4 + (2b - 6x)r^3 + (-3\alpha^2 + 11x^2 - 9bx + b^2)r^2 + (-6x^3 + 9bx^2 - (3b^2 - 9\alpha^2)x - 2\alpha^2b)r + (3\alpha^2bx - 6\alpha^2x^2 + \alpha^4) = 0. \quad (C1)$$

Using in (C1),

$$r = y - \frac{2b - 6x}{4}. \quad (C2)$$

After simplification and re-grouping of like terms, results in

$$y^4 + \left(-\frac{1}{2}b^2 - \frac{5}{2}x^2 - 3\alpha^2\right)y^2 + (\alpha^2b - 2bx^2)y + \left(\frac{3}{4}\alpha^2x^2 + \frac{1}{4}\alpha^2b^2 + \frac{1}{16}b^4 + \frac{9}{16}x^4 - \frac{5}{8}b^2x^2 + \alpha^4\right) = 0. \quad (C3)$$

(C3) is a depressed quartic and expressed as

$$y^4 + py^2 + qy + dr = 0 \quad (C4)$$

where

$$p = -\left(\frac{1}{2}b^2 + \frac{5}{2}x^2 + 3\alpha^2\right), \quad (C5a)$$

$$q = \alpha^2b - 2bx^2, \quad (C5b)$$

$$dr = \frac{3}{4}\alpha^2x^2 + \frac{1}{4}\alpha^2b^2 + \frac{1}{16}b^4 + \frac{9}{16}x^4 - \frac{5}{8}b^2x^2 + \alpha^4. \quad (C5c)$$

(C4) is made a perfect square after adding $y^2z + \frac{z^2}{4}$ to both sides, thus,

$$\left(y^2 + \frac{z}{2}\right)^2 = (z - p)y^2 - qy + \left(\frac{z^2}{4} - dr\right) \equiv (my + k)^2, \quad (C6)$$

where m and k are to be determined later on. As observed, (C6) is quadratic in y such that

$$\left(y^2 + \frac{z}{2}\right) = \pm(my + k). \quad (C7)$$

Now, consider having an equation which is quadratic in x ,

$$ax^2 + bx + c = 0. \quad (C8)$$

Appendix C (Continued)

(C8) has the solutions

$$x_{1,2} = -\frac{b}{2a} \pm \frac{1}{2a} (b^2 - 4ac)^{1/2} \quad (\text{C9})$$

and that (C8) is a perfect square when its discriminant is zero, thus

$$b^2 - 4ac = 0. \quad (\text{C10})$$

By comparing the constant coefficients of (C8) with that of the middle expression in (C6), and thereafter, paralleled in (C10) thus returns

$$q^2 - 4(z-p) \left(\frac{z^2}{4} - dr \right) = 0. \quad (\text{C11})$$

Simplification of (C11) leads to the resolvent cubic in z as

$$z^3 - pz^2 - 4drz + (4pdr - q^2) = 0. \quad (\text{C12})$$

Back substitution of (C5) in (C12) and simplification yields

$$\begin{aligned} z^3 + \left(\frac{1}{2}b^2 + \frac{5}{2}x^2 + 3\alpha^2 \right) z^2 - \left(3\alpha^2 x^2 + \alpha^2 b^2 + \frac{1}{4}b^4 + \frac{9}{4}x^4 - \frac{5}{2}b^2 x^2 + 4\alpha^4 \right) z + \frac{15}{2}b^2 \alpha^2 x^2 \\ - \frac{5}{4}\alpha^2 b^4 - \frac{1}{8}b^6 + \frac{9}{8}b^2 x^4 + \frac{5}{8}b^4 x^2 - 6\alpha^4 b^2 - \frac{57}{4}x^4 \alpha^2 - \frac{45}{8}x^6 - 19\alpha^4 x^2 - 12\alpha^6 = 0. \end{aligned} \quad (\text{C13})$$

The resolvent cubic roots after solving for z in (C13) are

$$z_1 = \frac{1}{6}w^{1/3} + 2H - \frac{1}{6}b^2 - \frac{5}{6}x^2 - \alpha^2, \quad (\text{C14a})$$

$$z_2 = -\frac{1}{12}w^{1/3} - H - \frac{1}{6}b^2 - \frac{5}{6}x^2 - \alpha^2 + I \frac{\sqrt{3}}{2} \left(\frac{1}{6}w^{1/3} - 2H \right), \quad (\text{C14b})$$

$$z_3 = -\frac{1}{12}w^{1/3} - H - \frac{1}{6}b^2 - \frac{5}{6}x^2 - \alpha^2 - I \frac{\sqrt{3}}{2} \left(\frac{1}{6}w^{1/3} - 2H \right), \quad (\text{C14c})$$

where

$$H = \left(8\alpha^2 x^2 + 2\alpha^2 b^2 - \frac{5}{3}x^2 b^2 + \frac{1}{3}b^4 + \frac{13}{3}x^4 + 7\alpha^4 \right) w^{-1/3} \quad (\text{C15a})$$

$$w = w_1 + w_2 + 12(w_3 + w_4 + w_5 + w_6 + w_7)^{1/2} \quad (\text{C15b})$$

Appendix C (Continued)

and the components of w are as follows:

$$w_1 = \left(-864b^2\alpha^2 + 36(16x^2 + 23\alpha^2)\alpha^2 - 12(x^2 + 5b^2)b^2 + 280x^4 \right) x^2, \quad (\text{C16a})$$

$$w_2 = 72(b^2 + 5\alpha^2)b^2\alpha^2 + 8(b^6 + 81\alpha^6), \quad (\text{C16b})$$

$$w_3 = \left(-3162\alpha^2x^2 - 9420\alpha^4 + 4110\alpha^2b^2 \right) \alpha^2x^4b^2, \quad (\text{C16c})$$

$$w_4 = \left(-4848\alpha^4 - 936\alpha^2b^2 + 684x^2b^2 - 648x^4 \right) \alpha^2x^2b^4, \quad (\text{C16d})$$

$$w_5 = \left(-108\alpha^2b^6 - 648\alpha^2x^6 - 8760\alpha^8 - 27(x^2b^6 - 10x^4b^4 + 33b^2x^6 - 40x^8) \right) x^2b^2, \quad (\text{C16e})$$

$$w_6 = \left(-3(4824\alpha^4x^4 + 3064\alpha^2x^6 + 4609\alpha^6x^2 + 1056x^8 + 2220\alpha^8) \alpha^2 - 432x^{10} \right) x^2, \quad (\text{C16f})$$

$$w_7 = -48(\alpha^6b^2 + 6\alpha^8)\alpha^2b^2 - 1200\alpha^{12}. \quad (\text{C16g})$$

It then follows that m and k in (C6) can be determined after equating the expanded RHS with the middle expression as

$$m^2y^2 + 2mky + k^2 = (z-p)y^2 - qy + \left(\frac{z^2}{4} - dr \right) \quad (\text{C17})$$

such that by comparing the LHS and RHS (C17) reveals that

$$m = \pm(z-p)^{1/2} \quad (\text{C18a})$$

and

$$k = -\frac{q}{2m}. \quad (\text{C18b})$$

More explicitly, after choosing m in (C18a) as

$$m = -(z-p)^{1/2} \quad (\text{C19a})$$

invariably makes

$$k = \frac{q}{2}(z-p)^{-1/2}. \quad (\text{C19b})$$

Appendix C (Continued)

Also, equating LHS and RHS of (C7) implies

$$y^2 - my + \left(\frac{1}{2}z - k\right) = 0 \quad (\text{C20a})$$

and

$$y^2 + my + \left(\frac{1}{2}z + k\right) = 0. \quad (\text{C20b})$$

Using quadratic formula, (C20) has the solution as

$$y_{1,3} = \frac{1}{2}m \pm \frac{1}{2} \left(m^2 - 4 \left(\frac{1}{2}z - k \right) \right)^{\frac{1}{2}} \quad (\text{C21a})$$

and

$$y_{2,4} = -\frac{1}{2}m \pm \frac{1}{2} \left(m^2 - 4 \left(\frac{1}{2}z + k \right) \right)^{\frac{1}{2}}. \quad (\text{C21b})$$

Using (C19) in (C21) implies that

$$y_{1,3} = -\frac{1}{2} \left\{ (z-p)^{\frac{1}{2}} \mp \left[-(z+p) + 2q(z-p)^{-\frac{1}{2}} \right]^{\frac{1}{2}} \right\} \quad (\text{C22a})$$

and

$$y_{2,4} = \frac{1}{2} \left\{ (z-p)^{\frac{1}{2}} \pm \left[-(z+p) - 2q(z-p)^{-\frac{1}{2}} \right]^{\frac{1}{2}} \right\}. \quad (\text{C22b})$$

Substitute (C5a), (C5c) and (C14a) in the terms in (C22) as:

$$(z-p)^{\frac{1}{2}} = \left(\frac{1}{6}w^{1/3} + 2H + \frac{1}{3}b^2 + \frac{5}{3}x^2 + 2\alpha^2 \right)^{\frac{1}{2}}, \quad (\text{C23a})$$

$$-(z+p) = -\frac{1}{6}w^{1/3} - 2H + \frac{2}{3}b^2 + \frac{10}{3}x^2 + 4\alpha^2, \quad (\text{C23b})$$

$$2q(z-p)^{-\frac{1}{2}} = (2\alpha^2b - 4bx^2) \left(\frac{1}{6}w^{1/3} + 2H + \frac{1}{3}b^2 + \frac{5}{3}x^2 + 2\alpha^2 \right)^{-\frac{1}{2}}, \quad (\text{C23c})$$

where

$$H = \left(8\alpha^2x^2 + 2\alpha^2b^2 - \frac{5}{3}x^2b^2 + \frac{1}{3}b^4 + \frac{13}{3}x^4 + 7\alpha^4 \right) w^{-1/3} \quad (\text{C24})$$

Appendix C (Continued)

Put (C23) in (C22)

$$y_{1,3} = -\frac{1}{2} \left\{ \left(\frac{1}{6} w^{1/3} + 2H + \frac{1}{3} b^2 + \frac{5}{3} x^2 + 2\alpha^2 \right)^{1/2} \mp \left[-\frac{1}{6} w^{1/3} - 2H + \frac{2}{3} b^2 + \frac{10}{3} x^2 + 4\alpha^2 + (2\alpha^2 b - 4bx^2) \left(\frac{1}{6} w^{1/3} + 2H + \frac{1}{3} b^2 + \frac{5}{3} x^2 + 2\alpha^2 \right)^{-1/2} \right]^{1/2} \right\} \quad (\text{C25a})$$

and

$$y_{2,4} = \frac{1}{2} \left\{ \left(\frac{1}{6} w^{1/3} + 2H + \frac{1}{3} b^2 + \frac{5}{3} x^2 + 2\alpha^2 \right)^{1/2} \pm \left[-\frac{1}{6} w^{1/3} - 2H + \frac{2}{3} b^2 + \frac{10}{3} x^2 + 4\alpha^2 - (2\alpha^2 b - 4bx^2) \left(\frac{1}{6} w^{1/3} + 2H + \frac{1}{3} b^2 + \frac{5}{3} x^2 + 2\alpha^2 \right)^{-1/2} \right]^{1/2} \right\}. \quad (\text{C25b})$$

Finally, substitution of (C25) in (C2) gives the roots in the main text

$$r_1 = -\frac{1}{2}(b-3x) - \frac{1}{2} \left(\frac{1}{6} w^{1/3} + 2H + \frac{1}{3} b^2 + \frac{5}{3} x^2 + 2\alpha^2 \right)^{1/2} + \frac{1}{2} \left[-\frac{1}{6} w^{1/3} - 2H + \frac{2}{3} b^2 + \frac{10}{3} x^2 + 4\alpha^2 + (2\alpha^2 b - 4bx^2) \left(\frac{1}{6} w^{1/3} + 2H + \frac{1}{3} b^2 + \frac{5}{3} x^2 + 2\alpha^2 \right)^{-1/2} \right]^{1/2}, \quad (\text{C26a})$$

$$r_2 = -\frac{1}{2}(b-3x) + \frac{1}{2} \left(\frac{1}{6} w^{1/3} + 2H + \frac{1}{3} b^2 + \frac{5}{3} x^2 + 2\alpha^2 \right)^{1/2} + \frac{1}{2} \left[-\frac{1}{6} w^{1/3} - 2H + \frac{2}{3} b^2 + \frac{10}{3} x^2 + 4\alpha^2 - (2\alpha^2 b - 4bx^2) \left(\frac{1}{6} w^{1/3} + 2H + \frac{1}{3} b^2 + \frac{5}{3} x^2 + 2\alpha^2 \right)^{-1/2} \right]^{1/2}, \quad (\text{C26b})$$

$$r_3 = -\frac{1}{2}(b-3x) - \frac{1}{2} \left(\frac{1}{6} w^{1/3} + 2H + \frac{1}{3} b^2 + \frac{5}{3} x^2 + 2\alpha^2 \right)^{1/2} - \frac{1}{2} \left[-\frac{1}{6} w^{1/3} - 2H + \frac{2}{3} b^2 + \frac{10}{3} x^2 + 4\alpha^2 + (2\alpha^2 b - 4bx^2) \left(\frac{1}{6} w^{1/3} + 2H + \frac{1}{3} b^2 + \frac{5}{3} x^2 + 2\alpha^2 \right)^{-1/2} \right]^{1/2}, \quad (\text{C26c})$$

$$r_4 = -\frac{1}{2}(b-3x) + \frac{1}{2} \left(\frac{1}{6} w^{1/3} + 2H + \frac{1}{3} b^2 + \frac{5}{3} x^2 + 2\alpha^2 \right)^{1/2} - \frac{1}{2} \left[-\frac{1}{6} w^{1/3} - 2H + \frac{2}{3} b^2 + \frac{10}{3} x^2 + 4\alpha^2 - (2\alpha^2 b - 4bx^2) \left(\frac{1}{6} w^{1/3} + 2H + \frac{1}{3} b^2 + \frac{5}{3} x^2 + 2\alpha^2 \right)^{-1/2} \right]^{1/2}. \quad (\text{C26d})$$

Appendix C (Continued)

Or equivalently, (C26) is compactly written as

$$r_1 = -\frac{1}{2}P - \frac{1}{2}Q + \frac{1}{2}R, \quad (\text{C27a})$$

$$r_2 = -\frac{1}{2}P + \frac{1}{2}Q + \frac{1}{2}S, \quad (\text{C27b})$$

$$r_3 = -\frac{1}{2}P - \frac{1}{2}Q - \frac{1}{2}R, \quad (\text{C27c})$$

$$r_4 = -\frac{1}{2}P + \frac{1}{2}Q - \frac{1}{2}S, \quad (\text{C27d})$$

where

$$P = (b - 3x), \quad (\text{C28a})$$

$$Q = \left(\frac{1}{6}w^{1/3} + 2H + \frac{1}{3}b^2 + \frac{5}{3}x^2 + 2\alpha^2 \right)^{1/2}, \quad (\text{C28b})$$

$$R = \left[\left(-\frac{1}{6}w^{1/3} - 2H + \frac{2}{3}b^2 + \frac{10}{3}x^2 + 4\alpha^2 \right) + (2\alpha^2b - 4bx^2)Q^{-1} \right]^{1/2}, \quad (\text{C28c})$$

$$S = \left[\left(-\frac{1}{6}w^{1/3} - 2H + \frac{2}{3}b^2 + \frac{10}{3}x^2 + 4\alpha^2 \right) - (2\alpha^2b - 4bx^2)Q^{-1} \right]^{1/2}, \quad (\text{C28d})$$

Appendix D: Test of Roots as Related to Coefficients (Vieta's Theorem)

Starting from the quartic polynomial

$$r^4 + (2b - 6x)r^3 + (-3\alpha^2 + 11x^2 - 9bx + b^2)r^2 + (-6x^3 + 9bx^2 - (3b^2 - 9\alpha^2)x - 2\alpha^2b)r + (3\alpha^2bx - 6\alpha^2x^2 + \alpha^4) = 0. \quad (D1)$$

(D1) has the following roots

$$r_1 = -\frac{1}{2}P - \frac{1}{2}Q + \frac{1}{2}R, \quad (D2a)$$

$$r_2 = -\frac{1}{2}P + \frac{1}{2}Q + \frac{1}{2}S, \quad (D2b)$$

$$r_3 = -\frac{1}{2}P - \frac{1}{2}Q - \frac{1}{2}R, \quad (D2c)$$

$$r_4 = -\frac{1}{2}P + \frac{1}{2}Q - \frac{1}{2}S, \quad (D2d)$$

where

$$P = (b - 3x), \quad (D3a)$$

$$Q = \left(\frac{1}{6}w^{1/3} + 2H + \frac{1}{3}b^2 + \frac{5}{3}x^2 + 2\alpha^2 \right)^{1/2}, \quad (D3b)$$

$$R = \left[\left(-\frac{1}{6}w^{1/3} - 2H + \frac{2}{3}b^2 + \frac{10}{3}x^2 + 4\alpha^2 \right) + (2\alpha^2b - 4bx^2)Q^{-1} \right]^{1/2}, \quad (D3c)$$

$$S = \left[\left(-\frac{1}{6}w^{1/3} - 2H + \frac{2}{3}b^2 + \frac{10}{3}x^2 + 4\alpha^2 \right) - (2\alpha^2b - 4bx^2)Q^{-1} \right]^{1/2}. \quad (D3d)$$

Now, given a general quartic polynomial as

$$r^4 + a_1r^3 + a_2r^2 + a_3r + a_4 = 0. \quad (D4)$$

Conclusion drawn after comparison of (D1) with (D4) is that

$$a_1 \equiv 2b - 6x, \quad (D5a)$$

$$a_2 \equiv b^2 - 3\alpha^2 - 9bx + 11x^2, \quad (D5b)$$

Appendix D (Continued)

$$a_3 \equiv 9bx^2 - 6x^3 + 9x\alpha^2 - 3b^2x - 2\alpha^2b, \quad (\text{D5c})$$

$$a_4 \equiv 3\alpha^2bx - 6\alpha^2x^2 + \alpha^4. \quad (\text{D5d})$$

Using Vieta's formula, the roots (r_1, r_2, r_3, r_4) , as related to the coefficients of the characteristic quartic equation [see (D1)] is verified as follows:

$$r_1 + r_2 + r_3 + r_4 = -a_1, \quad (\text{D6a})$$

$$r_1r_2 + r_3r_4 + r_2r_3 + r_1r_4 + r_1r_3 + r_2r_4 = a_2, \quad (\text{D6b})$$

$$r_1r_2r_3 + r_1r_2r_4 + r_1r_3r_4 + r_2r_3r_4 = -a_3, \quad (\text{D6c})$$

$$r_1r_2r_3r_4 = a_4. \quad (\text{D6d})$$

Test 1. $r_1 + r_2 + r_3 + r_4 = -a_1$.

The sum of all the roots from (D2) yields

$$r_1 + r_2 + r_3 + r_4 = -2P \quad (\text{D7})$$

and backsubstitution of (D3a) in (D7) leads to the confirmation of (D6a)

$$r_1 + r_2 + r_3 + r_4 = -2(b - 3x) = -(2b - 6x) \equiv -a_1. \quad (\text{D8})$$

Test 2. $r_1r_2 + r_3r_4 + r_2r_3 + r_1r_4 + r_1r_3 + r_2r_4 = a_2$.

Also, taking the product of two roots from (D2) at a time is analyzed as follows:

$$r_1r_2 = \frac{1}{4}(P^2 - PS - Q^2 - QS - RP + RQ + RS), \quad (\text{D9a})$$

$$r_2r_3 = \frac{1}{4}(P^2 + RP - Q^2 - RQ - PS - QS - RS), \quad (\text{D9b})$$

$$r_3r_4 = \frac{1}{4}(P^2 + PS - Q^2 + QS + RP - RQ + RS), \quad (\text{D9c})$$

$$r_1r_4 = \frac{1}{4}(P^2 + PS - Q^2 + QS - RP + RQ - RS), \quad (\text{D9d})$$

Appendix D (Continued)

$$r_1 r_3 = \frac{1}{4}(P^2 + 2PQ + Q^2 - R^2), \quad (\text{D9e})$$

$$r_2 r_4 = \frac{1}{4}(P^2 - 2PQ + Q^2 - S^2). \quad (\text{D9f})$$

Thus, (D9a) + (D9c) = (D10a), (D9b) + (D9d) = (D10b), and (D9e) + (D9f) = (D10c)

$$r_1 r_2 + r_3 r_4 = \frac{1}{2}(P^2 - Q^2 + RS), \quad (\text{D10a})$$

$$r_2 r_3 + r_1 r_4 = \frac{1}{2}(P^2 - Q^2 - RS), \quad (\text{D10b})$$

$$r_1 r_3 + r_2 r_4 = \frac{1}{4}(2P^2 + 2Q^2 - R^2 - S^2). \quad (\text{D10c})$$

Now, (D10a) + (D10b) = (D11)

$$r_1 r_2 + r_3 r_4 + r_2 r_3 + r_1 r_4 = P^2 - Q^2. \quad (\text{D11})$$

Finally, (D10c) + (D11) = (D12)

$$r_1 r_2 + r_3 r_4 + r_2 r_3 + r_1 r_4 + r_1 r_3 + r_2 r_4 = \frac{1}{2}(3P^2 - Q^2) - \frac{1}{4}(R^2 + S^2). \quad (\text{D12})$$

Breaking (D12) into term wise and applying (D3) such that

$$\frac{3}{2}P^2 = \frac{3}{2}b^2 - 9bx + \frac{27}{2}x^2, \quad (\text{D13a})$$

$$-\frac{1}{2}Q^2 = -\frac{1}{12}w^{1/3} - H - \frac{1}{6}b^2 - \frac{5}{6}x^2 - \alpha^2, \quad (\text{D13b})$$

$$-\frac{1}{4}(R^2 + S^2) = \frac{1}{12}w^{1/3} + H - \frac{1}{3}b^2 - \frac{5}{3}x^2 - 2\alpha^2. \quad (\text{D13c})$$

Lastly, backsubstitution of (D13) in (D12) confirms (D6b) as

$$r_1 r_2 + r_3 r_4 + r_2 r_3 + r_1 r_4 + r_1 r_3 + r_2 r_4 = b^2 - 9bx + 11x^2 - 3\alpha^2 \equiv a_2. \quad (\text{D14})$$

Test 3. $r_1 r_2 r_3 + r_1 r_2 r_4 + r_1 r_3 r_4 + r_2 r_3 r_4 = -a_3$.

It is known from (D2) that

$$r_1 r_2 r_3 = -\frac{1}{8}(P^3 + P^2Q - P^2S - PQ^2 - Q^3 - Q^2S - PR^2 + QR^2 + R^2S - 2PQS), \quad (\text{D15a})$$

$$r_1 r_2 r_4 = -\frac{1}{8}(P^3 - P^2Q - PS^2 - PQ^2 + Q^3 - QS^2 - P^2R - Q^2R + RS^2 + 2PQR), \quad (\text{D15b})$$

Appendix D (Continued)

$$r_1 r_3 r_4 = -\frac{1}{8} \left(P^3 + P^2 Q + P^2 S - P Q^2 - Q^3 + Q^2 S - P R^2 + Q R^2 - R^2 S + 2 P Q S \right), \quad (\text{D15c})$$

$$r_2 r_3 r_4 = -\frac{1}{8} \left(P^3 - P^2 Q + P^2 R - P Q^2 + Q^3 + Q^2 R - P S^2 - Q S^2 - R S^2 - 2 P Q R \right). \quad (\text{D15d})$$

Adding up (D15) gives

$$r_1 r_2 r_3 + r_1 r_2 r_4 + r_1 r_3 r_4 + r_2 r_3 r_4 = \frac{1}{4} \left(P S^2 + Q S^2 + P R^2 - Q R^2 + 2 P Q^2 - 2 P^3 \right). \quad (\text{D16})$$

Finally, the substitution of (D3) in (D16) confirms (D6c) as

$$r_1 r_2 r_3 + r_1 r_2 r_4 + r_1 r_3 r_4 + r_2 r_3 r_4 = - \left(9 b x^2 - 6 x^3 + 9 x \alpha^2 - 3 b^2 x - 2 \alpha^2 b \right) \equiv -a_3. \quad (\text{D17})$$

Test 4. $r_1 r_2 r_3 r_4 = a_4$.

Again, it is known from (D2) that

$$r_1 r_2 r_3 r_4 = \frac{1}{16} \left(2 P Q (R^2 - S^2) - (P^2 + Q^2) (R^2 + S^2) + R^2 S^2 - (2 P^2 - Q^2) Q^2 + P^4 \right). \quad (\text{D18})$$

Due to symbolic complexity which is beyond maple capabilities, a numerical program i.e., space simulation, has been run to confirm the validity of (D6d).

Appendix E: Derivation of Homogeneous Solution of All Order

By recalling (3.20) as

$$\frac{d\psi_{+1}(\xi)}{d\xi} = -j\alpha e^{-j(x+b)\xi} \psi_0(\xi), \quad (\text{E1a})$$

$$\frac{d\psi_0(\xi)}{d\xi} = -j\alpha \left(e^{+j(x+b)\xi} \psi_{+1}(\xi) + e^{-jx\xi} \psi_{-1}(\xi) \right), \quad (\text{E1b})$$

$$\frac{d\psi_{-1}(\xi)}{d\xi} = -j\alpha \left(e^{+jx\xi} \psi_0(\xi) + e^{-j(x-b)\xi} \psi_{-2}(\xi) \right), \quad (\text{E1c})$$

$$\frac{d\psi_{-2}(\xi)}{d\xi} = -j\alpha e^{+j(x-b)\xi} \psi_{-1}(\xi). \quad (\text{E1d})$$

It is observed after a series of steps (see Appendix B) that (E1) led to

$$\begin{aligned} & \frac{d^4\psi_{-2}(\xi)}{d\xi^4} + j(2b-6x) \frac{d^3\psi_{-2}(\xi)}{d\xi^3} + (3\alpha^2 - 11x^2 + 9bx - b^2) \frac{d^2\psi_{-2}(\xi)}{d\xi^2} \\ & + j(6x^3 - 9bx^2 + (3b^2 - 9\alpha^2)x + 2\alpha^2b) \frac{d\psi_{-2}(\xi)}{d\xi} + (3\alpha^2bx - 6\alpha^2x^2 + \alpha^4) \psi_{-2}(\xi) = 0. \end{aligned} \quad (\text{E2})$$

Now, the general solution to (E2) is a superposition of four homogeneous solutions,

$$\psi_{-2}(\xi) = Ae^{jr_1\xi} + Be^{jr_2\xi} + Ce^{jr_3\xi} + De^{jr_4\xi}. \quad (\text{E3})$$

The 1st derivative of (E3) is obtained as

$$\frac{d\psi_{-2}(\xi)}{d\xi} = j(r_1Ae^{jr_1\xi} + r_2Be^{jr_2\xi} + r_3Ce^{jr_3\xi} + r_4De^{jr_4\xi}). \quad (\text{E4})$$

Then solving for $\psi_{-1}(\xi)$ in (E1d) yields

$$\psi_{-1}(\xi) = \frac{je^{-j(x-b)\xi}}{\alpha} \frac{d\psi_{-2}(\xi)}{d\xi}. \quad (\text{E5})$$

Substitution of (E4) in (E5) leads to -1-order homogeneous solution as

$$\psi_{-1}(\xi) = -\frac{1}{\alpha} e^{-j(x-b)\xi} \left(r_1Ae^{jr_1\xi} + r_2Be^{jr_2\xi} + r_3Ce^{jr_3\xi} + r_4De^{jr_4\xi} \right). \quad (\text{E6})$$

Similarly, solving for $\psi_0(\xi)$ in (E1c) gives

$$\psi_0(\xi) = \frac{je^{-jx\xi}}{\alpha} \frac{d\psi_{-1}(\xi)}{d\xi} - e^{-j(2x-b)\xi} \psi_{-2}(\xi). \quad (\text{E7})$$

Appendix E (Continued)

The 1st derivative of (E6) returns

$$\begin{aligned} \frac{d\psi_{-1}(\xi)}{d\xi} = & -\frac{j}{\alpha} e^{-j(x-b)\xi} \left((r_1^2 A e^{jr_1\xi} + r_2^2 B e^{jr_2\xi} + r_3^2 C e^{jr_3\xi} + r_4^2 D e^{jr_4\xi}) \right. \\ & \left. -(x-b)(r_1 A e^{jr_1\xi} + r_2 B e^{jr_2\xi} + r_3 C e^{jr_3\xi} + r_4 D e^{jr_4\xi}) \right). \end{aligned} \quad (\text{E8})$$

Through substitution of (E3) and (E8) in (E7) gives 0-order homogeneous solution

$$\begin{aligned} \psi_0(\xi) = & \frac{1}{\alpha^2} e^{-j(2x-b)\xi} \left((r_1^2 - (x-b)r_1 - \alpha^2) A e^{jr_1\xi} + (r_2^2 - (x-b)r_2 - \alpha^2) B e^{jr_2\xi} \right. \\ & \left. + (r_3^2 - (x-b)r_3 - \alpha^2) C e^{jr_3\xi} + (r_4^2 - (x-b)r_4 - \alpha^2) D e^{jr_4\xi} \right). \end{aligned} \quad (\text{E9})$$

Also, $\psi_{+1}(\xi)$ can be solved for in (E1b) as

$$\psi_{+1}(\xi) = \frac{j}{\alpha} e^{-j(x+b)\xi} \frac{d\psi_0(\xi)}{d\xi} - e^{-j(2x+b)\xi} \psi_{-1}(\xi). \quad (\text{E10})$$

The 1st derivatives of (E9) leads to

$$\begin{aligned} \frac{d\psi_0(\xi)}{d\xi} = & \frac{j}{\alpha^2} e^{-j(2x-b)\xi} \left(r_1^3 - (3x-2b)r_1^2 + (2x^2 - 3bx + b^2 - \alpha^2)r_1 + \alpha^2(2x-b) \right) A e^{jr_1\xi} \\ & + \left(r_2^3 - (3x-2b)r_2^2 + (2x^2 - 3bx + b^2 - \alpha^2)r_2 + \alpha^2(2x-b) \right) B e^{jr_2\xi} \\ & + \left(r_3^3 - (3x-2b)r_3^2 + (2x^2 - 3bx + b^2 - \alpha^2)r_3 + \alpha^2(2x-b) \right) C e^{jr_3\xi} \\ & + \left(r_4^3 - (3x-2b)r_4^2 + (2x^2 - 3bx + b^2 - \alpha^2)r_4 + \alpha^2(2x-b) \right) D e^{jr_4\xi}. \end{aligned} \quad (\text{E11})$$

Substitution of (E6) and (E11) in (E10) concludes the +1-order homogeneous solution as

$$\begin{aligned} \psi_{+1}(\xi) = & -\frac{1}{\alpha^3} e^{-j3x\xi} \left(r_1^3 - (3x-2b)r_1^2 + (2x^2 - 3bx + b^2 - 2\alpha^2)r_1 + \alpha^2(2x-b) \right) A e^{jr_1\xi} \\ & + \left(r_2^3 - (3x-2b)r_2^2 + (2x^2 - 3bx + b^2 - 2\alpha^2)r_2 + \alpha^2(2x-b) \right) B e^{jr_2\xi} \\ & + \left(r_3^3 - (3x-2b)r_3^2 + (2x^2 - 3bx + b^2 - 2\alpha^2)r_3 + \alpha^2(2x-b) \right) C e^{jr_3\xi} \\ & + \left(r_4^3 - (3x-2b)r_4^2 + (2x^2 - 3bx + b^2 - 2\alpha^2)r_4 + \alpha^2(2x-b) \right) D e^{jr_4\xi}. \end{aligned} \quad (\text{E12})$$